Petrogenesis of orogenic peridotites and emplacement in the lower- and upper belt of the Seve Nappe Complex, Northern Sweden, Central Scandinavian Caledonides

S.D.A.van Bruchem
Master thesis, department of earth sciences, University of Utrecht
Utrecht, the Netherlands March 2017

1st Supervisor: dr. Herman van Roermund
2nd Supervisor: prof. dr. Martyn Drury

1.0 Abstract

The Scandinavian Caledonides (Sweden and Norway) are characterized by the presence of orogenic peridotites. The Seve Nappe Complex (SNC) which consists of high grade middle belt (granulite/eclogite facies) bounded on both sides by the middle grade upper- and lower Seve belts (lower-middle amphibolite facies) are scattered with these orogenic peridotites. Recent research has shown that the middle belt peridotites belong to the Mantle Wedge Peridotites (MWP) subtype. For the upper and lower Seve belt this is unknown. This MSc thesis focuses on the origin and emplacement mechanism of the orogenic peridotites in the upper and lower Seve belt. Fieldwork in Jämtland (North Sweden) is done to collect samples of these peridotite bodies in the upper- and lower- Seve belts. EMP- and XRF-analyses are done on these collected samples providing data for modelling P-T-t paths using Perple_X. The upper Seve belt originated in the mantle wedge overlying the subduction zone, the lower Seve belt has a sub-cratonic origin. The upper Seve belt has undergone metasomatism during the Finnmarkian (~500 Ma.) and Jämtlandian (~454 Ma.), the lower Seve belt heated up as a response to a hyperextended margin causing the dynamic recrystallization of olivine during the breakk-up of Laurentia and Baltica (615-590 Ma.). During the Jämtlandian the orogenic peridotites of both belts were incorporated in the country rock as a result of shearing, during the same time peak metamorphic conditions are reached in the order of 600 C° and 0.5 GPa for the upper belt and 750 C° and 0.5 GPa for the lower belt. The latest metamorphic overprint is the Scandian (420-410 Ma.) in which a retrograde metamorphism (greenschist facies) is observed .

Contents

2.0 Introduction

The Scandinavian Caledonides is a deeply eroded mountain belt in Norway and (western) Sweden. This implies that the bedrocks of the Scandinavian Caledonides contain important geological information about the physical and chemical processes that operate during orogenesis in the middle to lower crust. Peridotite is an ultramafic rock that originates from the Earth's mantle (Carlson 2004, Bucher 2011). Peridotites are therefore hard to study "in situ" as researchers cannot collect samples directly. However during orogenesis mantle peridotites can become emplaced into the continental crust (even up to higher crustal levels) by tectonic processes related to orogenesis. Such mantle rocks are called orogenic (or Alpine type) peridotites (Den Tex 1969). The Scandinavian Caledonides form one of the best places in the world to study such orogenic peridotites. In this MSc thesis orogenic peridotites, exposed along the Seve-Köli boundary in central Scandinavia, form the central research topic.

In Scandinavia the Caledonian mountain belt stretches from north to south for more than 2000 km. The Caledonian bedrocks thus dominate the "surface" geology of Norway and western Sweden (Gee, 2008). The Caledonian orogeny began with rifting and break-up of the supercontinent Rhodinia (Li et al., 2008). Initial rifting (600-700 Ma) was followed by further spreading and ocean floor formation, the ocean here was called Iapetus > 500 Ma. Baltica and Laurentia formed continents along the outer edge of the newly formed Iapetus Ocean. Around 550 Ma convergence between Baltica, Laurentia and/or Siberia started and resulted in subduction and progressive destruction of the Iapetus Ocean. This was then followed by a final collision between in this case the continents Laurentia and Baltica, in which the former overthrusted the latter. The final collision between Baltica and Laurentia is in the Scandinavian literature referred to as the Scandian orogeny (~430-390 Ma). There are however several other tectono-thermal events recognized in the Caledonides that characteristically all predate the Scandian orogeny. The latter involves intra-oceanic-, arc-micro-continent- and/or collisions between micro-continental fragments. They are respectively called Finnmarkian - (~500-490 Ma), Trondheim, (~480 Ma), Taconian (~460-450 Ma) and/or Jämtlandian orogenies (~460-450 Ma). From these the Trondheim- and Taconian orogenies occurred along the outermost continental margin/continent-ocean transition (COT) zone of Laurentia (= western part of Iapetus), while the Finnmarkian and Jämtlandian orogenies occurred along the Baltic COT margin (= eastern part of Iapetus; Brueckner and Van Roermund, 2004; Roberts et al., 2004). Including the Scandian all these orogenic events together, i.e. are related to closure of Iapetus and/or the final continental collision event, define the Caledonian Orogeny. Caledonian rock masses can be found in the Appalachians, Greenland, Scotland, Svalboard and Scandinavia etc. Consequently all Caledonian rock masses present in Scandinavia are referred to as the Scandinavian Caledonides, alternatively those in Greenland as the Greenlandian Caledonides etc.

The Scandinavian Caledonides consist of generally north-south striking nappes which were thrusted, during the Caledonian orogeny, progressively more eastwards over the continental margin of Baltica defined by its sedimentary cover and underlying Proterozoic/Archean basement. All allochthonous nappes are dominantly dipping (and thinning) towards the west and can be subdivided into the following 5 major nappe complexes (Roberts & Gee 1985; Gee et al., 2013). From top to bottom: the Autochthon, the lower- middle- upper- and uppermost Allochthons. The Autochthon consists of the Precambrian Baltic Shield/basement in the east (Fig 2) but also by some of the "sub-autochthonous" basement units that are exposed in tectonic windows underneath the allochthonous Caledonian nappes in the west (or more western parts of Norway/Sweden; Fig 2). The Allochthons are defined by Caledonian-metamorphosed, sedimentary cover rocks (+/- basement slivers). The lower- and middle Allochtons consist respectively of continental- and continent-ocean transition (COT) zone deposits which were formed during continental extension and the passive/active continental margin of western Baltica. The upper Allochton represents sediments and magmatic rocks (ophiolites etc.) originally deposited within the domain of the Iapetus Ocean. The Uppermost Allochthon consists of metamorphosed deposits and underlying basement units that define the outermost passive continental margin of Laurentia. This MSc thesis is essentially focused on the Seve Nappe Complex (SNC), which defines the upper part of the Middle Allochton in central Sweden/Norway. Here the SNC has been subdivided into three parts, called belts (Trouw, 1973, Zwart, 1974, Van Roermund and Bakker, 1984; Gee et al., 2013). From top to bottom these are called the western/upper-, the central/middle- and the eastern/lower belts. The metamorphic grade of the western and eastern belts is low/middle amphibolite facies, in contrast the central belt contains migmatites, granulites and eclogites, its metamorphic grade reaches up into the (U)HP/MT eclogite facies. Orogenic (or Alpine-type) peridotites occur within all three Seve belts (Zwart, 1974; Williams and Zwart 1977, Calon, 1977, Qvale & Stigh 1985; Bucher-Nurminen 1991). The origin, timing and crustal emplacement mechanisms of the orogenic peridotites in the SNC form a matter of fierce debate. This MSc thesis therefor deals with this topic. The various available tectonic models will be summarized and described in detail (chapters 3.5.1 to 3.5.3). However some orogenic Seve peridotites, all located in the central belt of the SNC, have recently been interpreted as mantle fragments that were resided in deeper parts of a mantle wedge above a subduction zone at the onset of early Caledonian subduction (Brueckner

and Van Roermund, 2004, 2007; Brueckner et al 2004, Clos et al., 2013;). According to these authors the central belt Seve orogenic peridotites were thus tectonically transported from the hanging wall mantle wedge into the subducting/educting continental crust (= central belt host rock gneisses) during the early Caledonian (Jämtlandian) orogeny (460-450 Ma) when continental subduction/eduction of SNC took place. At a later stage of this early Jämtlandian subduction process the subducted continental crust (including its peridotite cargo) had to return back to the surface due to positive buoyancy forces (= after slab break off). During this exhumation process, possible even later, water, present in the subducting sediments/continental crust and/or produced by prograde/retrograde dehydration reactions, caused post peak HPM serpentinization inside the central Seve belt orogenic peridotites. The recent discovery of UHPM-minerals inside one of these central belt orogenic peridotites (= Frinningen garnet peridotite) further strengthens this crustal emplacement model as the new UHPM mineral finding simply increased the maximal subduction depth from 100 to ~150 km (Majka et al 2014; Janák et al 2013).

However it is so far unknown how other orogenic Seve peridotites, i.e. those that occur within the western and eastern belts of the Seve Nappe Complex, or alternatively those of the Köli Nappe, were emplaced from the mantle into the continental crust by tectonic forces. The (early Caledonian) metamorphic grade of these two belts is (much) lower than that of the central belt (low to middle amphibolite facies grade. Zwart 1974; Van Roermund and Bakker, 1984; Van Roermund, 1985). This means that the latter two belts have never been subducted so deep into the mantle as the central belt. The aim of this MSc thesis is therefore to determine how the orogenic peridotite bodies in the western and eastern belts of the Seve Nappe Complex (SNC) were (tectonically) emplaced from the mantle into the continental crust.

Finding both recrystallized (foam texture) and primary olivine clasts can give an insight in the timing and PT conditions of recrystallization. Research has shown that dynamically recrystallized olivine grains can only form at temperatures above ~650°C (Bial & Trepman 2013). This work has shown that a temperature of 650-800 °C and a differential stress of 70-300 MPa lead to olivine being deformed with a strain rate of 10^{-13} to 10^{-15} s^{-1} (figure 1). In other words, finding these recrystallized olivine grains in nature means deformation has taken place, thus that the rock must have reached temperatures of at least 650-700 °C.
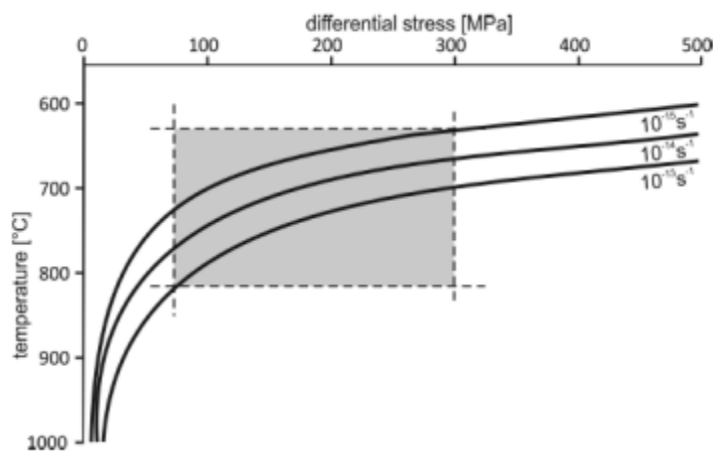
Figure 1. flow law for dislocation creep for olivine. temperatures ranging from 650-800°C and differential stresses from 70-300 mpa. (Bial & trepman 2013)

This Msc research is done using optical- and electron-microscopy techniques; i.e. a detailed study of the characteristic microstructures and/or mineral assemblages, present in thin sections that were made of orogenic peridotite samples collected in the field by the author (and colleagues), was performed. Results of this optical and electron microscopy study will be presented in diagrams/tables illustrating the relative timing of mineral growth versus deformation (events) observed/analyzed using mineral assemblages of the orogenic peridotites and/or their country rocks (chapter 5.2). In addition, some of the metamorphic PT-conditions will be calculated using the thermodynamic modelling program Perple_X (Conolly (2005,); Conolly (2009), chapter 6.3). The calculated PT conditions and associated P-T-t paths, will allow a better view of the mechanism and timing for tectonic emplacement of the orogenic peridotites into the SNC of northern Jämtland, central Sweden. In addition the obtained results will be compared to other crustal emplacement models proposed in the literature for other orogenic peridotites exposed in other

parts of the Scandinavian Caledonides (chapter 6.5). Hopefully this will result in a satisfying explanation for the crustal emplacement of mantle slices that are now exposed as orogenic peridotites at the surface in the Central Scandinavian Caledonides. This research will therefore strengthen or disprove current crustal emplacement models proposed for orogenic peridotites from the Scandinavian Caledonides (chapter 6.5).
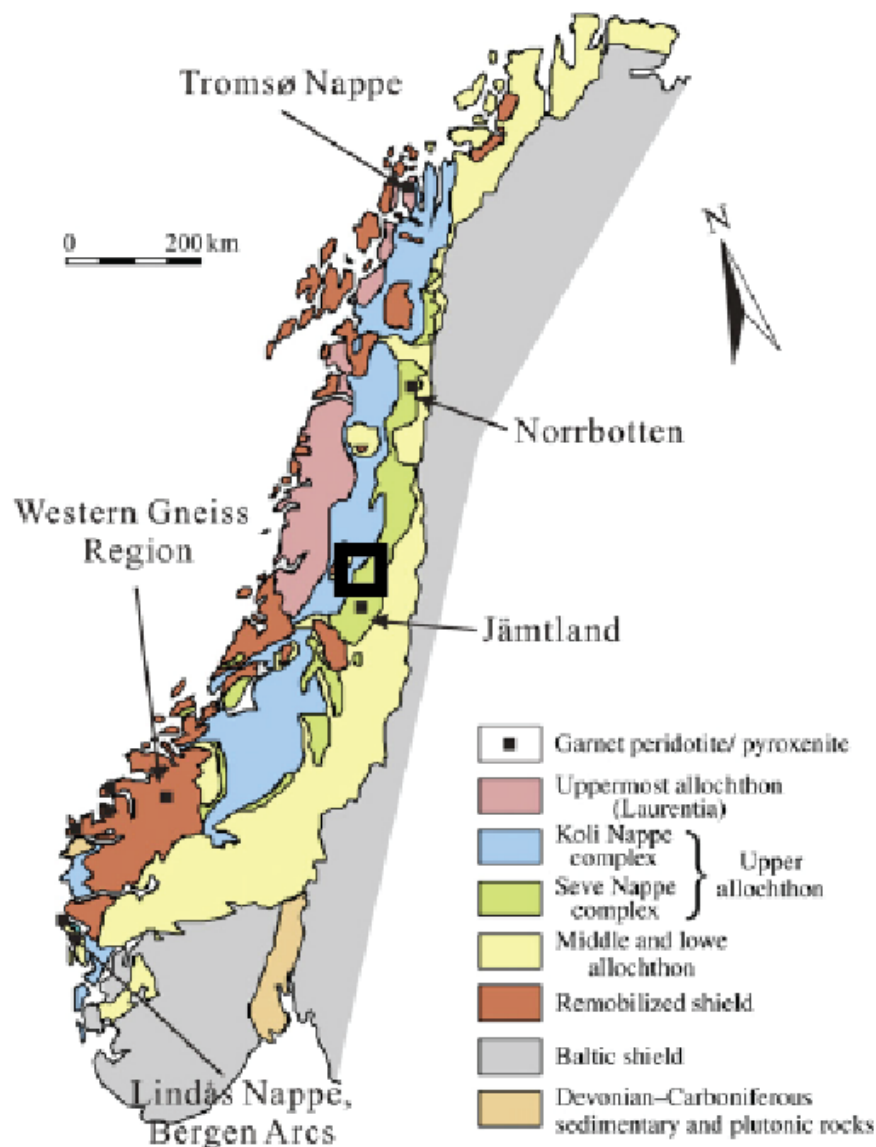
fegure 2. Simplified geological map of the Scandinavian Caledonides showing the major Allochtons (remobilized), basement, garnet peridotite locations and Devonian-Carboniferous sediments and plutonic of the Oslo area. The black square indicates the fieldwork area. (After Gee et al. 1985 and Brueckner & van Roermund 2004).

3.0 Geological background

3.1 Basic components of the Scandinavian Caledonides

The (Scandinavian) Caledonides were formed as a response to the closure of the Iapetus ocean and the final Scandian collision between Baltica and Laurentia (430-400 Ma), during which the former underthrusted the latter. However, recently, some other tectono-metamorphic events were discovered that predated the Scandian

orogeny. Including exhumation and erosion these orogenic events together have shaped the geometry of the Caledonian mountain belt in Scandinavia. Below, i.e. in the Fig caption of Fig 3 a summary is given of the timing and/or locations of the other Caledonian orogenic events.
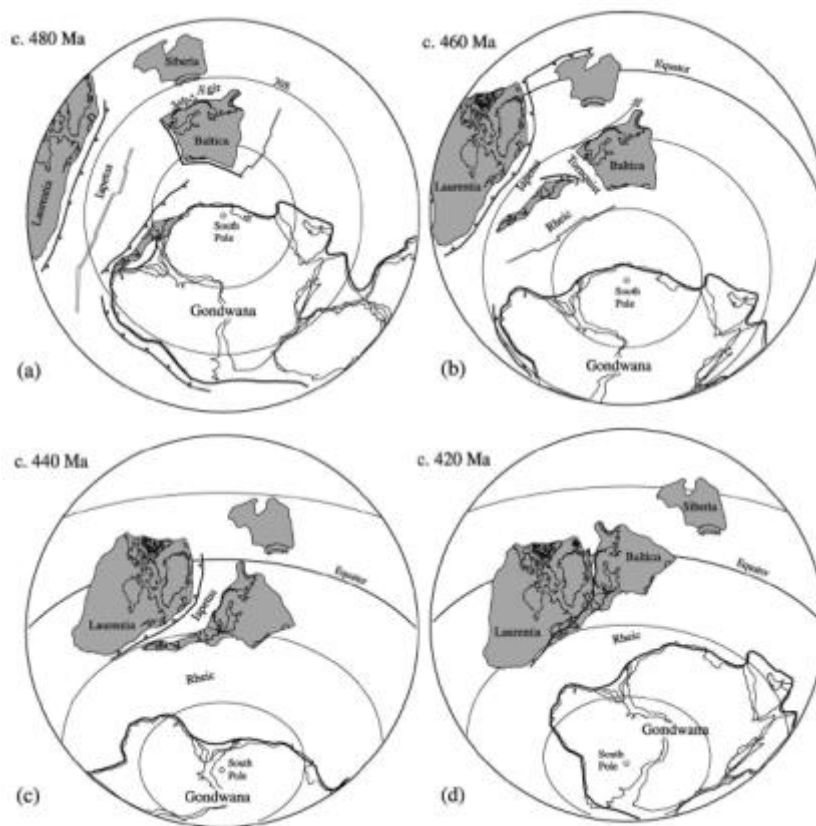
Figure 3. Simplified palaeo-geographic reconstructions from late Cambrian/early Ordovician to late Silurian time. Note: location of the geographic South Pole in all reconstructions. (a) Approximate position of Baltica, Siberia, Laurentia, Avalonia and Gondwana in latest Tremadoc/early Arenig time (= 500-480 Ma). The latter time period is broadly coeval with the Finnmarkian orogenic event (c. 500-480 Ma) which occurred along the "western" margin of Baltica involving oceanward subduction of Baltica (= upper part of Middle Allochton). Alternatively the Trondheim orogenic event (c. 480-475 Ma) is recorded by rocks of the 'Gula micro-continent' (= middle Köli Nappe/Upper Allochton) which at that time was located "offshore" of Baltica (it is sofar unknown however whether this offshore" position corresponds to the eastern or western side of the Iapetus/Ægir sea). Fossil evidence points so far towards the latter (=Laurentian side). Note 1: The Gula micro-continent is indicated on the schematic structural profile illustrated in Fig. 3. (b) Situation around the mid Llanvirn-late Caradoc (470-445 Ma), roughly at the time the Taconian orogenic event occurred along the eastern margin of Laurentia and the Jämtlandian orogeny along the western margin of the Baltica. Note 2: According to this reconstruction Baltica continued its anticlockwise rotation and drifted into more southerly, but look at South Pole position? latitudes, Avalonia is approaching the sw margin of Baltica. Note 3 the anti-clockwise rotation of Baltica is absent in reconstructions made by Li et al., 2008. (c) Early Silurian (early Llandovery/438-435 Ma) situation with Baltica approaching Laurentia across a rapidly closing Iapetus ocean. The Taconian and Jämtlandian Orogenies have ended, the Scandian is in progress. Avalonia (including accreted Laurentian marginal blocks) starts to dock with sw Baltica. (d) Situation in late Silurian time (420-410 Ma) during the Baltica/Laurentia Scandian continent-continent collision (After Torsvik (1998), Torsvik et al. (1996) and Cocks and Torsvik (2002)

3.2 Terrane map/Major tectono-stratigraphy of the Scandinavian Caledonides

The bedrocks of the Scandinavian Caledonides have been subdivided into 5 major groups (figure 2), from bottom to top: the Autochton, lower Allochton, middle Allochton, upper Allochton and finally the uppermost Allochton

(Zwart 1974). In the section below (section 3.2) the 5 groups will be discussed as to where they came from and what they represent in the Scandinavian Caledonides.

The Autochton forms the lowermost part of the Scandinavian Caledonides and is represented by the crystalline rocks that form the Baltic Shield in the east. The Baltic Shield consists of Archean to Proterozoic rocks that are overlain by Vendian to Silurian sediments (Hacker & Gans, 2005); the latter acted as a "substrate" to transport the overlying allochthonous nappes from west to east over the Baltic plate during the Caledonian Orogeny.

The lower Allochton is the lowermost transported units and consists of metasedimentary and crystalline rocks of late Proterozoic - Early Paleozoic age lithological similar to the sedimentary rocks overlying the Autochton. The lower Allochton represents the Baltoscandian foreland basin and platform (Hacker & Gans, 2005).

The Western Gneiss Complex (WGC) forms a tectonic window that is exposed along the SW coast of Norway (Fig 2). It consists of Proterozoic basement rocks/gneisses (and includes also some overlying cover sediments) that are reworked/overprinted by the Scandian (U)HP metamorphic event. According to Robinson et al. (2013) these reworked Caledonian basement units, exposed in tectonic windows along the Norwegian west coast, also belong to the lower Allochthon. It is worth mentioning that many orogenic peridotites occur in the WGC as well in some of the other basement windows (Qvale and Stigh, 1985; Bucher-Nurminnen 1989, 1991; Brueckner et al., 2010).

The middle Allochton is locally dominated by highly deformed Precambrian crystalline rocks that are overprinted/reworked by a Caledonian tectono-metamorphic event, the metamorphic grade of the latter corresponds to that of the greenschist facies but it can reach up to amphibolite facies grades in the westernmost areas along the Norwegian west coast and in parts of Finnmark and Troms (Roberts & Gee 1985). Apart from these crystalline rocks the dominant rock type of the middle Allochton consists of meta-sandstones which are subjected to high ductile strains and locally intruded by dolerite dikes around 680-580 Ma old (Roberts & Sturt., 1977; Greiling et al., 2007). The middle Allochton represents the western outermost edge of the continental margin of Baltica. This continental margin was fractured, intruded by a basic dike swarm and became strongly extended during the break up from Rhodinia (Fig 3). Since 2009 (Gee et al. 2009) part of the Upper Allochton is added to the Middle Allochton. More specific, the Seve Nappe is added which is divided into three belts: an eastern, central and western belt. The metamorphic grade of the eastern and western belt is amphibolite, the central belt reaches up to eclogite facies. Only recently the central belt is interpreted to represent a fossil subduction zone (Clos et al. 2013; Gee et al. 2014). However, the spatial dimensions of this fossil subduction zone are so far unknown, causing for a hotly debated research topic (Majka et al. 2013); Grimmer et al. 2015). The eastern and western belt of the SNC both show no evidence for subduction as the recorded metamorphic pressures in these belts are too low for subduction (chapter 6.3).

The eastern, central and western belts of the SNC represent the Continent-Ocean-Transition (COT) zone. The Seve nappe can be followed at least 1000 km along the length of the Caledonides (Andréasson 1994) and comprises of high-grade schists, gneisses, amphibolites and migmatites. In the Central belt of the Seve nappe some garnet peridotites are found, the western and eastern belts both contain orogenic spinel bearing peridotite bodies of 10's m to 100's m scale, but no garnet peridotites. The Köli nappe (Upper Allochtons), which represents oceanic (Iapetus Ocean) and island-arc terranes (Micro-continents). The transition between the Seve and Köli nappe, which is tectonic at some places, is marked upwards by a decrease in metamorphic grade. The Köli nappe has a metamorphic grade of lower to upper greenschist facies (Gee et al. 2010).

The uppermost Allochton (in the Central Caledonides) consists of the Rödingsfjället (RNC) and Helgeland Nappe Complexes (HNC). Both nappes consist of gneisses, schists, psammites, conglomerates, dolomites, calcitic marbles, and variable amounts of amphibolites, greenstones and sporadically some serpentinites (Robert & Gee 1985). The uppermost Allochton is interpreted to represent the easternmost continental margin of Laurentia, its

metamorphic grade is variable but usually of amphibolite facies grade, however middle to upper greenschist facies assemblages have also been observed. In contrast to the underlying, lower Allochthonous nappes, tectonic transport directions of nappes formed during the Taconian orogeny are all directed to the west (Roberts et al 2002).
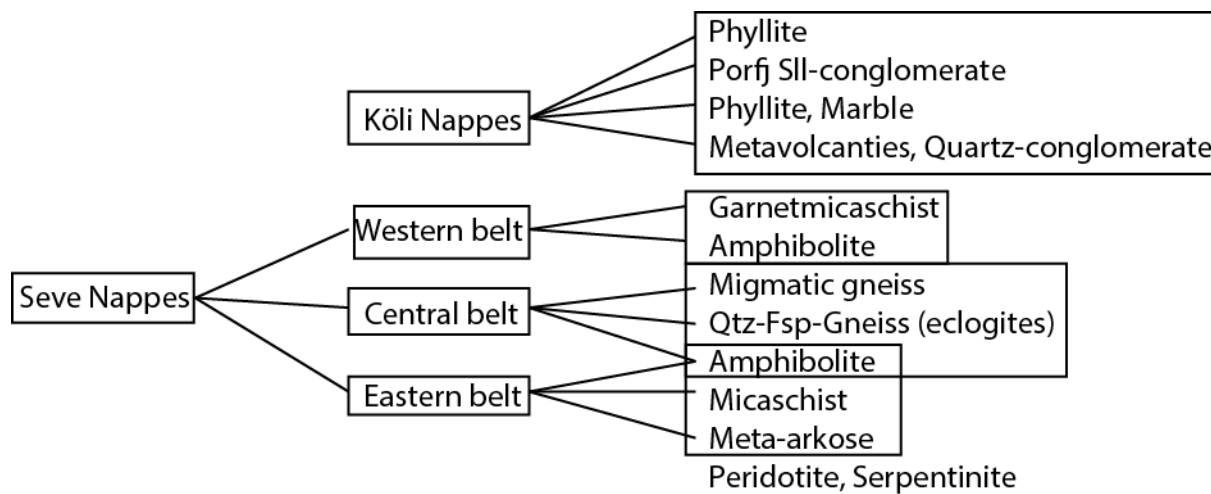
Figure 4. Basic tectonostratigraphic column succession of the Tängen-Inviken area. Samples taken during fieldwork are indicated in the figure. (Modified after van Roermund & Bakker, 1984)

3.3 The Seve Nappe Complex in N. Jämtland and S Västerbotten

The Seve Nappe Complex in N. Jämtland and S Västerbotten (SNC) is divided into three parts (Zwart, 1974, Williams and Zwart 1977; Van Roermund and Bakker, 1984). From top to bottom these are called the Western/Upper, Middle/Central and Eastern/Lower belts (new terminology after Gee et al., 2008 & 2013). The Caledonian metamorphic grade of the Western and Eastern belts is lower/middle amphibolite facies that of the Middle belt granulite to eclogite facies (Fig. 5). Classically the SNC formed part of the Upper Allochton (Robert & Gee, 1985; Stephens and Gee, 1989) but more recently researchers (Gee et al. 2008, 2013) have decided that the SNC forms part of (the upper part of) the Middle Allochton. The SNC is now interpreted to represent the continent-ocean transition (COT) zone, contrary to the Upper Allochton which represents now exclusively the oceanic domain of the eastern Iapetus Ocean. The SNC can be followed for more than 1000 km from north to south (Fig 2). Ultramafic mantle slices are found in all 3 major belts of the SNC (Zwart, 1974, Williams and Zwart 1977). These ultramafic bodies are mainly spinel bearing dunites and/or harzburgites which means that, predating their crustal incorporation, these orogenic peridotites have been through one kind of depletion/melting process. Central belt Seve orogenic peridotites contain 2 generations of the HP garnet-olivine mineral assemblage (A.o. Frinningen Garnet Peridotite, FGP; Van Roermund, 1989) which can only be formed, depending on temperature, at depths > 80 km. The Frinningen Garnet Peridotite is interpreted as a Mantle Wedge Garnet Peridotite (van Roermund 2009; Gilio et al. 2014).

The western/upper Seve belt consists of garnet-mica schists interlayered with quartzitic, garnet bearing, micaschists and meta-amphibolites (Zwart 1974). The central belt consists of migmatitic ky-kspar gneisses (with eclogite and/or granulite assemblages), quartzo-feldspathic gneisses and meta-amphibolites. Recent discoveries have shown that at least one of the ultramafic bodies have undergone early Caledonian UHP metamorphism (Brueckner and Van Roermund 2004, 2007; Janak et al. 2013). Since then possible micro-diamond occurrences were also reported from more norther locations in the Avardo gneiss (=central/middle Seve belt; Majka et al. 2014). The eastern belt consists of meta-arkoses, quartzites, garnet-micaschists, amphibolites and some minor calcsilicates/marbles (figure 4) (Zwart 1974; Van Roermund and Bakker, 1984).

It should be noted that the Central belt is the subduction zone during the Jämtlandian orogeny (Brueckner & van Roermund 2004), as the highest pressure-temperature conditions are found in the Central belt. Thus the boundaries of this fossil subduction zone are the contacts between the Western-Central and the Central-Eastern belt. The Eastern belt is thus found beneath the subduction zone, where the Western belt is found on top of it.
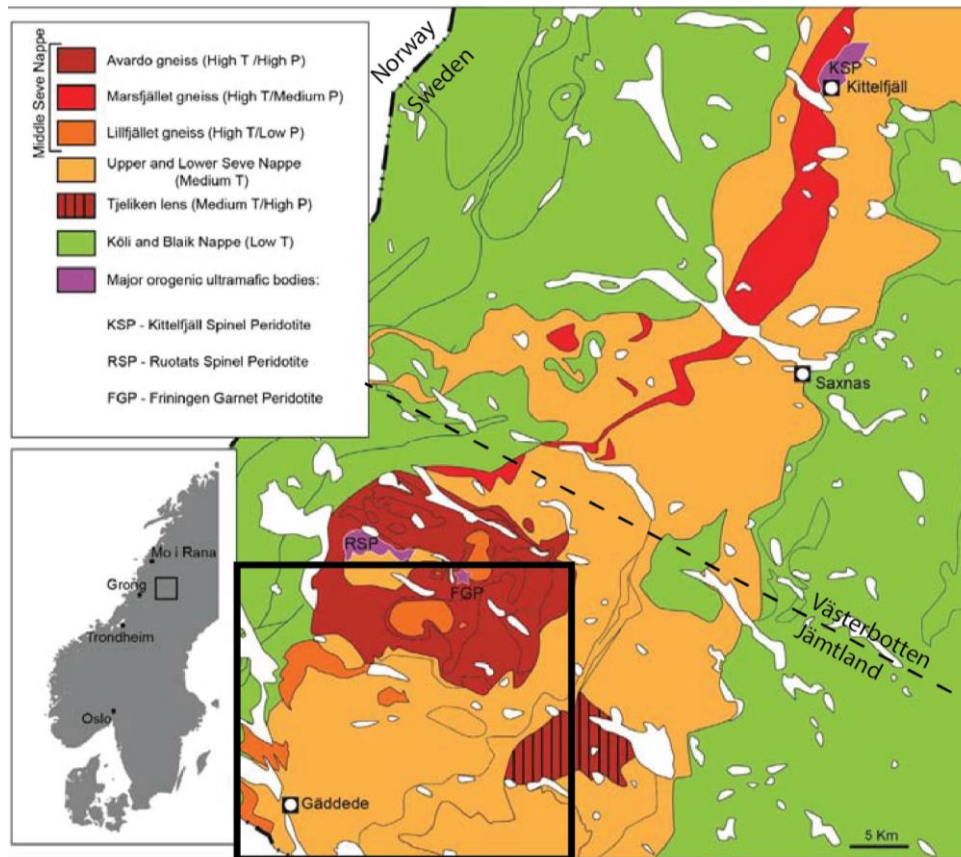
Figure 5. Metamorphic map of the SNC in northern Jämtland and S. Västerbotten. The metamorphic grade of the western and eastern belts are that of the lower/middle amphibolite facies, the central belt is HP-MT granulite- to eclogite facies (after Clos et al., 2014).The black square indicates the research area. Note also that the metamorphic pressure recorded by mineral assemblages of the central belt is variable from north to south.
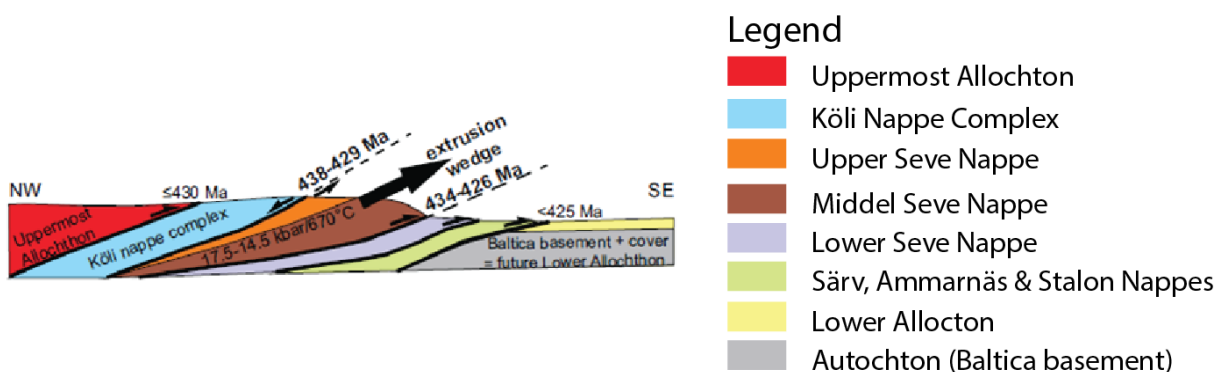
Figure 6. Schematic cross section through, approximately, the Västerbotten-Jämtland boundary. (Grimmer et al. 2015)

3.4 Peridotites

3.4.1 Primitive mantle composition and (decompression) melting

Peridotites are ultramafic rocks which make up most of the Earth's mantle (Bucher & Grapes, 2011). Using cosmochemical estimates a mean bulk composition for the Earth's mantle was determined by Palme and O'Neill (2003). For simplicity reasons the average bulk mantle composition will be called here primitive mantle (=PM). This PM bulk rock composition is plotted as a black star in the Cpx-Opx-Ol diagram of figure 7 below. Also indicated in the same figure 7 are the compositional fields for lherzolitic, harzburgitic and dunitic rocks. In addition experimental evidence has demonstrated that the PM mantle composition can be modified by HP melting (= decompression melting; Walter, 1998/1999). Experimental work has also demonstrated that, depending on the amounts of melt (in vol%) extracted from a PM bulk mantle composition, the residual/refractory bulk rock compositions will change from lherzolite to harzburgite and then to dunite. Chemical analyses of the bulk rock compositions (BRC) of natural orogenic peridotites do overlap with this chemical melting trend (Bodinier and Godard, 2005).

3.4.2 Melting
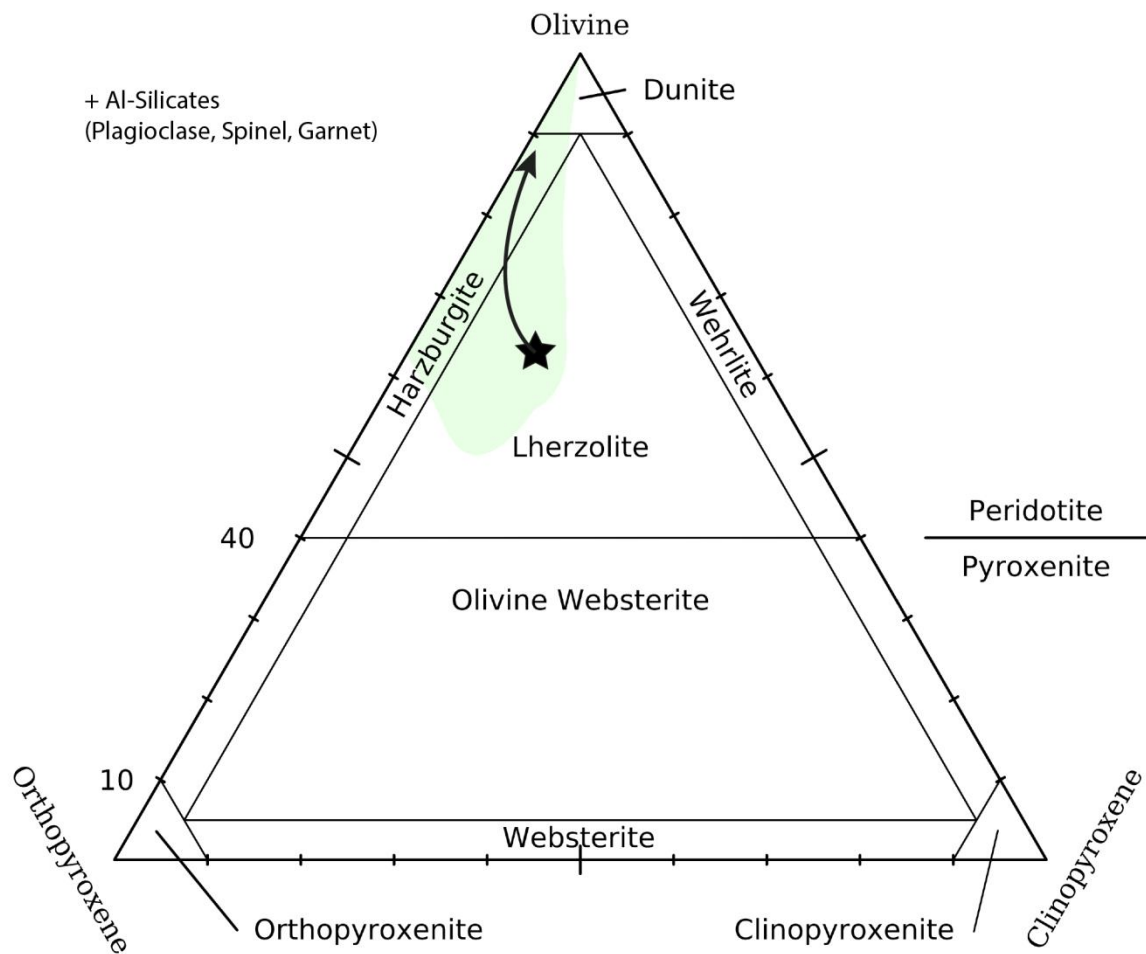
Figure 7. triangular classification diagram of ultramafic rocks based on the mineral modes expressed in terms of ol-opx-cpx. the star represents the pm bulk rock composition of the upper mantle, the arrow shows increasing depletion of the ultramafic rock. lherzolite is the starting composition, a more depleted stage is harzburgite and the most depleted stage is dunite (after bodinier & godard, 2004). there can also be al-silicates (spinel, garnet, plagioclase) in every field of the figure. These are not shown but can be very important in showing a part of the geologic history the rock has gone through. so these fields can also be divided into for example spinel dunite or spinel harzburgite.

By chemical differentiation related to (adiabatic) decompression-HP melting, a PM bulk rock composition can become depleted in major elements like Si, Ca, K, Na, Al and Fe. The latter elements will partition into the melt, as such the residual bulk (mantle) rock composition will become enriched in Mg and Cr. Bulk rock compositions of Primary (PM) or "only little" depleted mantle will thus plot in the lherzolite field (indicated in Fig 7), and consist of the following silicate-minerals which are ordered from more to less abundant: Olivine (Ol), orthopyroxene (OPX), clinopyroxene (CPX) including an Al-bearing phase such as garnet, spinel or plagioclase. During the depletion/decompression melting in the Earth's mantle the first mineral that will be progressively be removed is CPX as Ca partitions first out into the melt. Depending on pressure the second mineral that will be "removed" is OPX when Si partitions into the melt, leaving Ol as the remaining mineral behind in the refractory host rock. Thus the most depleted refractory stage is represented by the dunite field, followed by harzburgite and then lherzolite (figure 7). The above described melting process has taken place continuously throughout Earth's history. It simply occurs each time when a rising/upwards moving mantle mass (plume or convection cell?) intersects the dry peridotite solidus. At relatively "shallow" depths, but still at high T (1250-1500°C), subsequent isobaric cooling of the refractory rock will transform the refractory peridotite volume from asthenospheric- (T>1200°C) into lithospheric conditions (T<1200°C). As such the melting process will result in the formation of sub-continental- and/or sub-oceanic lithospheric mantle (SCLM and SOLM).

Although the melting and cooling processes of both types of lithospheric mantle are roughly similar they are not the same in terms of P and age. The latter parameter determines whether you are talking about sub-oceanic lithospheric mantle (SOLM) or sub-continental lithospheric mantle (SCLM). In addition oceanic crust is generally not older than 150-200 Ma (Rowley 2003) as it is eventually reincorporated back into the mantle through subduction. Normally continental crust does not get reincorporated in the mantle due to positive buoyancy forces. However, the age at which continental crust was formed varies (Archean–Cenozoic), thus the underlying lithospheric mantle can also be of Archean-Cenozoic age. During the Archean the mantle temperature was generally higher than the present day mantle. Archean mantle melting events are thus expected to extract higher volumes of partial melts from PM than possibly can occur in modern times.

3.4.3 Mantle rocks (peridotites) classified according to their geological setting

Ultramafic rocks are derived directly from the mantle. Ultramafic rocks can however be formed also by direct crystallization/fractionation from (mantle-derived) basic melts such as basalt (Wyllie, 1969). Examples of this "igneous" type of peridotite are mainly found as minor peridotite layers (5-10%) within otherwise gabbroic rocks (90-95%) defining large layered igneous complexes like Skaergaard (Den Tex 1969). More important is that similar igneous peridotites are now also commonly described from the basal sections of ophiolites (oceanic "Moho" level). However in order to lower the solidus temperature of a dry peridotite melt the Fe content of the system has to be "high". This means that solidification/crystallization will produce olivine mineral compositions that are characterized by relatively low Mg numbers (Mg# < 84-86). This can easily be determined in the lab allowing for rapid identification after field work. Thus although scientists cannot directly study in the field rocks that come from the (upper) mantle, they can still study, at the "surface" of the earth, ultramafic rocks that were brought to higher crustal levels either in the form of a) xenoliths transported by magma/liquids b) Solid mantle material (SOLM/SCLM/asthenosphere) that was emplaced from the (shallow/deep) mantle into the continental crust by tectonic processes related to orogenesis (this type is called orogenic peridotites which includes here the classic ophiolite- and Alpine types). Only in recent years a third peridotite type has been added to this list c) samples dredged (mechanically/drilled) from the floor of the ocean, this type is called abyssal peridotite.

3.4.4 Further classification of orogenic peridotites/Subtypes of orogenic peridotites.

Based on their geological setting 3 main groups of peridotites can thus be recognized in the field: 1) xenolithic peridotite, 2) orogenic peridotite, and 3) Abyssal peridotite. Note that the orogenic peridotite group is also known in the (older) literature as the group of Ophiolite and Alpine type peridotites. When looking at peridotite occurrences exposed in the Scandinavian Caledonides two groups of peridotite were identified (Qvale and Stigh 1985). Unfortunately they are referred to as either the igneous type or the so called Alpine type peridotites. In this context it is important to mention that in the geological past Alpine type (now orogenic) peridotites were subdivided in 2 sub-groups called the ophiolitic- and the rootzone sub-types by Den Tex (1969). In this classification system the ophiolitic subtype represented (sometimes dismembered) obducted oceanic crust (this ophiolite subtype includes SOLM, but the SOLM fragment can be detached from the overlying ophiolite by tectonic processes, as such they are found as isolated peridotite masses within schist/gneiss). At that time this ophiolitic subtype was found in mountain belts of Caledonian- or younger age. More important along sutures defined by thin plates. The latter was a very important field observation as it clearly excluded garnet-olivine (HP-mineral) protolith assemblages characteristic for garnet peridotite. As such the rootzone subtype consisted of SCLM fragments (spinel - and garnet peridotite) that became incorporated in the continental crust either by underplating during continent-continent collision or by deep level ductile imbrication of the continental crust during orogenesis (Cuthbert & Carswell 1990). Here the rock-association (spinel/garnet) peridotite and eclogite/ HP granulitic gneiss typically defined a geological setting that was characterized by a thick (=doubled) continental

crust (note: at that time the geological meaning of eclogite/eclogite facies was not yet known). The rootzone type was found in orogens of Caledonian- and older age.

If we further discriminate between spinel- and garnet bearing peridotites we can find the following major difference. Spinel bearing peridotites can be classified as either an ophiolitic as well as a rootzone peridotite. Garnet bearing peridotites cannot be of the ophiolitic type as the pressure needed to form garnets (>100 km depth) is never reached in ophiolitic type peridotites. Another problem was that during the time Den Tex couldn't explain the emplacement of garnet peridotites into continental crust as UHP terranes did not exist yet and thus the only way of how peridotites could be incorporated was by underplating or imbrication of continental crust. However, by these mechanisms you can only explain the emplacement of spinel bearing peridotites but not garnet bearing peridotites. Den Tex came up with a solution that garnet peridotite occurrences resembled rising hot mantle diapirs which were emplaced in thick continental crust. It wasn't until the discovery of UHPM (Brueckner 1998; Janak et al. 2013; Majka et al 2014) that a satisfying explanation could be given for the aforementioned problem. Brueckner & Medaris (2000) divided the different types of peridotite in two categories: crustal- and mantle types. The crustal category resided in the "shallow" crust prior to subduction. The mantle category is, in some cases, derived from the mantle wedge and is, in turn, divided into two classes: the subduction zone class and the relict. The subduction zone type is further divided into 'prograde', 'high-pressure – high temperature' and 'ultra-high temperature' types (Brueckner & Medaris 2000). The relict type peridotite is derived from "ancient", subcontinental lithosphere and shows no evidence of processes related to oceanic subduction. Both types of peridotites have a more complex metamorphic history than their surrounding country-rocks, which indicates that peridotites are formed as predominantly solid bodies (Den Tex, 1969). This formed the onset of detailed microstructural studies as the question how solid rocks can show creep came up. This has been basically the first evidence of convection processes in the mantle.

Brueckner (1998) and Brueckner & Medaris (2000) came up with continental subduction into the mantle down to levels which passed the spinel-garnet phase boundary. Through subduction continental crust can penetrate up to 140 km deep into the mantle where the overlying mantle wedge can then be incorporated in the crust. Peridotites incorporated like this are now called mantle wedge garnet peridotites (MWGP)(Van Roermund 2004). Once slab break-off has taken place the crust, together with the incorporated MWGP, returns to the surface due to positive buoyancy forces. Another explanation of the occurrence of garnet bearing peridotites is that the ultrabasic material was already present in the crust prior to subduction. During subduction the crust reached depths of > 140 km where through prograde metamorphism the olivine-garnet assemblage of the garnet peridotite was formed. This type is called the Subduction Zone Garnet Peridotite (SZGP). However, the SZGP will give the age of the orogeny, whereas the MWGP will have a garnet-olivine age that pre-dates the orogeny.

3.5 Current large scale Tectonic models for the formation of the Caledonides

In the following section popular/recent large scale tectonic models for the formation of the Caledonides are described. These large scale tectonic models are presented in a cartoon-like format. The section is however needed to see when/where in these large scale orogenic models peridotites can be emplaced from the mantle into the continental crust. More important, are these models consistent with the proposed crustal emplacement model for the orogenic peridotites of the Seve Nappe Complex (SNC) i.e. as proposed later in this MSc thesis for the orogenic peridotites exposed in the Seve Nappe in central Sweden.

3.5.1 Roberts 2003

The first event in the Roberts model is called the Finnmarkian event which has been dated at 505 Ma (Sturt et al. 1978). The Finnmarkian involved the outermost Baltoscandian margin (SNC) - the continent-ocean transition zone - comprised of the upper Allochton and parts of the Middle Allochton (Roberts 2003). The aforementioned parts of the Caledonides are believed to have subducted beneath a magmatic arc. This arc may have been largely

oceanic and positioned in the Ægir Sea between Baltica and Siberia or it may have been a partly continental block which had earlier rifted from Baltica (Gayer et al. 1987) (figure 3)
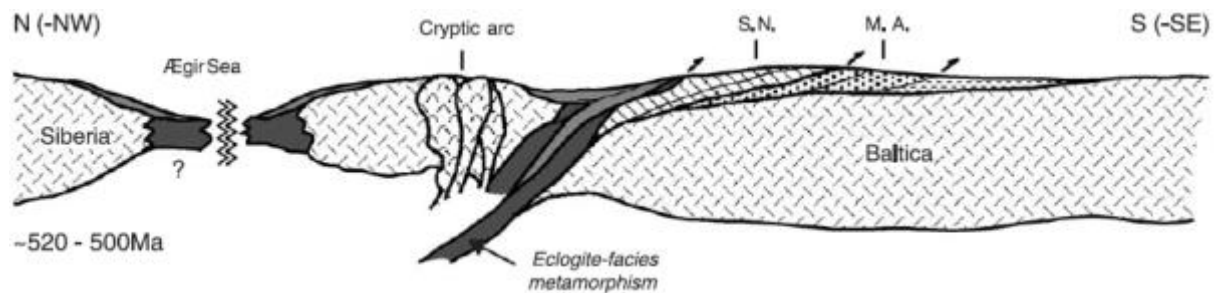
Figure 8. schematic, composite profile illustrating the finnmarkian event, in late cambrian time, ca. 520-500 ma. the profile relates to the nothernmost parts of Norway and parts of Sweden. oceanward subduction of the continetnal margn/ocean transition zone down to at least eclogite-facies dpeths was followed by rapid exhumation and emplacement of finnmarkian nappes onto the baltoscandian margin. baltica is considered to have faced siberia at this time, across the Ægir sea. a microcontinental block (rifted off baltica) has been inferred to have been involved – the 'barents microcontinent' of gayer et al. (1987). s.n. – Seve nappes; m.a. - middle allochton. (after roberts 2003)

The second event is called the Trondheim event which involved the Köli Nappes and took place at ~480 Ma. During the Trondheim event deformation and metamorphism, including eclogite obduction, occurred. Dating on these suprasubduction-zone ophiolites have yielded U-Pb zircon ages of c. 493-482 Ma (Dunning 1987; Sturt & Roberts 1991; Roberts et al. 2002). The ophiolites are believed to be obducted upon epicontinental rocks of the Gula Complex, which rifted off Baltica. Fossils found in the overlying Støren Nappe show a maximum age of Mid to Late Arenig constraining the metamorphic event to Early Arenig (Roberts 2003).
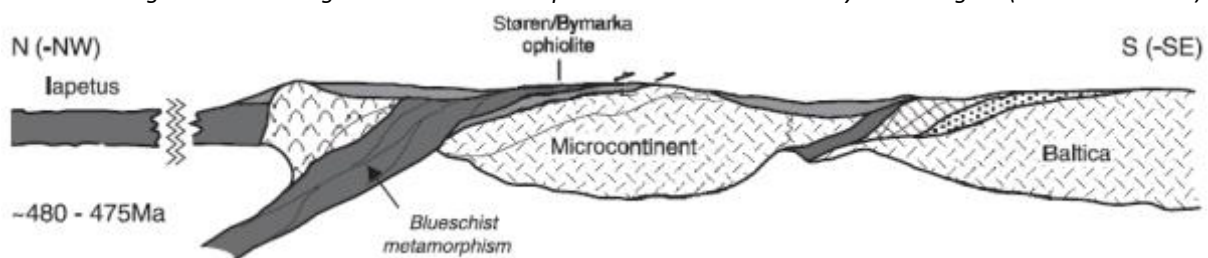
Figure 9. schematic, composite pofile illustrating the Trondheim even, in latest tremadoc to early arenig time, c. 480-475 ma. the profile relates to the trondheim region of mid norway. again, oceanward subduction is inferred, down to at least blueschist-forming depths, prior to or partly coeval with early to mid arenig, ophiolite obduction onto mainly epicontinental köli nappe rocks (gula complex) covering the 'gula microcontinent'. the earlier, finnmarkian-accreted, magmato-sedimentary complexes (seve/kalak nappes etc.) are shown farther s-se, draping the margin of baltica. by this time, baltica had started to rotate anticlockwise, eventually to face laurentia, across the iapetus ocean. (after roberts 2003)

The third event is the Taconian event and occurred Mid to Late Ordovician (~460 Ma). The Taconian event included the Uppermost Allochton and some of the highest and most outboard Köli terranes. The Taconian event occurred along the eastern margins of Laurentia, remote from Baltica at that time, and involved arc complex accretion and eastwards subduction (Fig 10). After–westwards accretion, as a result of eastwards subduction the accreted material got exhumed and detached from Laurentia and transported onto the nappes of the Baltoscandian margin of Baltica during the younger Scandian orogeny.
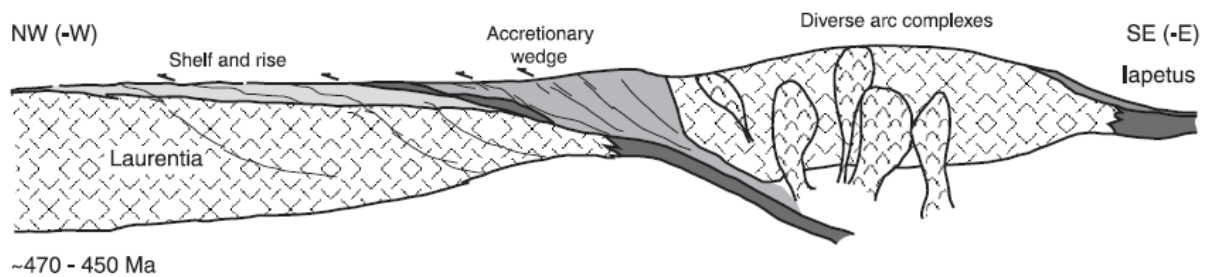
Figure 10. Schematic, composite profile showing the palaeotectonic setting during the taconian event, in mid to late ordovician (llanvirn to caradoc) time, c. 470-450 ma. in this case, subduction and accretion, including eclogite generatoin and ophiolite obduction, occurred along the continental margin of laurentia, quite remote from baltica. parts of these laurentian shelf-and-rise and peri-laurentian arc-complex terrans were later detached and retransported onto the nappes carpeting the baltoscandian margin of baltica during the scandian collisional event. (after roberts 2003)

The final collisional event creating the Caledonides as they are today is called the Scandian orogeny which took place between 430-400 Ma. This orogeny occurred as a reaction to the oblique collision of Baltica and Laurentia, where the former underthrusted the latter. Evidence from monazite geochronology from UHP rocks in the Western Gneiss Region (WGR) show that subduction to depths of >125 km at 407 Ma and subsequent exhumation took place in an extremely short geologic time of only 10 million years. As such this phenomenon is rightly called 'dunk tectonics' by Brueckner and van Roermund (2004). All Allochtons were involved in the Scandian orogenesis, including those already affected by the Finnmarkian, Trondheim, Taconian or Jämtlandian tectonothermal events (Roberts 2003).

The post-Scandian events exist solely of late-stage extensional deformation event arising from gravitational collapse. During these events major, low-angle, ductile detachments with a top –W to –SW shear sense.

3.5.2 Brueckner and van Roermund 2004

Brueckner and van Roermund admit that their model is still incomplete as it is not dealing with the 425 Ma Bergen Arcs event or the 452 Ma eclogite formation event in the Tromsø Nappe (north Norway), or the 415-340 Ma event in NE Greenland. Instead, their focus goes out to 3 or more major subduction and eduction events resulting in HP/UHP terranes.

The model from Brueckner and van Roermund also states the Finnmarkian as the first tectonothermal event in the evolution of the Scandinavian Caledonides. They think a microcontinent subducted to depths of up to 60 km (fig. 11A), the microcontinent reached these depths because it was dragged/pulled along with previously subducted oceanic lithosphere. Eventual slab breakoff or crustal delamination resulted in positive buoyancy thus eduction. The ultramafic rocks which invaded the microcontinent are interpreted as 'prograde subduction peridotites'. During eduction it is thought to have a less high T (<500°C) at ~480-470 Ma. Another possibility is an arc-continent collision to the north and an arc-microcontinent collision in the south, if this scenario proves to be true the HP terrane should be emplaced directly on Baltica.

A The Iapetus/Aegir Sea system at >500 Ma.
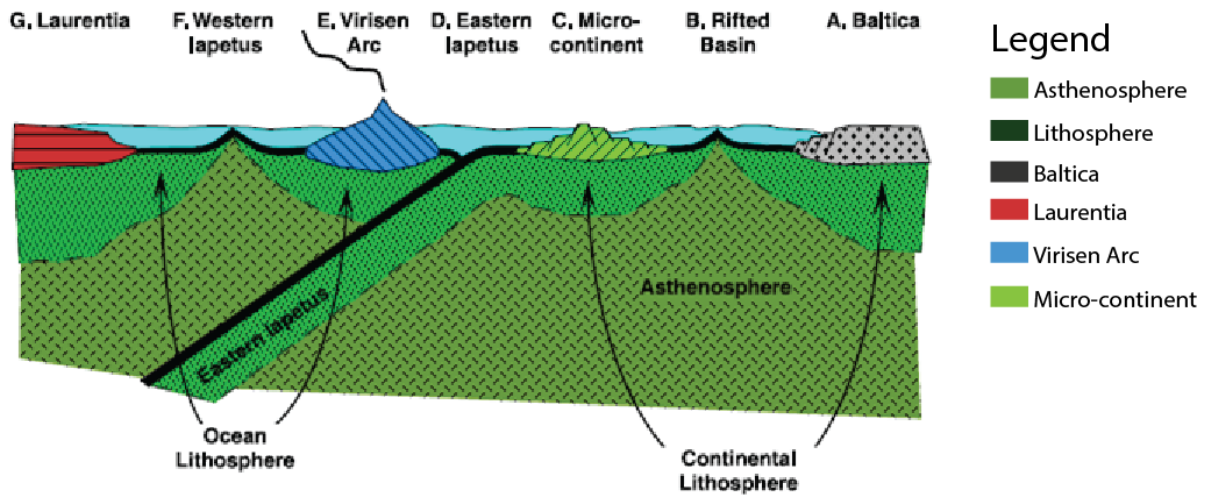
B The Finnmarkian Subduction at 500 Ma.
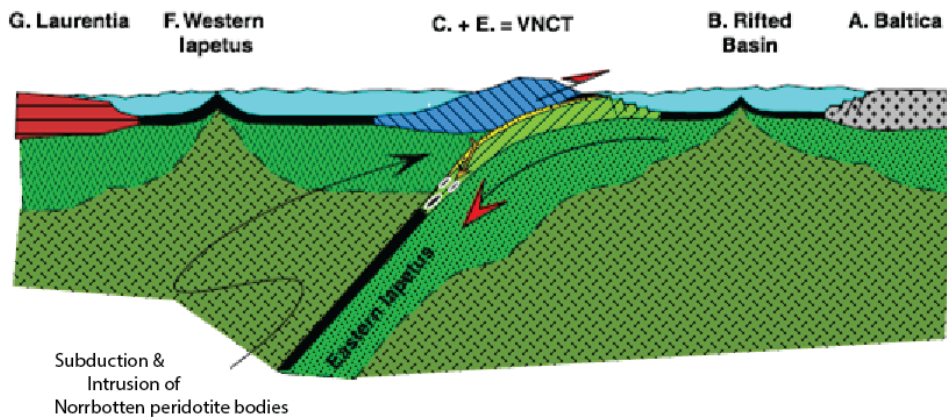
Figure 11. (a) conifguration of the iapetus ocean prior to the finnmarkian orogeny. (B) Part of the finnmarkian orogeny in which an arc-microcontinent collision led to the subduction of the microcontinent to eclogite facies metamorphism and the introduction of peridotite bodies from the mantle wedge. vnct: Virisen/Norbotten composite terrane.

The second event predating the Scandian orogeny is the Jämtlandian orogeny (~454 Ma) first recognized by Brueckner & van Roermund (2004; 2007). The Iapetus Ocean was an ocean littered with arcs, microcontinents and peninsulas (Brueckner & van Roermund 2007); it is therefore not surprising that during the Jämtlandian orogeny nearly the same happened as during the Finnmarkian. Following the same line of reasoning during the Jämtlandian a magmatic arc or microcontinent subducted beneath the Virisen Norbotten Composite Terrane (VNCT) up to eclogite forming depths and became exhumed in a geological short time. The main difference with the Finnmarkian is that the mantle wedge now does not show oceanic affinity but is continental (Brueckner et al. 2004). Another possibility for the Jämtlandian is the collision of 2 arc systems and the western part of Baltica (Central Seve Belt) where the Finnmarkian occurred 50 My earlier in the north than the Jämtlandian in the south.

However, this would not explain the subcontinental lithosphere mantle affinity found in the south.

C. The Jämtlandian Orogeny at 454 Ma.
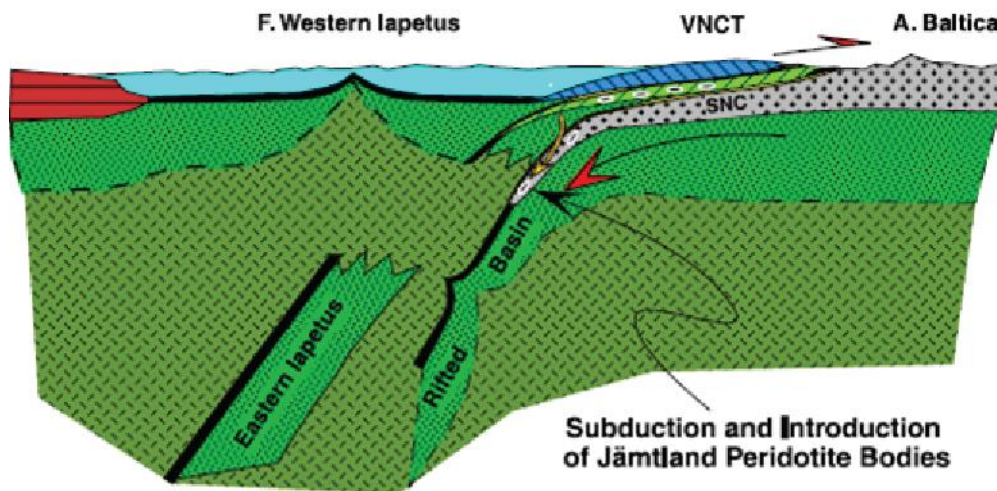
D. Eduction of Jämtlandia at ~435-440 Ma.
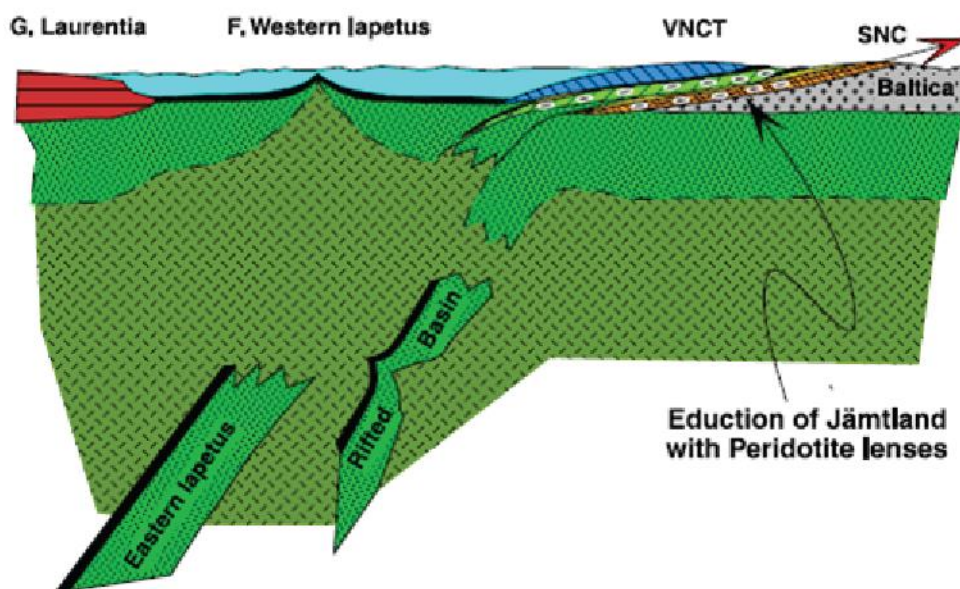
Figure 12. schematic section showing the jämtlandian orogeny and the subsequent eduction. (A) the Jämtlandian orogeny showing the subduction of the COT of baltica beneath the vnct. eclogite facies conditions were achieved during the subduction, the main difference with the finnmarkian is the affinity of the overlying mantle wedge which is continental compared to oceanic during the finnmarkian. (B) the eduction of Jämtlandia as a response to slab breakoff. the educted material is emplaced on top of the baltic shield. (Brueckner & van Roermund 2004)

The Scandian orogeny occurred as a reaction to the closure of the Iapetus Ocean and is responsible for the final nappe stacking found in the present day Caledonides. The collision started ~425 Ma but peak metamorphic conditions were not achieved until ~418-400 Ma. The WGR must have been forced into the mantle for UHP conditions and peridotite invasion. Easiest model to explain this is the simple subduction of Baltica beneath Laurentia. However, this does not explain the oceanic affinity of the subcontinental lithosphere. The garnet peridotites show a sub-Baltic affinity, it is hard to distinguish between Laurentia and Baltica affinity though as both underwent a major cycle of crustal growth and metamorphism at ~1750 Ma (Kalsbeek et al. 1993). An intracratonic fault in Baltica might be another explanation for the subduction of the WGR into the mantle. This

fault would have to cut through the crust into the underlying subcontinental mantle. The crustal material in the footwall will than have been pushed or dragged along the fault into the mantle to UHP conditions. Studies suggest that during continent-continent collision extremely high pressures capable of forming these enormous faults do exist. The WGR has been educted at tremendous speed (~10 mm/yr, Terry et al. 2000; Carswell et al. 2003) because the eclogites now visible in the field do not show extensive retrogression. Another explanation which does not require the low angle detachment fault is significant extension after subduction. This would have allowed the WGR to simply be pulled out of the mantle along with the underlying lithosphere.
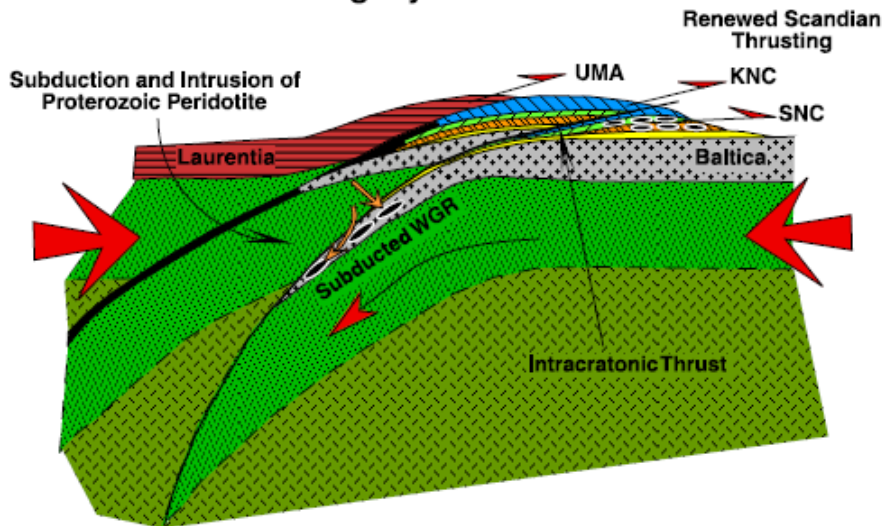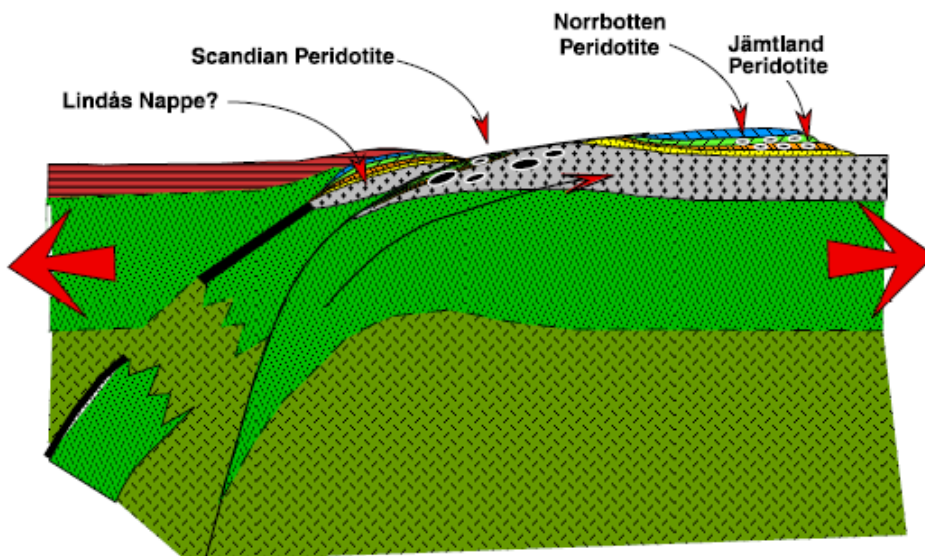
Figure 13. schematic section showing the scandian orogeny and subsequent exhumation of the Western gneiss region. (A) the scandian orogeny as a result of the closing of the iapetus ocean. subduction of baltica beneath laurentia reached up to eclogite facies metamorphism. note that some of the previously HP/uhp terranes could be resubducted into the mantle. (B) post-scandian exhumation of the WGR as a result of orogen-normal extension.note the extreme thinning of the allochtonous terranes as a result of extreme shearing during extension (brueckner & van roermund 2004).

3.5.3 Hacker & Gans 2005

The third model is from Hacker and Gans; they say that at 480-470 Ma, during the Trondheim event, an unnamed arc collided with Gula-Seve-Baltica which later got exhumed (figure 14). During this event ophiolite emplacement took place which can cause near UHP-metamorphism. The second event recognized is the Jämtlandian event as in Brueckner & van Roermund (2004). The Jämtlandian orogeny involved westward subduction of the Seve Nappes and maybe the Köli Nappes followed by thickening, heating and exhumation. No subduction related magmatic arc has been found which thus a more complicated tectonic setting. The third event is an areally extensive magmatic episode at ~445-432 Ma which resulted in the formation of new oceanic crust and intrusions in the Uppermost Allochton and Köli Nappes. These plutons in the Köli Nappe are derived from either melting mantle in a continental rifting system or from melting mafic crustal rock at T ~900°C and 10-15 kbar. Plutons of this age are solely found in the upper Köli Nappe and at stratigraphic levels above the Köli Nappe indicating this event took place before the final emplacement of the Uppermost Allochton and Köli Nappes on to Seve Nappe. The fourth event recognized is the Scandian Orogeny consisting of eastward propagating nappe emplacement at ~437 Ma in the west and ended at ~415 Ma in the east. Hacker & Gans conclude that there are four different scenarios in which continental crust can subduct up to eclogite forming conditions; 1) If the continental material becomes denser than the surrounding material, 2) if it is attached to sinking oceanic lithosphere, 3) if it is overlain by denser material pushing it downwards or 4) if it is attached to sinking continental lithosphere. The first theory is impossible as the WGR is too felsic in composition to ever reach greater-than-mantle density. The second theory is also impossible because 10-20 M yr. earlier ophiolite emplacement took place which requires large scale thrusting between Baltica and the WGR. The third scenario might be possible, with just a few kbar more the pressure would have caused eclogite formation resulting in an increase in density thus sinking into the mantle would be possible. The fourth scenario might also be possible as continental crust is capped at 20-30 km with 2.95-3.05 g/cm^3. This means that when high-pressure minerals form the density could become high enough for the crust to sink under its own weight and thus can drag attached continental material with it.

A.~480–470 Ma: subduction of Gula–Seve–Baltica(?) beneath pre-Llanvirn Köli Nappes (e.g., Støren); exhumation of subducted Gula–Seve–Baltica(?) & emplacement of Støren etc.

B. ~450–445 Ma: subduction of Seve beneath pre-Llanvirn Köli Nappes; exhumation of subducted Seve; burial & exhumation of Høyvik Group (Middle Allochthon)

C. 445–432 Ma: formation of marginal-basin ophiolites (e.g., Solund–Stavfjord) of Köli Nappes; rift magmatism in Köli Nappes; arc magmatism in Uppermost Allochthon

D. 435–415 Ma: continental collision; formation of Laurentian plateau(?); burial & exhumation of Köli, Lindås, & Seve Nappes & Vestranden

E. 415–400 Ma: continental subduction

Figure 14. the tectonic histroy according to hacker and gans 2005. (A) the trondheim event involving subduction of gula-seve-baltica beneath Köli nappes and subsequent exhumation and emplacement onto the baltoscandian margin. (B) the jämtlandian event involving the subduction of the seve nappes beneath kÓli nappes and subsequent exhumation. (C) Areally extensive magmatic period resulting in new oceanic crust and intrustions in the Köli nappes and upper allochton. (D) Scandian orogeny as a reaction to the collision of laurentia and baltica in which the former overthrusts the latter. (E) Subduction of baltica to uhp depths. (hacker & gans 2005).

4.1 Sample collection

Samples have been collected during the fieldwork in 2015 in Jämtland, Sweden. A geological map (fig 15) first made by Trouw (1973) and the Swedish Geological Survey (Zachrisson 1993, Zachrisson & Greiling 1993) is used to determine where the relevant peridotite bodies were. The latter has been made based on earlier work done by students of Leiden University in the 70's and 80's, under the supervision of Prof. H.J. Zwart. During this fieldwork a preliminary selection was made as to which localities of peridotite and country rock should be visited and subsequently sampled by the author (positions found in figure 15). The localities have been chosen in such a manner that a good balance between country rock (used for modelling P-T conditions) and peridotite (used for metamorphic growth phases) is represented in this thesis. Figure 15 shows the area in which the samples have been taken. All hand samples have been marked by pen so that the original position can be reconstructed.
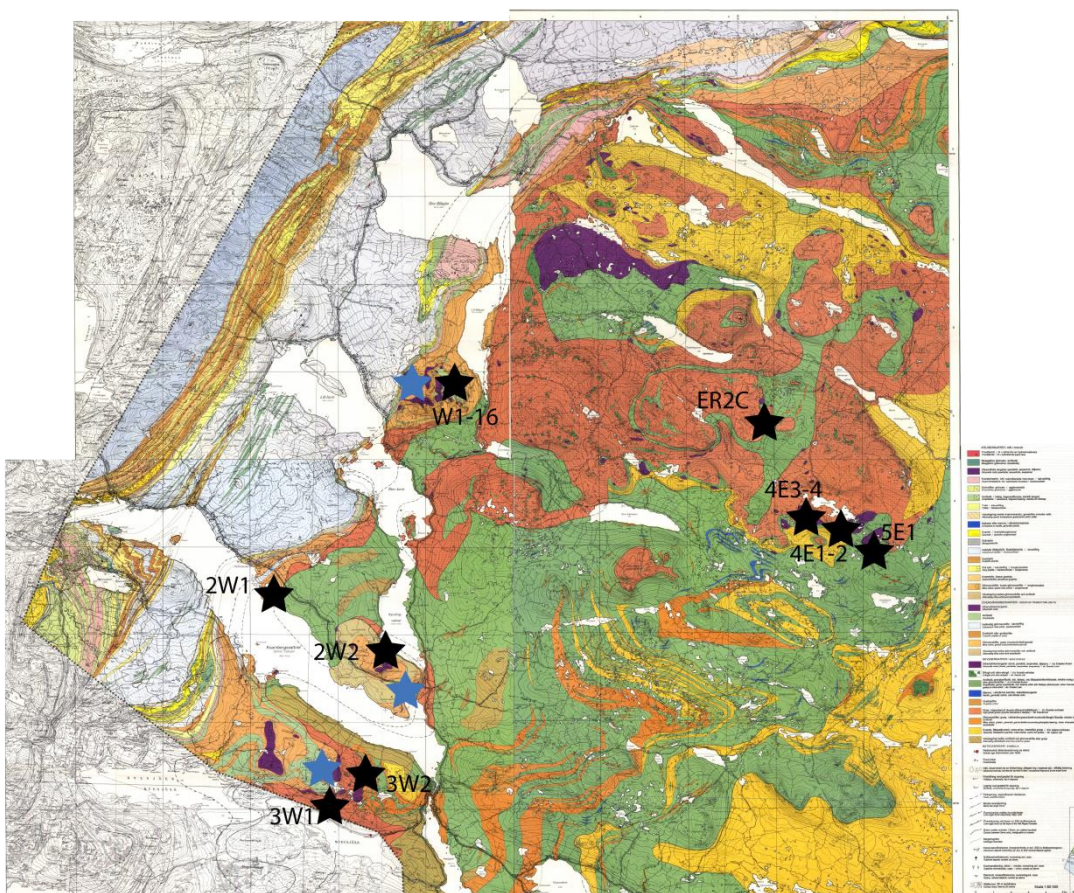
Figure 15. Geological map showing all sample locations taken for this thesis. The black stars show the sample locations of the peridotites together with the name of the sample location. The blue stars show sample locations of the country rock.

4.2 Sample preparation

From the hand samples a selection has been made as to which samples are to be cut to smaller blocks making it easier to produce thin sections from them. These thin sections (30μm thick) were subsequently marked in correspondence to the rock it has been made from. Multiple thin sections from the same rock were made in order to get the best overview of the rock possible. Thin sections were made perpendicular to the foliation. A selection

of the thin sections was further carbon-coated for further chemical analysis using Scanning Electron Microscope (SEM) and Electron Microprobe (EMP) techniques (Chapter 11.1).

4.3 Optical microscopy

The first structural and analysis was done using optical microscopy. From this work the mutual growth relationship between different minerals was established. Identification of minerals is based on their optical characteristics in plain polarized / cross polarized light. Using this data a further selection was made for carbon coating and chemical analysis. A LEICA-microscope has been used to make overview / more detailed pictures. Apart from these overview / more detailed pictures have been chosen to show the criteria for different growth relationships.

4.4 Scanning Electron Microscope (SEM)

Chemical analyses are done at the tabletop-SEM at Utrecht University and the joint environmental laboratory in Utrecht. Backscatter electron imaging is used to provide a view of the sample in the SEM. Electron-dispersive X-ray spectroscopy (EDX) is used to determine the chemical composition of minerals at chosen spots. EPX measurements performed on a table top SEM procedure produce semi-quantative result expressed as normalized chemical data. The chemical analyses are run under high-vacuum conditions using a 15 kV electron beam.

4.5 Electron microprobe (EMP)

Electron microprobe analyses are performed on the FEG-JEOL of the Utrecht University in the joint environmental laboratory in Utrecht. EMP measurements were done using an acceleration voltage of 15 kV, a beam current of 20 nA. The difference with the SEM is that the EMP produces quantitative data (1.5% accuracy), which makes it possible to discriminate between hydrous and anhydrous minerals.

4.6 X-Ray Fluorescence (XRF)

Samples (a total of 7) have been crushed and subsequently melted to produce XRF-pearls used for XRF-measurements. Measurements have been done at the Thermo ARL 9400 sequential XRF (±1.5% S.Ω.) at Utrecht University and the joint environmental laboratory in Utrecht. Results of the most representative samples can be found in section 5.3.

4.7 Numbering system

The numbering system is done as follows:

- *The first number of each sample represents the day of the fieldwork it was taken on.*
- *The first letter indictates whether it is taken from the Western or Eastern belt.*
- *The second number shows how many different outcrops were sampled during a day.*
- *The second letter shows if there are more than one samples used in this thesis.*

So for example 4e1a shows that the rock has been sampled on the fourth day, taken from the eastern belt, that it was the first outcrop to be sampled that day and that there is more than 1 sample analysed in this thesis.

There is one exception to this rule which is ER2C, this sample is taken form the Eastern belt and is collected by colleagues thus numbered different.

Perple_X

Perple_X is a collection of Fortran77 programs for calculating and displaying phase diagrams, phase equilibria and thermodynamic data. It uses specific bulk rock compositions as input data. The software uses Gibbs Free Energy minimization to compute psuedosections under the assumption of chemical equilibrium throughout a certain bulk rock volume.

5.0 Results

In the next section the structures and the different growth relations are described. This is done by looking at overprinting relations of minerals using their optical properties. For larger scale structures overview pictures (Appendix B) are used. From this a paragenetic diagram is produced which is later combined with the Perple_X psuedosections (chapter 6.3).

5.1 Structures

5.1.1 Upper Seve Nappe

Most samples taken from the Upper Seve Nappe at positions 2W1, 2W2, 3W1 and 3W2 (fig 17) do not show a clear foliation. However, some samples do show a foliation which consists of serpentine veins in between the larger olivine grains which show an elongation. Samples taken at positions W1-16 show a stronger foliation, but also expressed by serpentinization. In some Upper Seve Nappe samples chromite minerals show a foliation, although this is not clearly defined (Appendix w16).

5.1.2 Lower Seve Nappe

Samples taken from the Lower Seve Nappe (4E1, 4E3, 5E1-2) consistently show a clear foliation (Appendix 4e1) (nearly mylonitic) expressed by veins of olivine, orthopyroxene and serpentine (figure 20A&D) between larger M1 olivine grains. Some samples show open folding (Figure 20F, sample 4E3). Recrystallization structures in olivine are found in sample 4E1A (Appendix). Olivine grainsize has been measured which resulted in grains between 185 and 567 µm. Combining the grain size with a deformation mechanism map shows that the termperature and differential stresses operating in order to result in this are 700-785°C and 30-100 MPa, respectively.
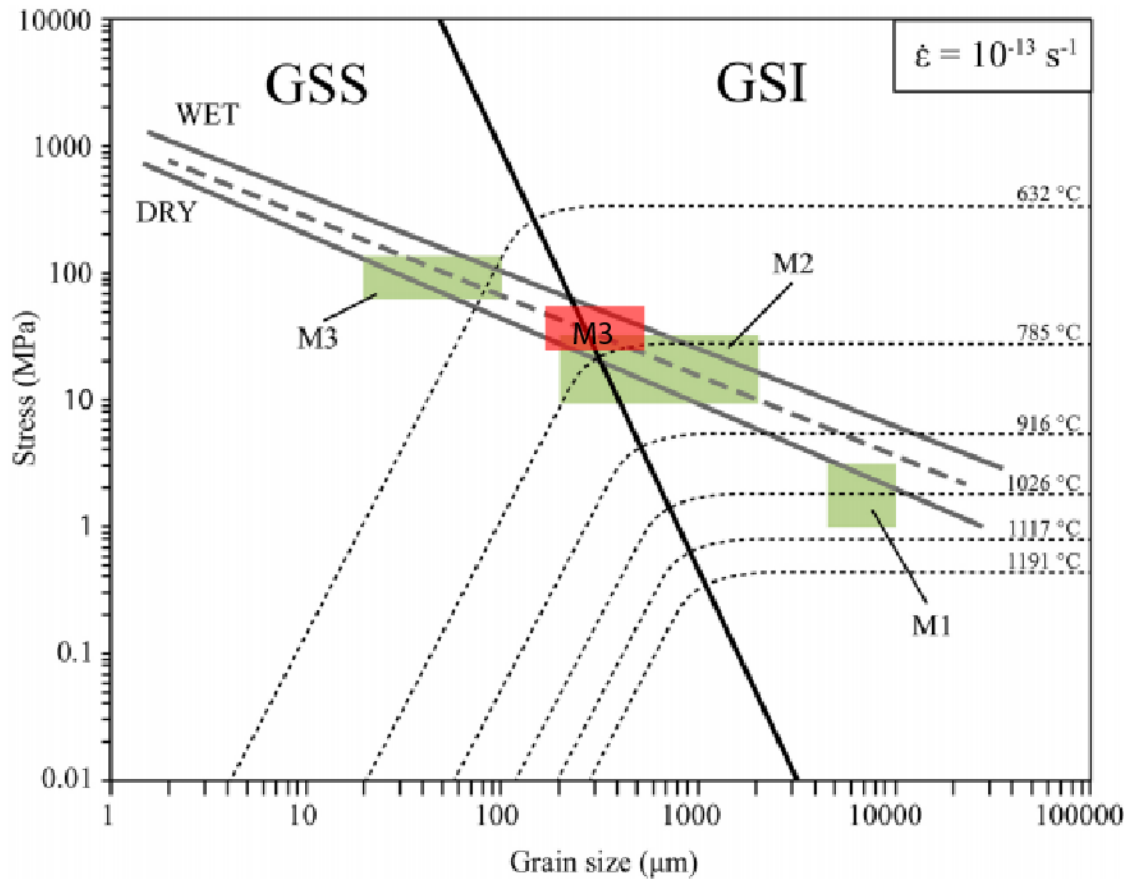
Figure 16. Deformation mechanism map for olivine at a constant strain rate (10^{-13} s^{-1}).Grey lines represent stress VS recrystallized grain size diagram for olivine. Solid grey lines being piezometers for "dry" (Van der Wal et al., 1993) and "wet" conditions (Jung & Karato, 2001). Green areas are interpreted conditions for the Frinningen Garnet Peridotite (Central Seve belt) of Gilio et al. (2015). The red area is the interpreted conditions for the M2 olivine of the Eastern Seve belt. (modified after Gilio et al., 2015)

5.2 Metamorphism

5.2.1 Upper Seve Nappe
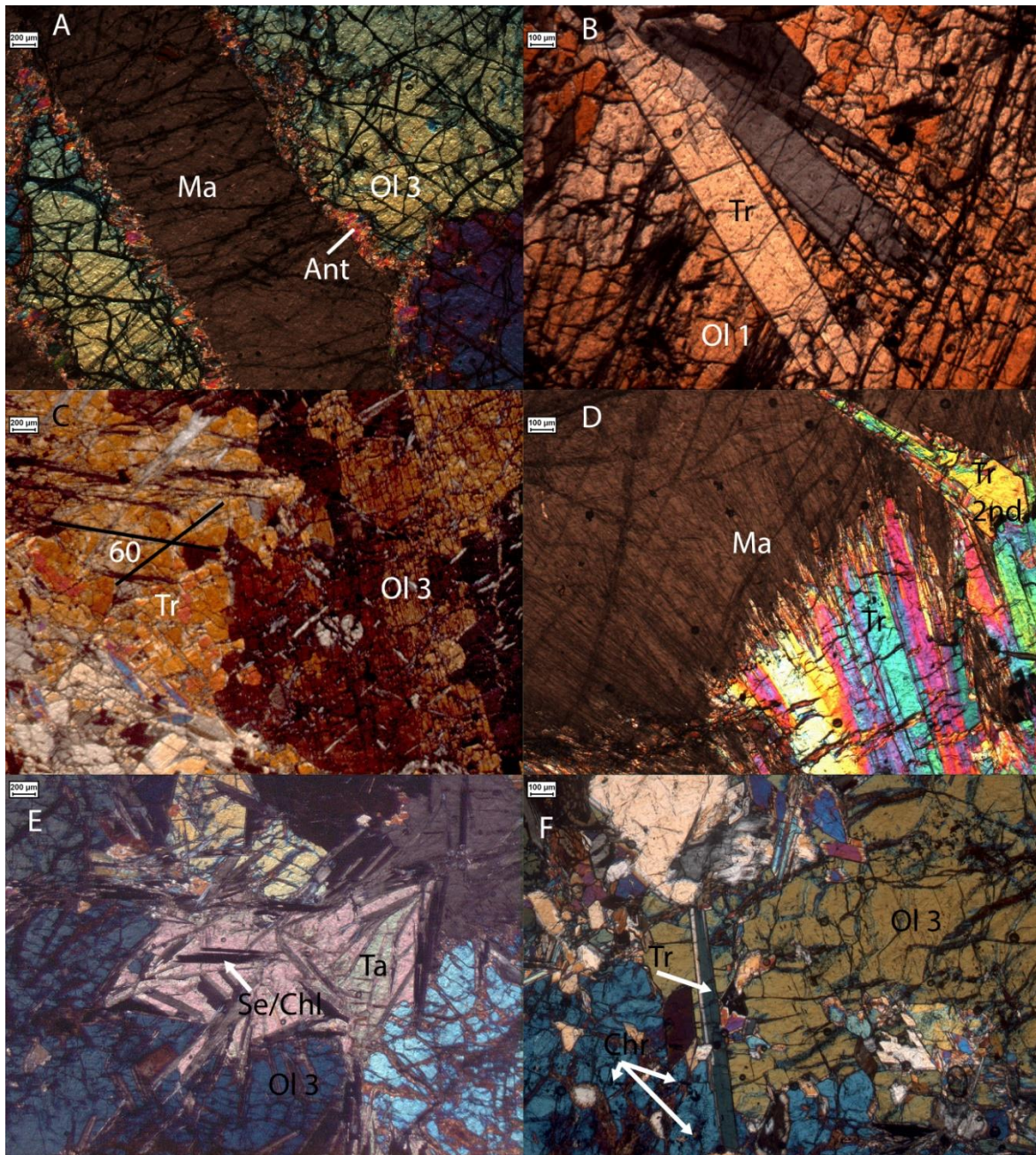
Figure 17. Optical microscopy figures showing relative growth time of different minerals in the Upper Seve belt. A) M4 Magnesite grows over a large (~1 cm) M3 olivine grain, the interface between the magnesite and olivine consists of anthophyllite, which is also present as very thin, elongated grains in the magnesite. B) M4 Tremolite grains growing over olivine grains (M3), the olivine grain shows signs of deformation (subgrain formation) in the upper right corner. C) Amphibole next to olivine grains (M3), the amphibole (interpreted as tremolite) grows slightly later than the olivine though the difference is small enough to be interpreted as M3 tremolite. d) magnesite growing together with tremolite M4, the top right corner shows a very late stage growth of tremolite growing over both the carbonate and M4 tremolite. this is interpreted as M5 tremolite .E) Talc minerals growing at the same time as the Olivine grains, thus these are M3 talc and olivine minerals. the black elongated minerals growing over the talc and olivine are serpentine and chlorite thus M5 mineral assemblage. f) tremolite mineral growing over a first generation olivine. in the left bottom corner a second order olivine grain contains chromite inclusions.

M1 (protolith)

The M1 mineral assemblage represents the protolith of the Upper Seve Nappe peridotites and consists of olivine and chromite (figure 17B). The M1 olivine grains are on the mm- to (very rarely) cm-scale, highly fractured and frequently overgrown by serpentine. The chromite crystals range from a few µm- to a few mm and show a well-rounded shape (figure 17F).

M2 (retrograde metamorphism)

The M2 mineral assemblage consists of serpentine (antigorite) and magnetite. The magnetite crystals are most often found directly next to serpentine veins or in contact with serpentine. They range from mm- to cm-scale and are often well-rounded. The deformation phase D1is best expressed in the serpentine grains which make up the foliation in most of the samples. Furthermore magnetite grains have oriented themselves in thin bands throughout the sample.

M3 (peak metamorphism)

The D2 is characterized by the second growth of olivine, together with the growth of talc and tremolite (fig 17B&C). These renewed grains are much larger than the M1 olivines, as such they can grow up to several centimeters. M2 olivines can be distinguished from the M1 olivine on the basis that the second generation is slightly less fractured and contain many small inclusions, which turn out to be magnetite (M2). This mineral assemblage (Ol-Tr-Tlc) represents the peak metamorphic conditions (estimated to be 600C°, 0.5-0.8 GPA. Chapter 6.3.1).

M4 (retrograde metamorphism)

The M4 assemblage consists of serpentine, magnesite, chlorite tremolite and talc (fig 17A&D). The M4 serpentine form in most samples thin lines breaking up larger olivine clasts, in some samples it forms large (several mm's thick) veins of massive antigorite. The carbonate consists of magnesite and calcite cutting M3 olivine grains.
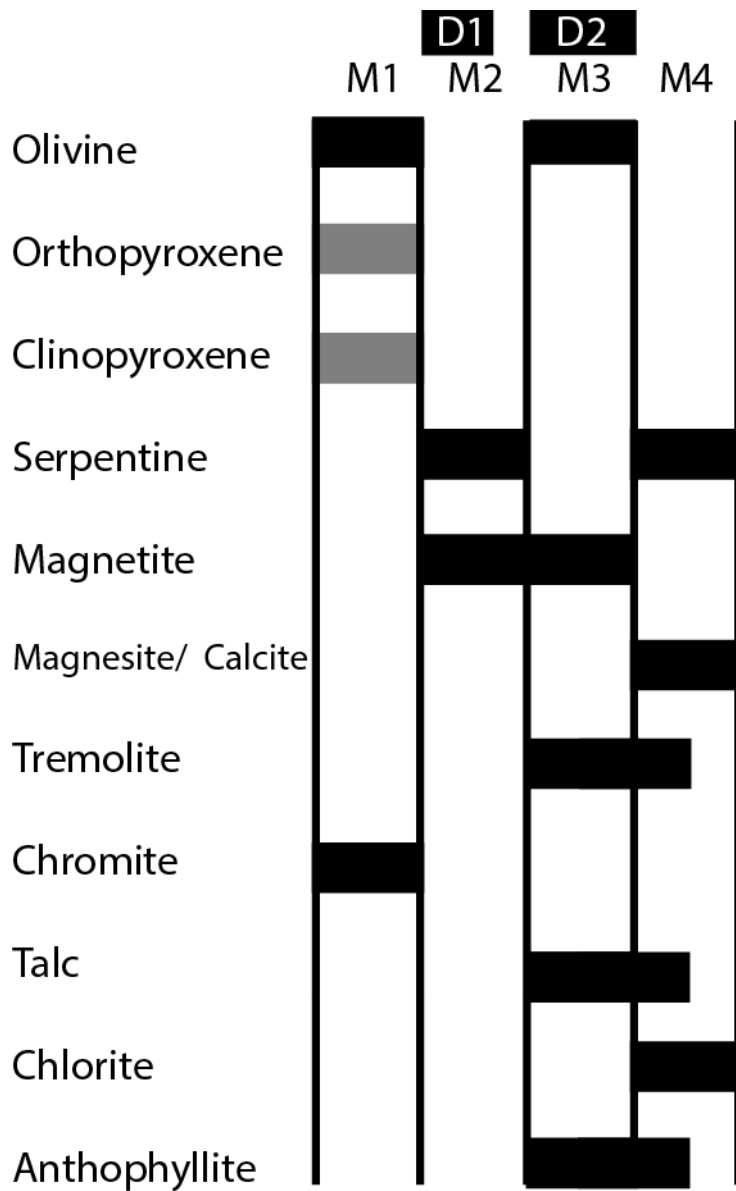
Figure 18. Paragenetic diagram for the orogenic peridotites of the Upper Seve Nappe. The grey bars are thought to be part of the protolith assemblage based on previous work on orthopyroxene and clinopyroxene. (Calon, 1979).
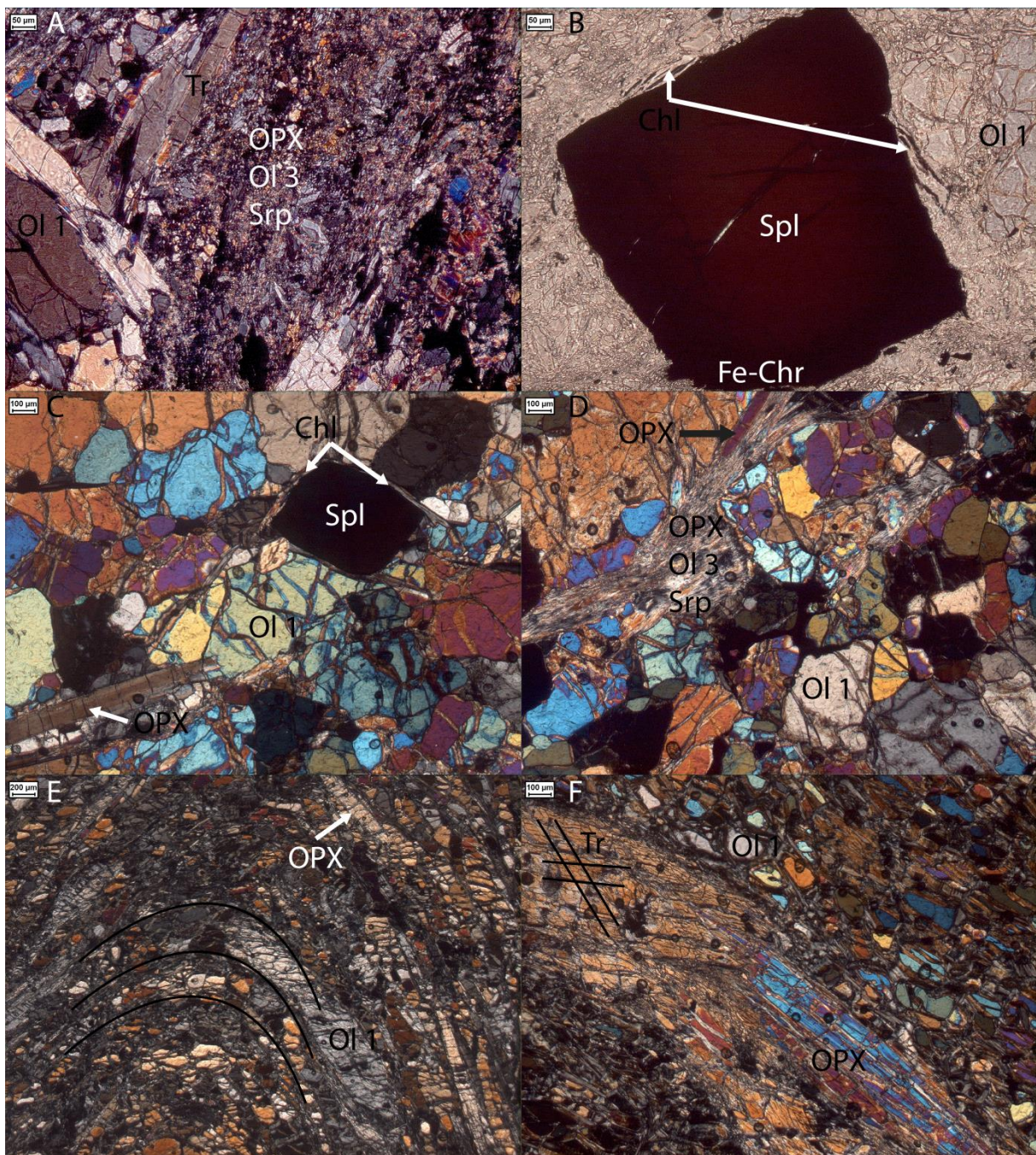
Figure 19. Optical microscopy photo's showing relative growth of the different minerals in peridotites of the lower seve nappe. A) primary olivine being cut by a mylonitic band of M3 orthopyroxene, olivine and serpentine. b) medium-high al-chromite with a darker rim consisting of high Fe-chromite. the chromite is surrounded by a small rim of chlorite. c) large orthopyroxene growing together with M1 olivine. Note the small rim around the chromite consisting of chlorite. D) mylonitic band cutting M1 olivine and surrounding a large orthopyroxene grain. E) Folded harzburgite showing the fold hinge. f) large M1 orthopyroxene grain being slowly replaced by tremolite. Above these minerals small recrystallized M3 olivine grains are shown.

M1 (Protolith)

The M1 assemblage of harzburgites and dunites of the Lower Seve Nappe peridotites consists of olivine, orthopyroxene and chromite/spinel. The protolithic olivine grains are fairly uncommon in the samples as most of them have been dynamically recrystallized at peak metamorphic conditions (M3, figure 19C); the protolithic grains still visible are mm- to cm-scale and show intense fracturing. The M1 orthopyroxene is also rare in the M1 samples as most of them have been reworked to tremolite, which has a size of several mm's in length, in a later metamorphic event. The chromite crystals are equidimensional and show a rim of ferro-chromite suggesting a later overgrowth phase (M2).

M2 (Retrograde metamorphism)

The M2 assemblage is characterized by serpentine growing together with magnetite and chlorite (although very little magnetite is found). Also during the growth of serpentine, magnetite and chlorite a rim of ferro-chromite formed around the protolithic chromites. The serpentines grow primarily in small localized shear bands, which is where the small (μm-scale) magnetites can also be found.

M3 (peak metamorphism)

The M3 metamorphic assemblage is characterized by the dynamic recrystallization of olivine and the growth of metamorphic orthopyroxene. The orthopyroxene crystals are small (μm) and are found in the previously mentioned shear bands. The olivine crystals range from several μm's to mm's, they are fractured and show many different orientations due to the recrystallization process.

M4 (Retrograde metamorphism)

The M4 is characterized as the latest growth stage of serpentine together with chlorite (fig 19B&C). Some lesser amounts of tremolite and talc have been found which probably grew for a short time between M3 and M4. However, for the formation of talc water is required; thus water must have been introduced in the system around this time.
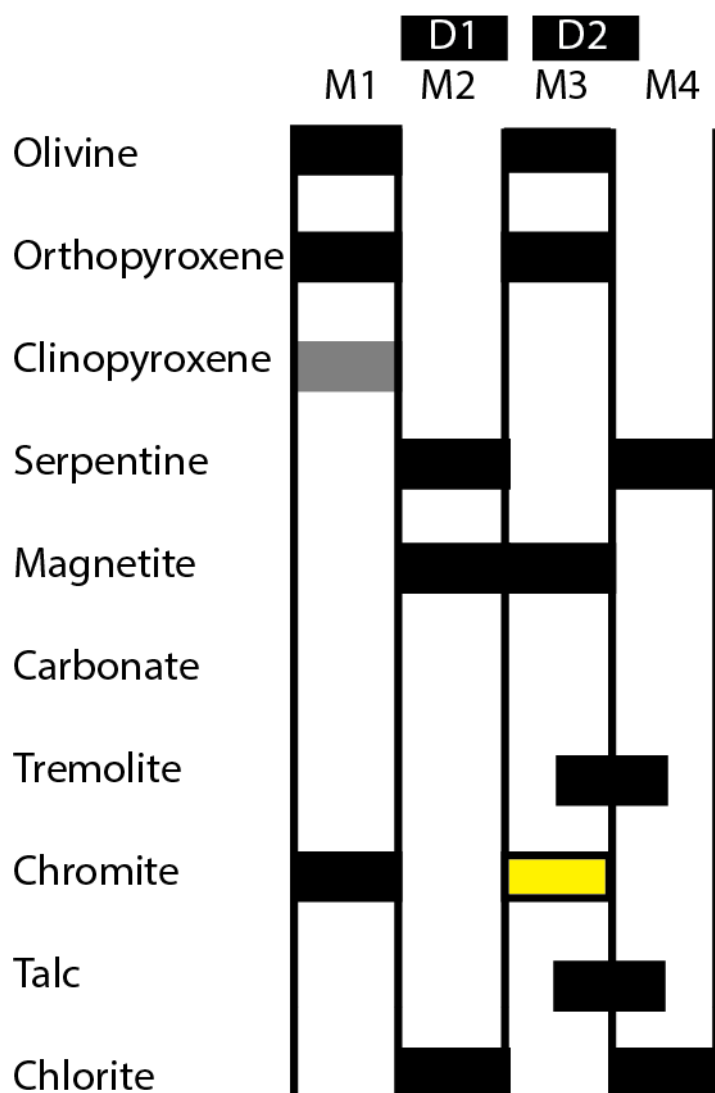
Figure 20. paragenetic diagram applicable to the Lower Seve nappe peridotite. the yellow block represents the growth of ferro-chromite as a ring around M1 chromite (fig 19 C), the grey block is thought to be part of the protolithic assemblage in less depleted peridotites.

5.2.3 Country rock
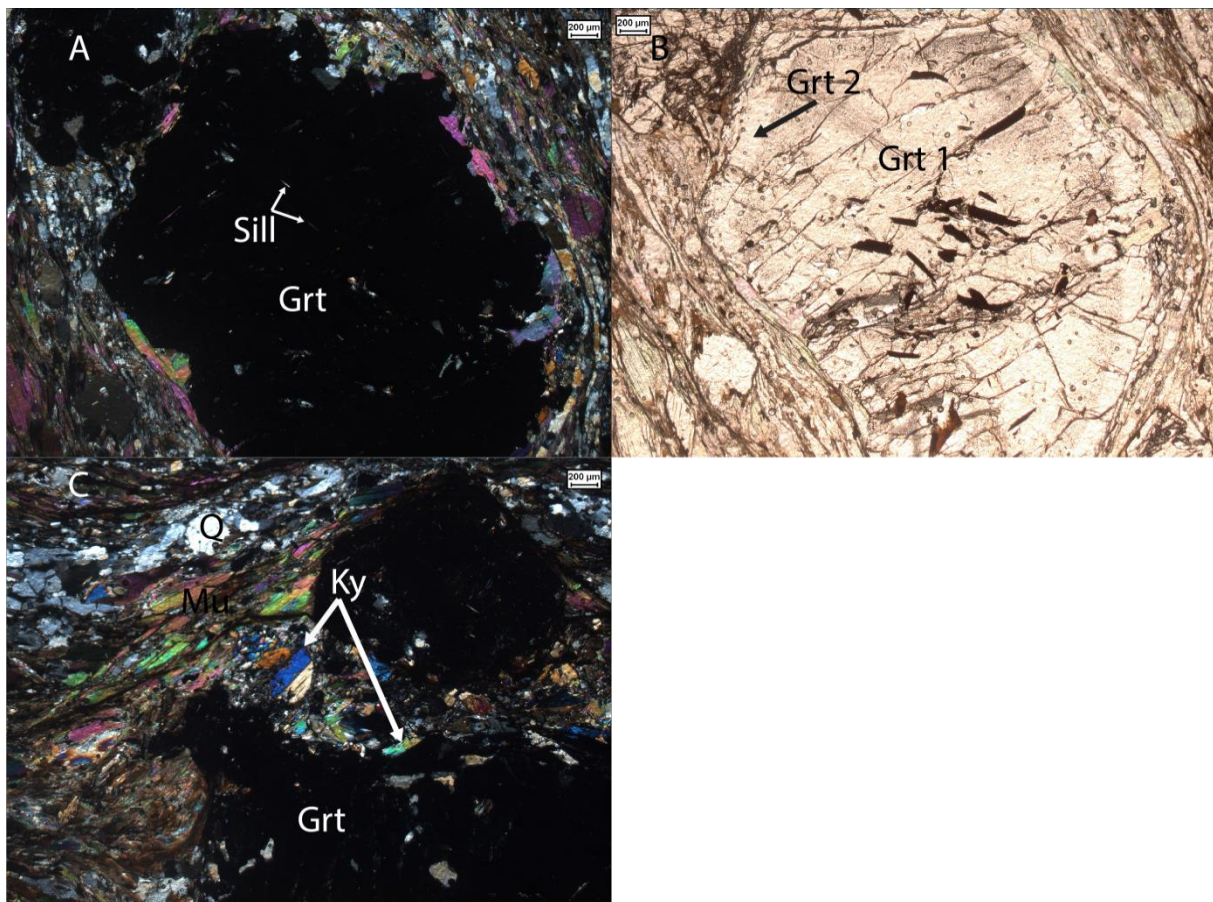
Figure 21. photo's showing relative growth relationship between different minerals in the country rock (sample 2C1B). A) sillimanite grains in a garnet core; the garnet is surrounded by quartz and mica. b) Same spot as A but now in plane polarized light showing (at least) 2 stages of garnet growth, i.e. the outer rim is lighter than the core. c) Kyanite grains replacing sillimanite. This also clearly shows late muscovite growing around the garnet.

M1

The M1 assemblage is characterized by muscovite, biotite, quartz and albite. Although muscovite, biotite and quartz are stable throughout the entire PT-path the discrimination between the different generations is somewhat hard and vague. Inclusions in other minerals, such as garnet, and the foliation curving around garnet give a fair idea of the different generations. Biotite and muscovite, which are the most abundant minerals in the M1 assemblage, are several mm's large. Quartz minerals are dynamically recrystallized to mm-scale. Rutile is solely found as inclusions in garnet minerals and is elongated with an elongation of 5:1. Sillimanite are hard to find as they are very small (<mm's).

M2

The M2 assemblage consists of quartz, garnet, biotite, rutile, sillimanite and anorthite. Most of these minerals have been overprinted by later stages making it hard to distinguish between the different metamorphic assemblages. The rutile and sillimanite are found as inclusions in garnet cores and in lesser amounts in the rim of garnets.

M3

The M3 assemblage consists of garnet, biotite, muscovite, quartz, kyanite and plagioclase. The garnet core contains mainly CaO and MnO, 5.59% and 11.15% respectively. The rim of the garnet contains more FeO and MgO at the expense of CaO and MnO. The CaO and MnO values decrease to 2.23% and 1.82% where the FeO and MgO values increase from 25.39% to 33.76% and 0.80% to 4.01% respectively. Kyanite is found growing at the rim of garnet and growing over earlier foliations.

M4

The M4 is a retrograde metamorphic phase going back to the starting composition; while between M3 and M4 the latest foliation formed curving around the M3 garnets. As M1, M4 consists of quartz, muscovite and albite.
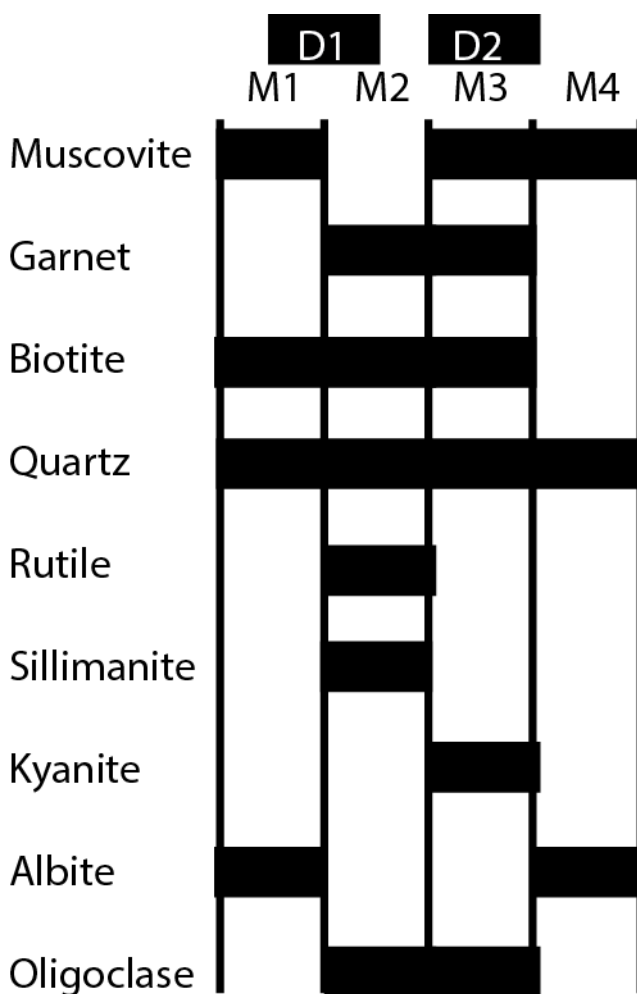
Figure 22. Paragenetic diagram for the country rock of the upper Seve nappe (2C1 & 2C2).

5.3 Chemical data

5.3.1 Country rock

XRF data for the country rock (sample 2C1, sillimanite bearing gneiss from the Upper Seve Nappe) is shown in the table below. The total amount of mass is 86.52%. These results will later be used for modelling PT-conditions using Perple_X (figure 42).

Component	Wt%
Al	18.97
Ca	1.57
Cr	0.01
Fe	6.99
K	4.85
Mg	2.22
Mn	0.13
Na	1.75
Si	61.84
Ti	0.84

Main elements

Component	Wt%	Component	Wt%
Ag	0.0020	Sr	0.0183
Au	0.0017	Nb	0.0037
Ba	0.0981	Ni	0.0021
Ce	0.0029	Pb	0.0016
Co	0.0313	Rb	0.0193
Er	0.0094	S	0.0634
Ga	0.0034	V	0.0181
Gd	0.0030	W	0.2413
Hg	0.0039	Y	0.0039
I	0.0015	Zn	0.0127
La	0.0025	Zr	0.0424

Trace elements

5.3.2 Upper Seve Nappe

XRF-data has been taken from sample 3W2 is shown in the table below. The total amount of mass is 99.63%. These results will later be used in Perple_X modelling.

Component	Wt%
Al	0.73
Ca	3.31
Cr	0.53
Fe	9.53
K	0.03
Mg	39.51
Mn	0.14
Na	0.00
Si	45.47
Ti	0.01

Main elements

Component	Wt%
Ba	0.07
Ni	0.27

P	*0.02*
Sr	*0.00*
Zr	*0.00*

Trace elements

Nearly all samples taken of peridotites have olivine with a Mg# of 91-93 except samples taken at location W1-16 which show a Mg# of 94 (inclusions in spinel) to 97. Measurements taken from spinel/magnetite grains show a major depletion in Al, having most of the time no Al in them at all which suggests that these are metamorphic spinels as primary chromites are expected to contain Al. The majority of the spinel minerals show a roughly 50-50 composition of Cr^{3+} and Fe^{3+} with a slight tendency towards the Fe^{3+} (fig 24). The average Cr# is 0.25 taken from 37 measurements.

5.3.3 Lower Seve Nappe

XRF-data taken from sample 4e1 is shown in the table below. The total amount of mass is 99.75%. These results will later be used in Perple_X modelling.

Component	Wt#
Al	*0.34*
Ca	*0.13*
Cr	*0.43*
Fe	*9.30*
K	*0.00*
Mg	*43.28*
Mn	*0.15*
Na	*0.00*
Si	*45.71*
Ti	*0.01*

Main elements

Component	Wt%
Ba	*0.08*
Ni	*0.30*
P	*0.02*
Sr	*0.00*
Zr	*0.00*

Trace elements

The Lower Seve Nappe shows a Mg# of 91-92 consistent in all sample locations, the average value is 91.63 calculated of 92 measurements. As in the Upper Seve Nappe, the chromite grains show a depletion of Al, although the grade of depletion is less suggesting more primary M1 chromites are still observable compared to the Upper Seve Nappe. The average Cr# is 54 calculated from 45 measurements.

5.4 Chemical compositions of peridotite minerals

5.4.1 Olivine

The olivines present in peridotites of the lower and upper belt of the Seve Nappe Complex show two different phases of growth. M1, which are the protolith olivines and M3, which represent the peak metamorphism condition. Both types of olivine are forsteritic in composition. The western belt olivines show an average Mg# of 91-93 except for the 1W1-16 samples, which have a mg# of 95-99.Where the eastern belt olivines show a similar Mg# of 91-92 (fig 23). Between the two different structures (primary and dynamically recrystallized) of olivine in the Eastern belt no difference in Mg# is found, this distinction is therefore solely based on structure. When plotting the Mg# against the NiO wt% there is not a large difference between the eastern and western belt. The only difference is that the eastern belt has on average more NiO wt%, the difference being in the order of 0.1 wt% (fig 23). The average NiO wt% of the eastern belt is 0.30 where the western is lower with 0.23. The NiO wt% in the eastern belt shows no difference regardless of olivine structure.
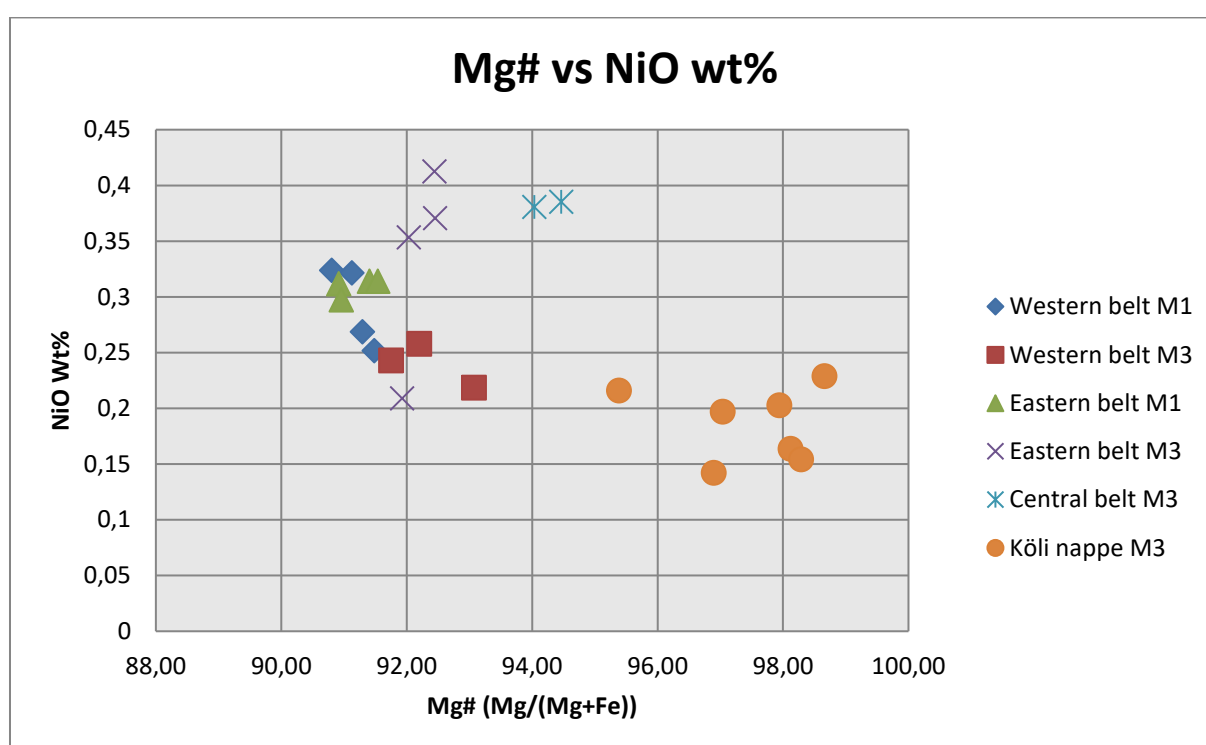
Figure 23. Mg# vs NiO wt% in olivine of peridotites in the Köli nappe, Seve Eastern, Central and Western belt in which a distinction is made between M1 and M3 olivine minerals. Data based on EMP measurements (appendix).

5.4.2 Spinel

There are two different types of spinel in this thesis: M1 spinel (chromite) and M2 spinel (magnetite) which got altered during serpentinization. M1 spinel is in general large (up to 1 cm) and solitary compared to M2 spinel which is clustered in bands and much smaller (0.5 cm at the most). The structural formula of spinel is a solid solution between Al^{3+}, Fe^{3+} and Cr^{3+} in the B-position of the crystal lattice and Fe^{2+} and Mg^{2+} in the A-position.

The main difference in spinel composition between the eastern and western belt is a much higher Fe^{3+} component in the western belt and the presence of chromites in Eastern belt samples (figure 24). All measurements were, however, taken in the core of the spinels as these are less prone to secondary alteration processes. Measurements have shown that the closer one gets to the rim, the higher the Fe^{3+} content becomes. This is consistent throughout all samples, this reworking of spinel can be explained by serpentinization. Another result of serpentinization is formation of chlorite around the edges of spinel (fig 19B). Spinels which contain a high amount of aluminum are

part of the protolith, while spinels with a lower aluminum content are altered by secondary processes. Looking at the western belt no primary/M1 spinel can be found (fig 24B&D). All measurements, whether it is a core or rim analysis, plot in the magnetite field.

The Cr#* (Cr/(Cr+Al+Fe^{3+})) of the Eastern belt spinels vary between 0.51-0.75 and the Mg# (Mg/(Mg+Fe^{2+})) between 0.08-0.54 (figure 26). Comparing this to the Western belt shows that Cr#*'s are higher in the Eastern belt as the Western belt Cr#*'s are between 0-0.4 where the Mg#'s are lower, between 0.04-0.06. The second type of spinel recognized in this thesis consists solely of magnetite($Fe^{2+}Fe^{3+}_2O_4$), with a Fe^{3+}# > 0.60. This end-member is formed as a result of serpentinization and therefore does not represent the M1 assemblage.

Arguments for what kind of protolith Western and Eastern belt samples have can be found in the Al^{3+} content. Al can only be found if there are minerals which can incorporate it in their crystal structure, as dunite consists of >90% olivine there is little to no room for Al. Thus if a BRC shows a low Al-content a dunite is most probable the protolith. Harzburgite, a less depleted mantle rock can contain Al, though in low amounts. Al in harzburgites is incorporated in Al-silicates such as spinel, and minor amounts in clinopyroxene. A high Al component suggests a lherzolite as protolith where Al-silicates and clinopyroxenes are more abundant. Therefore, the protolith of the Eastern Seve belt is probably a harzburgite, whereas no M1 spinels are found in the Western belt no indication can be given to what the protolith can be. However, chlorites can also give an indication to the protolith. If chlorite was formed next to magnetite it is very well possible that the Al in the chlorite came from the magnetite which previously was spinel. In the Western belt chlorite is found growing randomly over previous mineral assemblages which can suggest that the Al required to form chlorite came through infiltration/percolation of water which, in turn, can be an argument that the protolith did not contain enough Al to form chlorite thus having a dunite protolith (figure 17E).
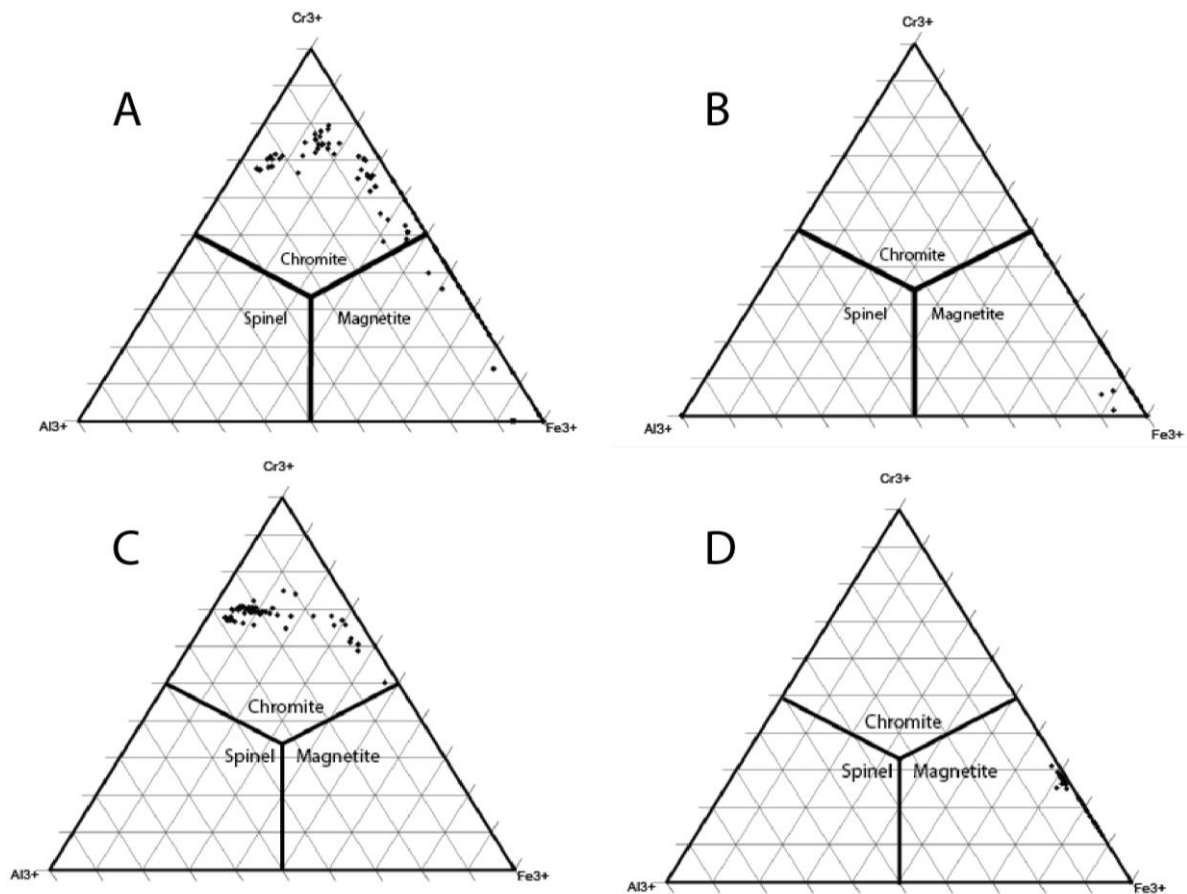
Figure 24. Triangular diagrams showing the composition of all measurements done on spinel. A) SEM measurements of the lower Seve nappe. b) SEM measurements of the upper Seve nappe. c) microprobe measurements of the lower Seve nappe. d) microprobe measurements of the upper Seve nappe.

If a 3D section is considered (fig. 25B) a second discrimination can be made apart from the difference in elements placed in the B-position in the spinel group. The second discrimination made is which element is placed in the A-position, Fe^{2+} or Mg. A clear trend can be found in figure 25A, the points calculated from Gilio et al. (2015) plot in the spinel area (Central belt), whereas samples, taken during this thesis, from the Western and Eastern belt both show a lower Mg# and higher Fe^{3+} content. However, serpentinization causes spinel to first transform to chromite and subsequently to magnetite.
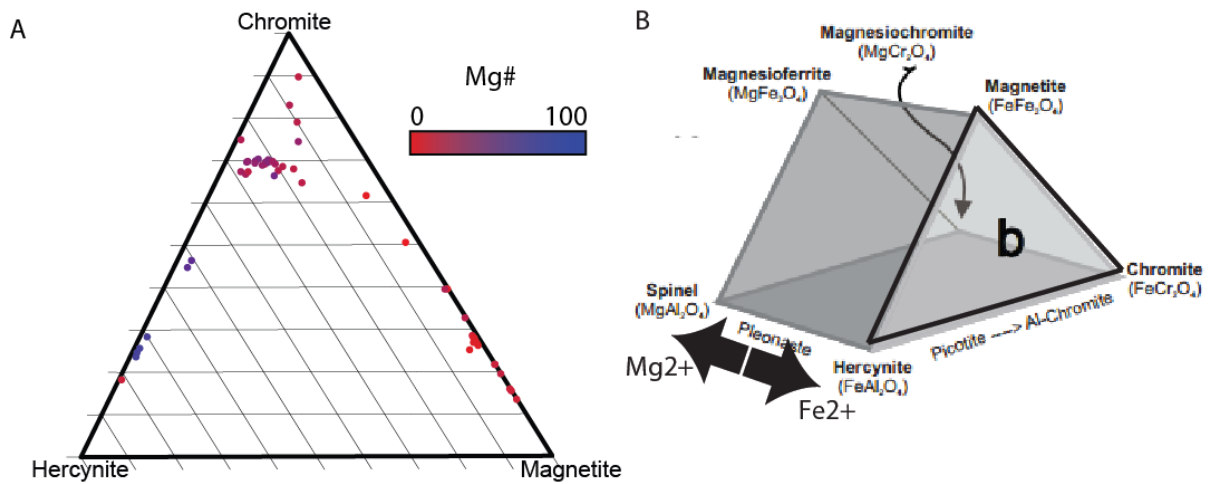
Figure 25. A) Triangular diagram showing the composition of measurements (both for this thesis and other research (Gilio et al. (2015) and Clos et al. (2014)) done on spinel. B) The thick lines represent the triangle shown in A, a higher Mg# results in points' positions to be further towards the back of the 3D-diagram.

Figure 26 shows the retrograde reaction of spinel to chromite to magnetite as the Cr#* first increases as a result of losing Al^{3+} to chlorite or other minerals and subsequently Cr^{3+} removes from the system making place for Fe^{3+} while at the same time decreasing the Mg# and increasing the Fe^{2+} content for the entirety of the reaction. The Mg released during this reaction is incorporated in serpentine (mainly antigorite) (chapter 6.1).

A closer look to figures 26 to 29 shows two distinct reactions; A high T reaction, consisting of the replacement of Al^{3+} by Cr^{3+} in the B-position and a low T reaction consisting of 2 parts, the first being the replacement of Cr^{3+} by Fe^{3+} and the second the replacement of Mg^{2+} by Fe^{2+}. Comparing figure 27 and 28 shows the high-T reaction, during this reaction Al^{3+} is removed from the system with decreasing Mg#'s (figure 27) while at the same time the Cr^{3+}# increases with increasing Fe^{2+}# (figure 28). This comparison quantifies the reaction.
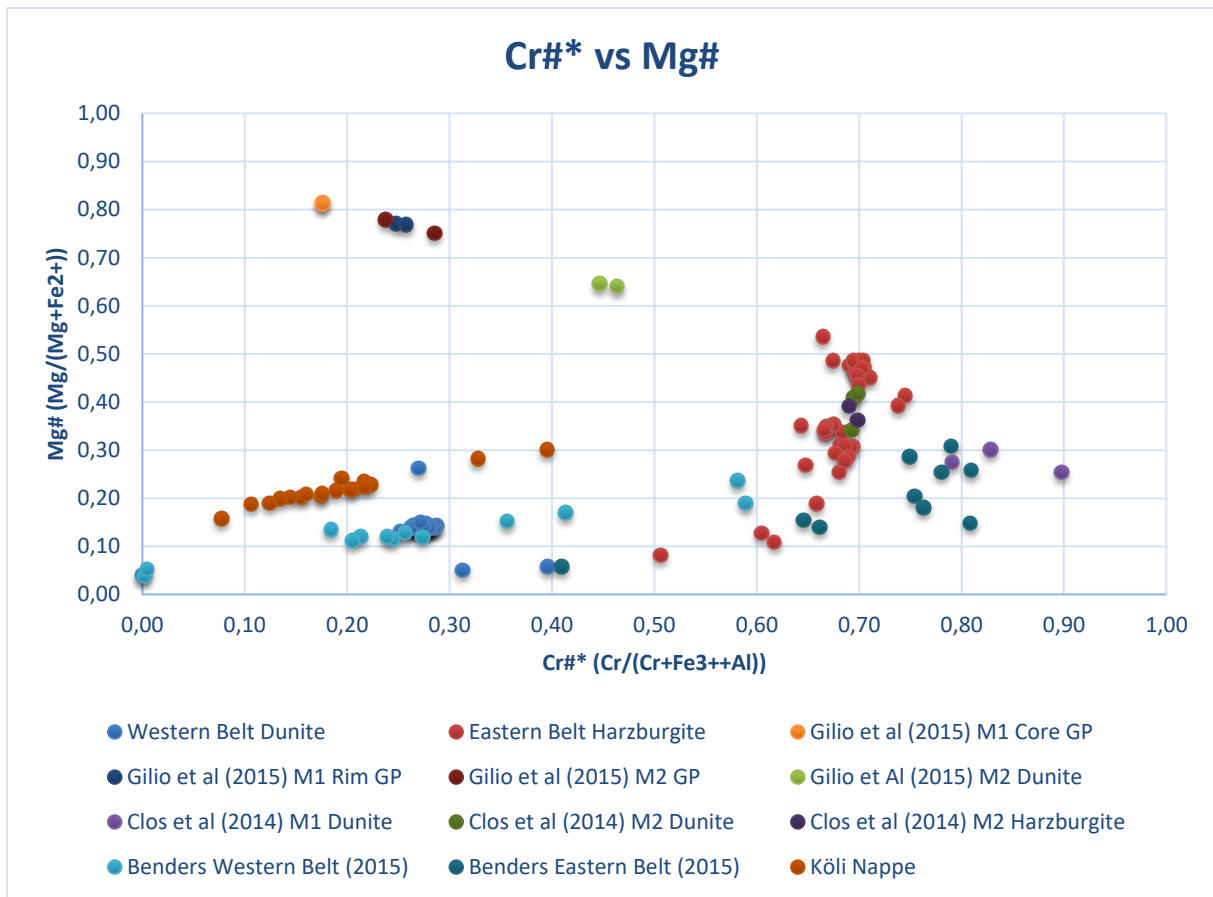
Figure 26. Spinel classification diagram. this classification is based on the elemental components present in the a-position (Mg^{2+}, Fe^{2+}) vs b-position (Cr^{3+}, Al^{3+} and Fe^{3+}) in spinel. data from spinels taken from the eastern and western belt follow a linear trend (or line) when the results are compared to other researchers working on spinels from the central belt. This line represents the metamorphic trend for spinel. The curve towards the left bottom corner represents serpentinization.
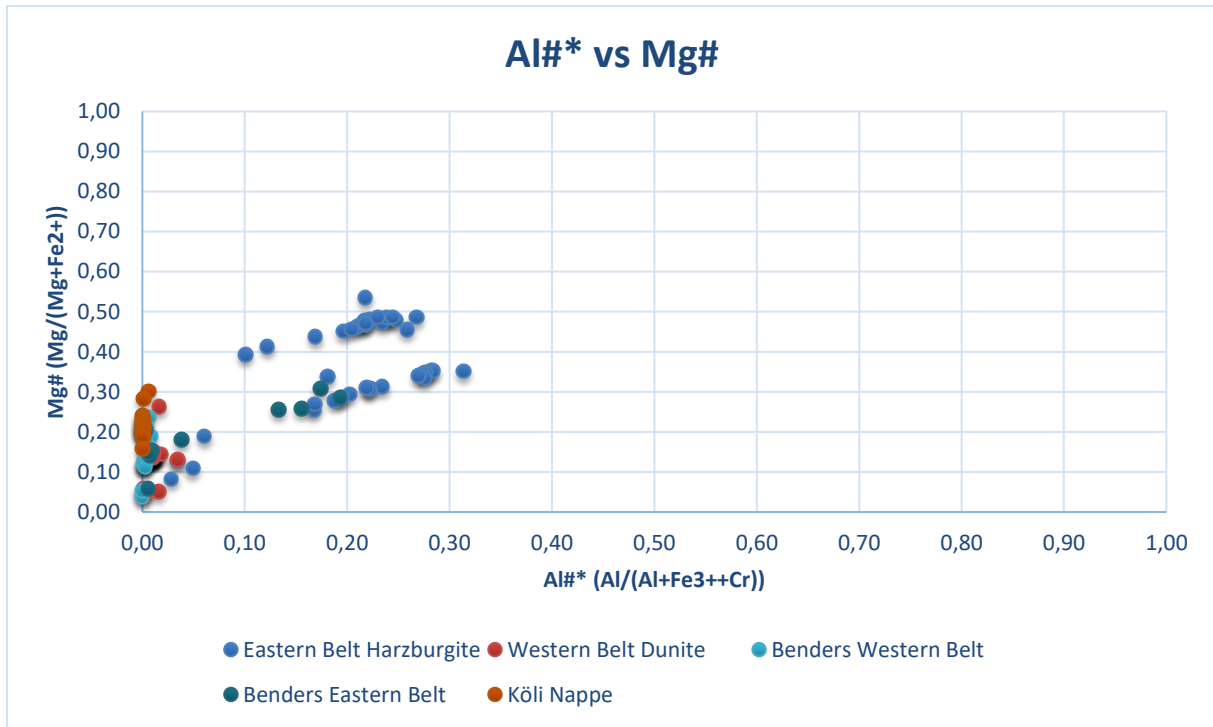
Figure 27. Spinel classification diagram illustrating the Al# vs Mg# in spinel.
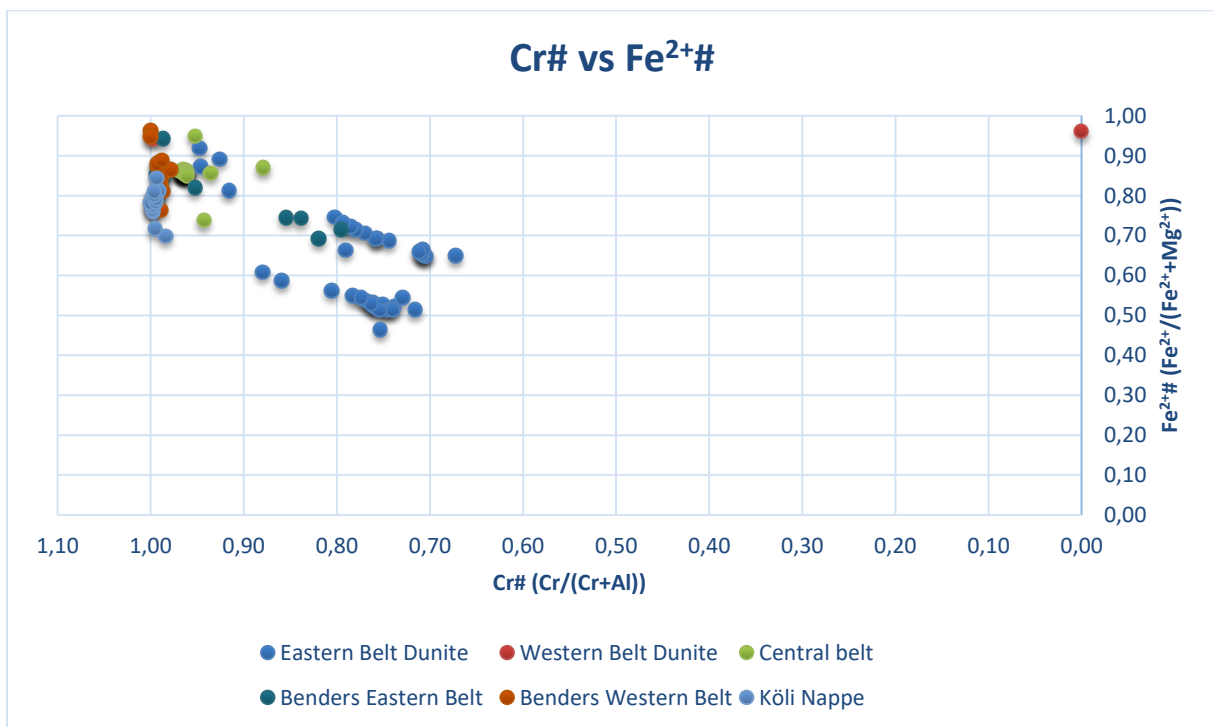
Figure 28. Spinel classification diagraqm illustrating the Cr# vs Fe^{2+}# in spinel.

Figure 29 shows what happens in the A- and B-positions of the spinel crystal structure during retrograde metamorphism. The y-axis shows what happens in the B position, the x-axis that of the A position. With decreasing metamorphism Fe^{3+} replaces first Al^{3+} and subsequently Cr^{3+}, in the A position Fe^{2+} replaces Mg^{2+}.
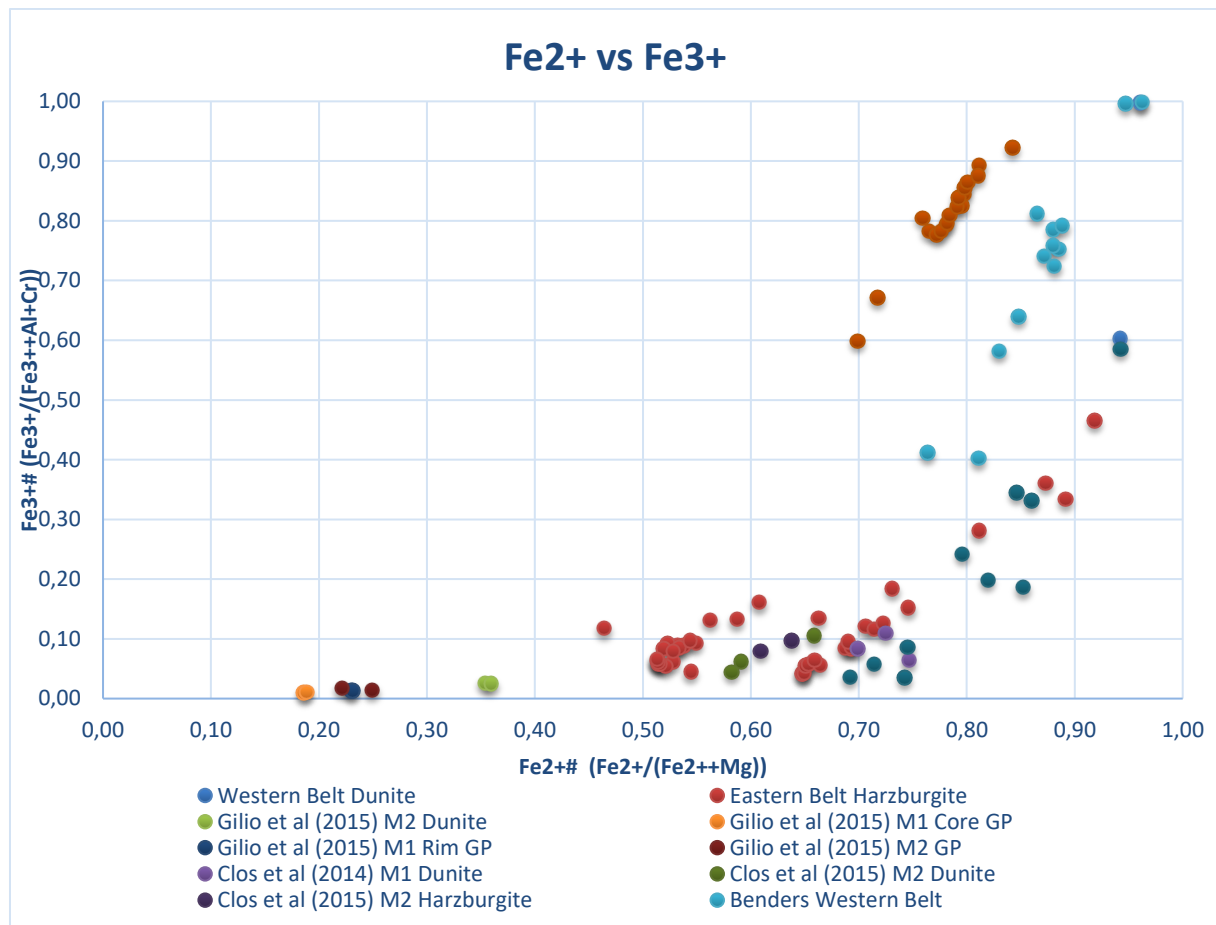
Figure 29. Ferric vs ferrous iron in spinel in peridotites of the Köli Nappe, Western, Central and Eastern Seve belt. A higher amount of Fe^{3+} means higher oxidation which might give an indication to the amount of serpentinization.

5.5 Other minerals

5.5.1 Amphiboles

Amphiboles found in the eastern and western belt both show a high Ca and Mg wt% of 11.9-12.5% and 21.1-24.5% respectively. Based on the nomenclature of Hawthorne et al. (2012) the upper belt amphiboles are tremolites and edenites (fig 31). Some of the M3 amphiboles in the Eastern Seve belt are anthophyllites (fig 30) which probably represent retrograde orthopyroxenes, the other amphiboles in the Eastern belt are tremolites. As very little to no clinopyroxene was present in the protolith of the Western nor the Eastern belt the introduction of Ca has probably come, partly from fluid infiltration/percolation during subduction and partly from hydrating clinopyroxenes forming Ca-rich amphiboles where the latter is mainly the case for the Eastern belt. Amphiboles taken from other research (Clos et al., 2014, Benders, 2015 and Gilio et al., 2015) show no occurrence of Mg-Fe-Mn amphiboles, Ca-amphiboles found in those researches show similar results compared to this thesis. There is one exception which is the occurrence of pargasite in Gilio et al. (2015). This is a Na-rich amphibole where the Na is probably derived from surrounding clinopyroxenes. The P-T conditions calculated for this metamorphic assemblage are 3.1 GPa and 825°C, Na-rich amphiboles are found to grow under high pressure in a water-undersaturated environment (Koons, 1982). Increasing the water content shifts the stability field of Na-rich

amphiboles resulting in Na-rich micas instead. Therefore the pargasite found in Gilio et al. (2015) must have grown in water-undersaturated conditions.
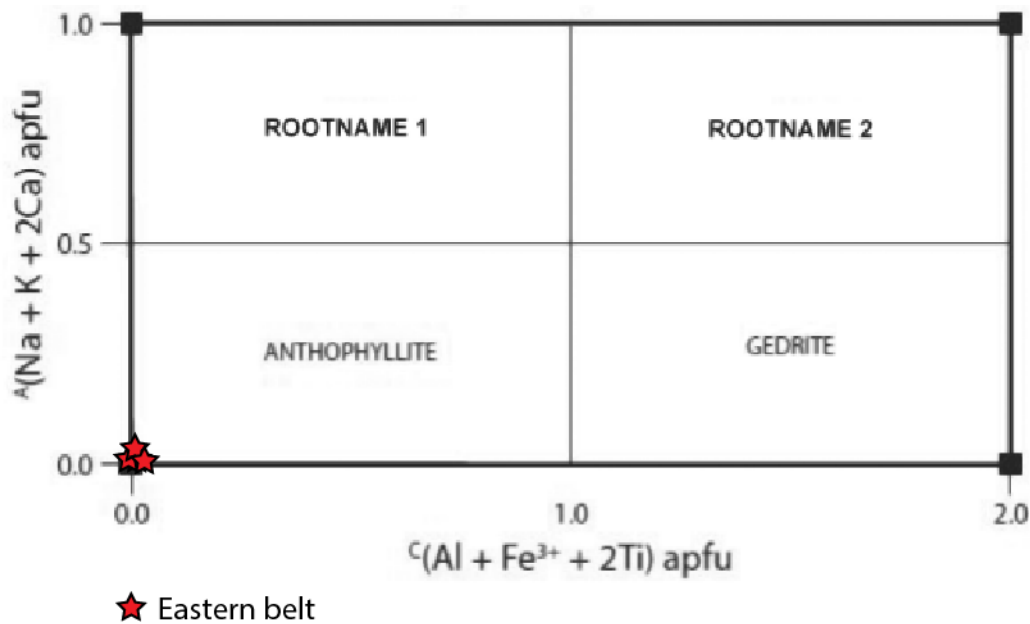
Figure 30. Classification diagram of Mg-Fe-Mn amphiboles after the latest nomenclature (Hawthorne et al., 2012). Mg-rich amphiboles found in the Eastern belt are found to be anthophyllites.
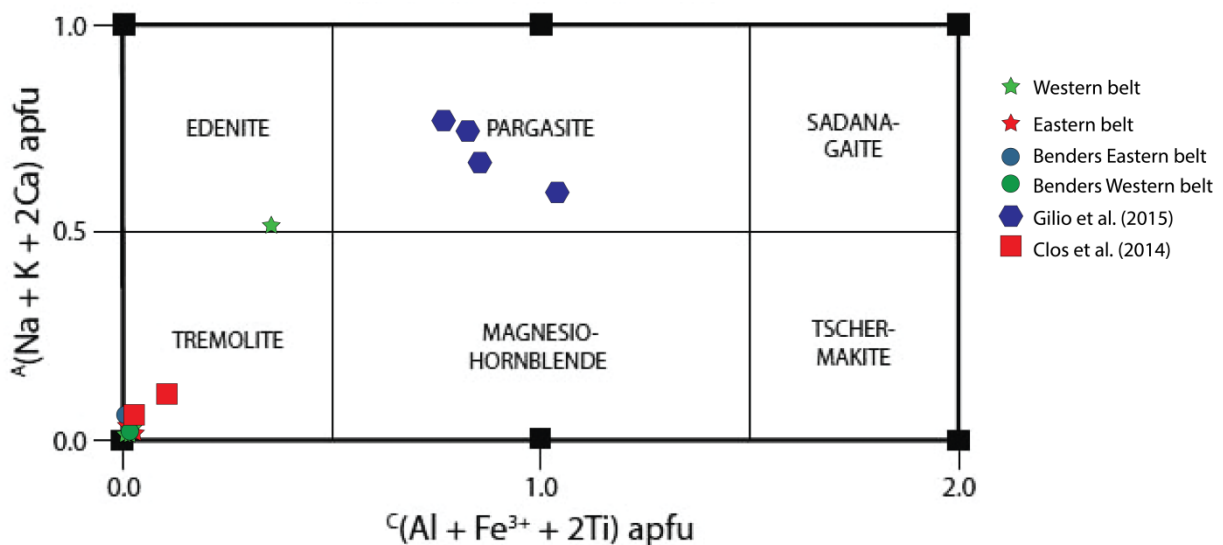
Figure 31. Classification diagram of calcium amphiboles after the latest nomenclature (Hawthorne e al., 2012). upper belt amphibolites are classified as tremolite with one exception being the edenite. Amphiboles from the Eastern belt are tremolites and anthophyllites (figure 30).

5.5.2 Chlorite

Chlorites found in the eastern and western belt show a high mg wt% of 19.8-33.5%. According to the classification system of Zane & Weiss (1998) all chlorites plot in the mg-chlorite field (fig 32). The chlorite of the lower belt all have 2.2-3.5 wt% Cr_2O_3, they are found at rims of the chromites which is probably where they got the chromium from (fig 19 B&C). Compared to Benders (2015), chlorites in this thesis show a slightly higher Al^{3+} and Fe^{2+} content. The protolith of the Eastern belt is a harzburgite which contains Al in spinel, this could explain the presence of Al

in the measured chlorites. However, the Western belt has a dunite as protolith which does not have Al in the same amounts as harzburgites. Yet, the Western belt chlorites show a higher Al content than the Eastern belt where it is expected to be less. This could be explained by either having a different protolith as thought or by fluid infiltration. As chlorites in the Western belt are found growing randomly over previous mineral assemblages where Eastern belt chlorites are found at the edges of spinel. It lies within reason that the Eastern belt chlorites are formed as a result of transformation of spinel to chromite. Western belt chlorites are probably formed as a result of fluid infiltration from the underlying subduction zone which is often rich in Al.
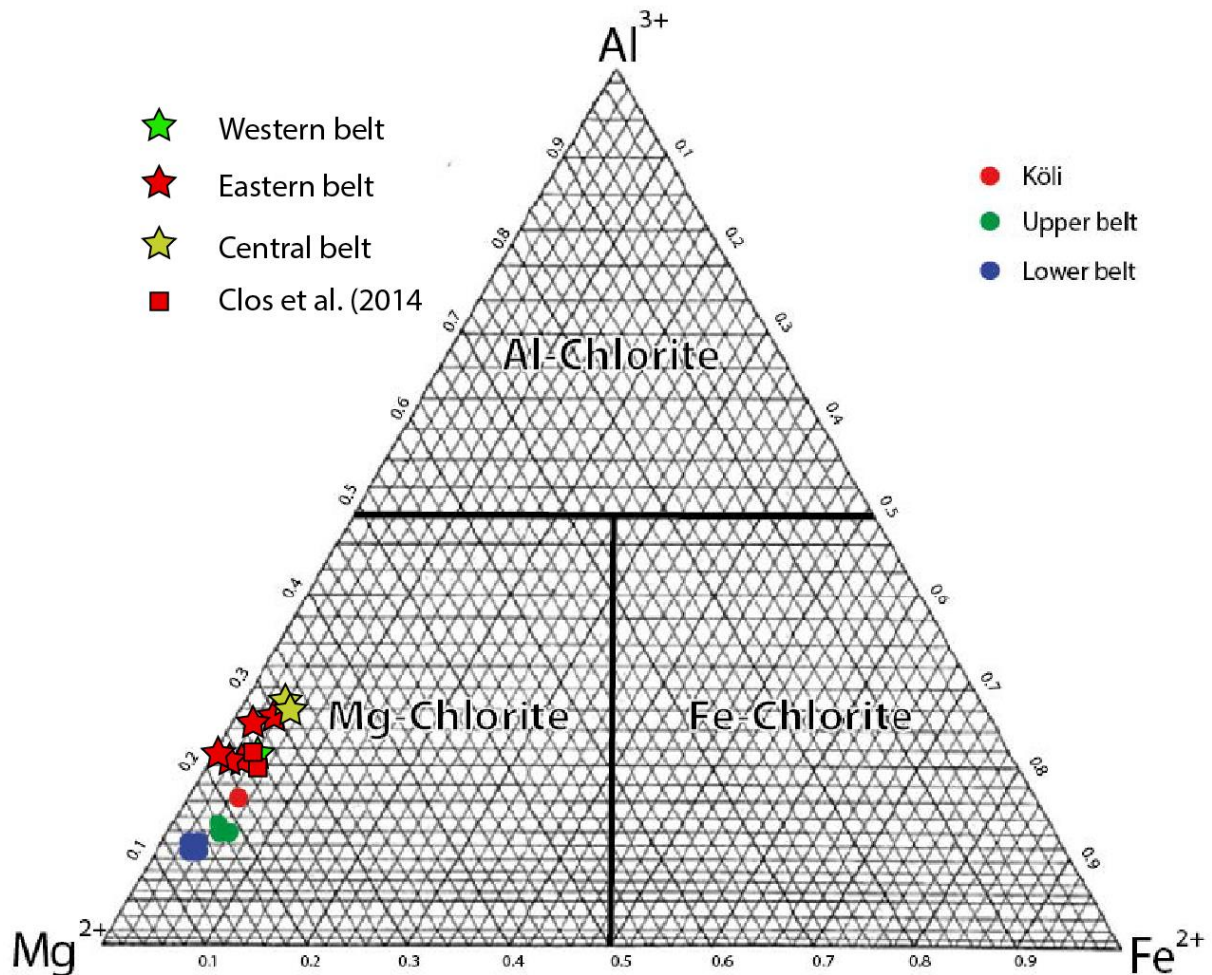
Figure 32. chlorite classification diagram. Both belts plot as mg-chlorites in the classification system after Zane & Weiss (1998).

5.5 Chemical composition of country rock minerals

Garnet found in sillimanite-kyanite bearing schists residing between the Central and Western belt show one continuous trend in Mg, Fe, Mn and Ca from core to rim. This continuous trend suggests that the garnet has grown in one phase as a result of prograde metamorhpishm..
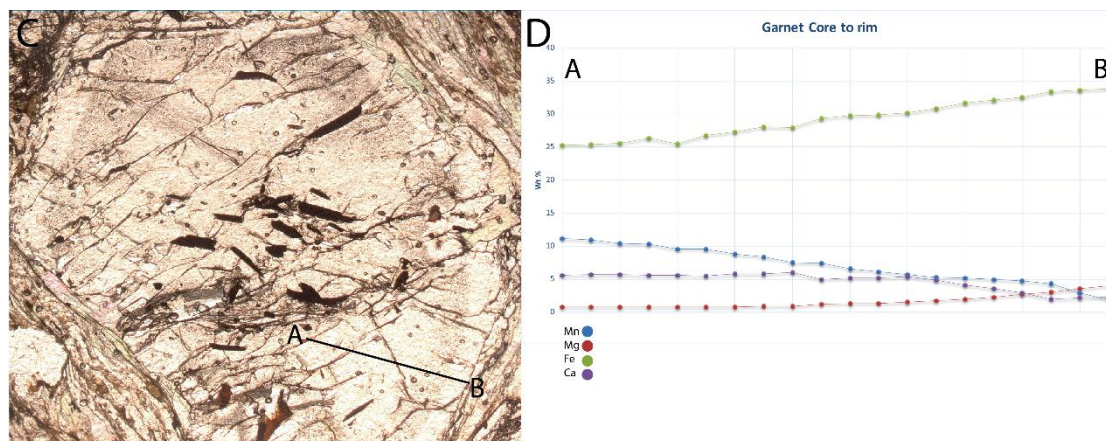
Figure 32 A) Image of garnet and location of the line measurement. B) Element oxide Wt% profile of line A-B. Note the smooth trend throughout the line which suggests this garnet has grown in one stage.

Element maps as shown below (figure 33) show clearly show a high amount of Al at the right rim of the garnet. Further measurements have shown this is kyanite growing together, and in contact, with the garnet. This observation led to the suggestion that garnet grew in 2 phases, during which the 2nd phase kyanite grew as well.
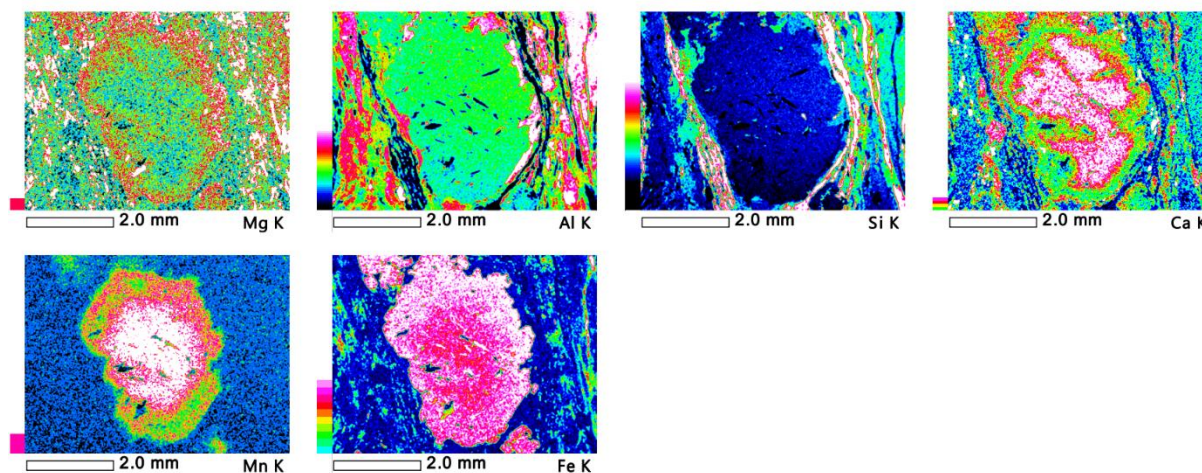
Figure 33. Multiple element maps of a garnet. Brighter colors indicate a higher wt%. 100 frames have been made with 0.02 seconds per measured point.

Perple_X (Conolly 2005 & 2009) modelling shows (figure 34), using isopleths of pyrope, grossular+spessartine and almandine, the core grew at a temperature and pressure of 466 °C and 4.6 kbar, respectively (starting position of the arrow figure 34). Using isopleths for multiple points along a line measurement can give a good view of changing PT-conditions during garnet growth. The changing PT-conditions for these garnets show an increase in temperature of 30°C and an increase of 1.3 kbar to 5.9 kbar in pressure when taking points from the core towards 75% outwards to the rim. As can be seen in figure 32A, the rim is clearer compared to the core. However, using the isopleth method shows a temperature of 746 °C and a pressure of 4.5 kbar (figure 32). The isopleth method in Perple_X does not take into account a change in BRC during growth of different minerals.

Therefore, the more calculations you make the less accurate they become. In figure 34 Grossular and Spessartine are taken together because they both have such low values(<0.1) that the resolution of the modelling programme is no longer reliable. Comparing the PT-conditions to the minerals observed at the core and rim of the garnet a discrepancy is found; kyanite is growing mainly at the rim of the garnet where the core contains sillimanite fibers. It is therefore suggested that the XRF-measurements of sample 2c1b is in relation to the core of the garnet rather than the rim. More advanced modelling for this is encouraged.
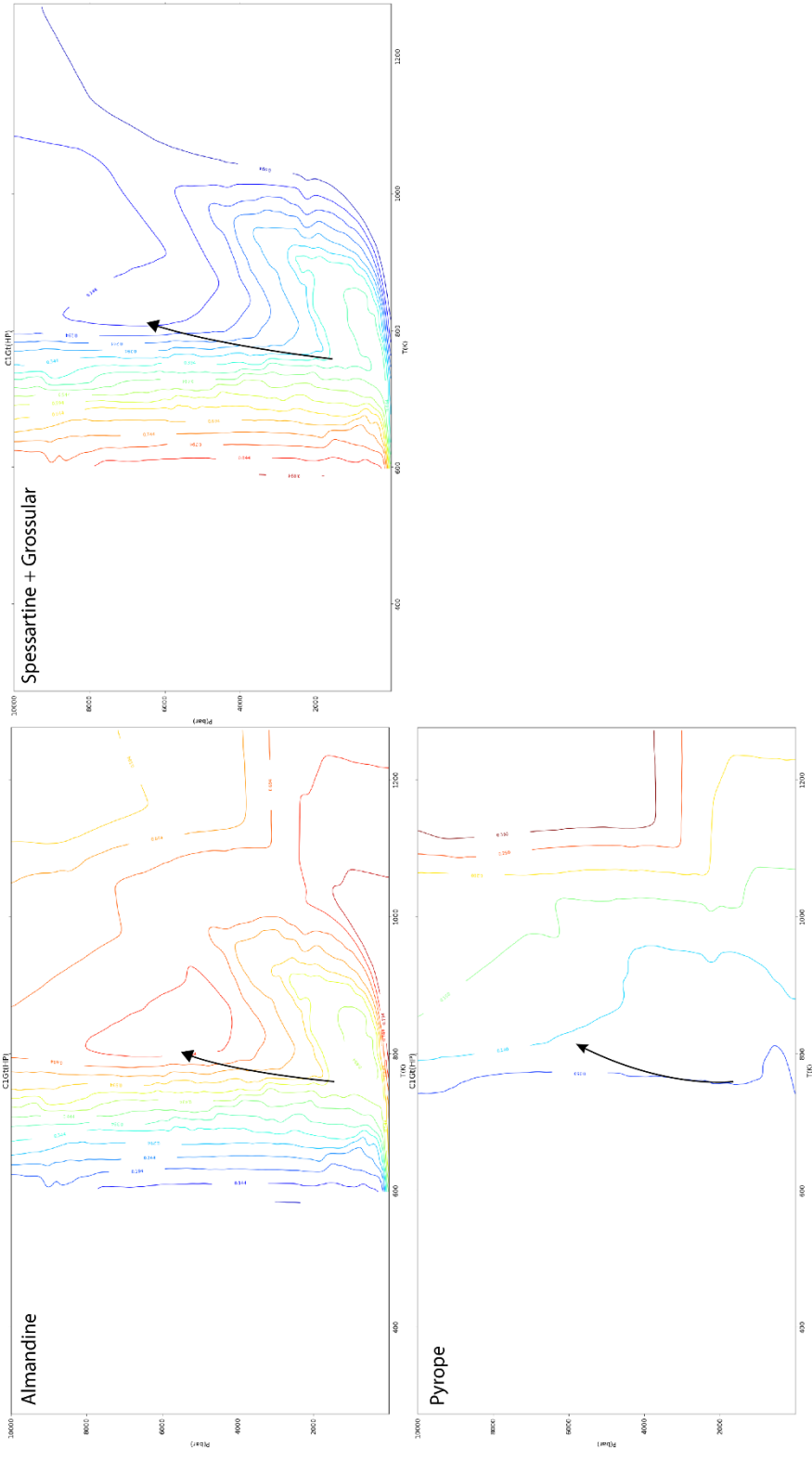
Figure 34. Isoplets for the different endmembers of garnet analysed from sample 2c1b. the arrow indicates the change in PT-conditions from core to rim.

6.0 Discussion

6.1 The effect of serpentinization on mineral chemistry of peridotites

The Mg# of olivine of the eastern and most of the western belt peridotites show that they have undergone very little serpentinization as the olivine Mg# does not reach above 93.1. One locality of the western belt shows mg# >96, this is interpreted on the geological map (fig 15) as Seve Nappe, which obviously cannot be true as these peridotites should have had the same geological history as the other bodies sampled in the western belt in this thesis. I therefore suggest that sample locations W1-16 belong to the Köli Nappe; Sjöstrand (1977) had the same idea. However, this was later changed to Seve Nappe by the Swedish Geological Survey (1990).

The spinels in peridotites of the western and eastern belt show an important difference, which is that the western belt spinels consist solely of magnetite ($Fe^{2+}Fe_2^{3+}O_4$) (figure 24B&D) where the eastern belt spinel still contain chromite ($Fe^{2+}Cr_2O_4$) (figure 24 A&C) with reasonable levels of Al^{3+}. This means that the western belt must have had serpentinization due to the following reactions.

$$14Fo + 10\,En + 31\,H_2O \rightarrow Atg \quad (1)$$
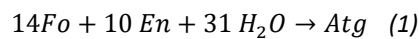
Reaction 1 shows the process of serpentinization which happens when a dry peridotite gets wetted. Olivine together with orthopyroxene forms antigorite. When all olivine is used up the remaining orthopyroxene reacts according to equation 2.

$$45En + 55\,H_2O \rightarrow Atg + 14\,Tlc \quad (2)$$

$$34\,Fo + 51\,H_2O \rightarrow Atg + 20\,Brc \,(3)$$
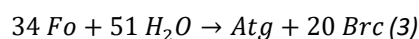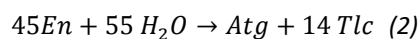
Equation 3 shows what happens when there is no more orthopyroxene but only olivine. However, no brucite is found in any sample, thus following this observation the olivine must have been used up before the peridotite ran out of orthopyroxene. Written in chemical formulae's the following reaction (reaction 4 & 5) occurs during serpentinization:

$$3Fe_2SiO_4 + 2H_2O \rightarrow 2Fe_3O_4 + 3SiO_{2(aq)} + 2H_2 \quad (4)$$

$$3Mg_2SiO_4 + SiO_{2(aq)} + 2H_2O \rightarrow 2Mg_3Si_2O_5(OH)_4 (5)$$
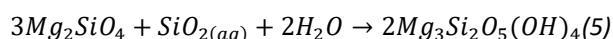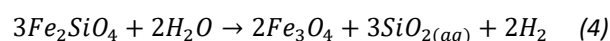
Equation 4 shows what happens with the fayalite exponent of olivine during serpentinization. Serpentine cannot contain all the iron released during this reaction, antigorite's chemical formula is $Mg_{2.25}\,Fe_{0.75}\,(OH)_4\,Si_2O_5$ so it is able to take up some of the iron. However, all the excess iron forms magnetite. Equation 5 shows the chemical reaction of the serpentinization of the forsterite component of olivine, which forms chrysotile when it is wetted. However, reaction 4 is irreversible, so when peridotites are subsequently brought back to their higher PT-conditions magnetite does not transform back to spinel or chromite, which results in a higher Mg# of olivine (Bucher 2011) as chrysotile and antigorite transform back to olivine. With this knowledge the western belt must have had fluids running through them where the eastern belt had very little to no fluids infiltrating as the spinels found there are M1 protolith composition with chromites and ferro-chromites at the rims.

The spinel composition of the eastern and western belt peridotites show one clear difference; western belt spinels all consist of magnetites where the eastern belt consists of chromite (figure 24A). A trend which shows enrichment in iron toward the rim of spinel is observed in the eastern belt (Photo 4e1). This rim is interpreted as metamorphic spinel. As spinel/chromite goes from high to low pressures/temperatures Al partitions out of the spinel(Barnes & Roedel 2001). Depending on bulk rock composition chromites/spinels can be relatively Al-rich to Al-low. Lherzolites are commonly more Al-rich than harzburgites and dunites. As all peridotites in this thesis are

harzburgites or dunites the Al-content in the chromites is low, where Al#'s don't reach higher numbers than 0.31 in the Eastern belt and 0.01 in the Western belt (figure 24). Growing at the rim of the chromite are chlorite minerals, Merlini et al. (2009) noted that chlorites are chromium-rich when they have a Cr_2O_3 between 2-6 wt%. All measurements of chlorites surrounding chromites have a wt% of 3-4% Cr_2O_3. The chlorites have therefore probably grown as a response to the breakdown of spinel/chromite. Chemical equation (6) shows what happens during this process (after Merlini, 2009). Chromite and antigorite, together with water and oxygen, transform to ferrianchromite and Cr-chlorite.

$$2(Mg_{0.60}Fe_{0.40})(Cr_{1.30}Al_{0.70})O_4 + \frac{3}{2}(Mg_{2.57}Al_{0.32}Fe_{0.11})Si_2O_5(OH)_4 + H_2O + \frac{1}{12}O_2$$

$$\rightarrow$$

$$\frac{7}{6}(Mg_{0.40}Fe_{0.60})(Cr_{1.85}Fe_{0.08}Al_{0.07})O_4 + \frac{1}{2}(Mg_{9.18}Fe_{0.34}Al_{1.60}Cr_{0.88})(Al_2SiO_6)O_{20}(OH)_{16} \quad (6)$$
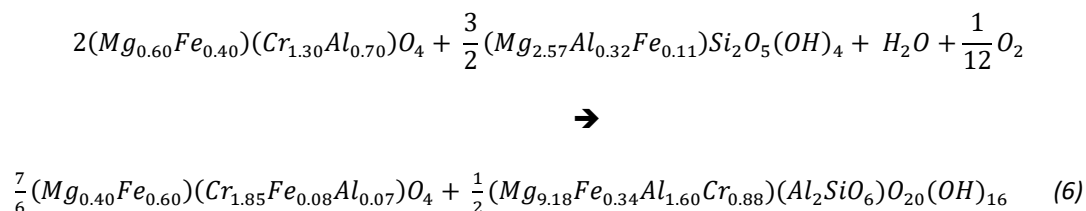
The above equation is applicable to the eastern belt but not to the western belt. The western belt deviates from equation 6 because it has a much higher Fe^{3+} content, thus the conditions for the western belt must have been more oxidizing (Kapsiotis et al., 2009).

The presence of talc means that the Western belt peridotites have been formed from forsterite by an H_2O-CO_2 fluid, or alternatively SiO_2 input is required depending on the amount of talc formed (equation 7) (Birtel, 2002). As the Western belt peridotites are thought to come from a mantle wedge the infiltrating CO_2-rich fluid probably comes from the underlying subducted slab. Sediments are known to contain CO_2 which they release at higher pressures and temperatures.

$$4Fo + 5CO_2 + H_2O = Tlc + 5Mgs \quad (7)$$
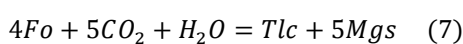
Equation 7 takes place at 400-580 °C between 0.35-0.7 GPa. Silica can also be delivered from pyroxene, which would result in the formation of dolomite or calcite instead of magnesite. However, no dolomite or calcite is found in any of the samples ruling this probability out. Talc found as matrix indicates a decrease in pressure causing the fluid to become oversaturated in resulting in talc precipitation. Even further retrograde evolution will result in the precipitation of antigorite veins (Birtel, 2002).

6.2 Peridotite origin

The chemical composition of peridotites depends on tectonic setting in which they are emplaced and/or evolved. The amount of depletion depends on the pressure and temperature conditions under which the partial melt, which eventually produces the peridotite, formed. Fluid infiltration/percolation can alter the bulk rock composition by adding or removing elements. The latter process has certainly taken place in both belts discussed in this thesis by introducing calcium to the system, forming tremolite. Arai et al. (1994) produced a classification system of the different types of peridotite based on the Mg# [Mg/(Mg+Fe)] in olivine and Cr# [Cr/(Cr+Al)] in spinel (fig 35). For comparison data has been taken from the research of Gilio et al. (2015) on garnet peridotites. Gilio et al. argued that all their peridotites have a subcratonic origin. Comparing the data from this MSc thesis to the data of Gilio et al. shows that they have similar Mg#'s. The large difference in Cr# can be explained by a smelting phase refertilizing the garnet peridotites; this smelting phase did not occur in the Eastern or Western Seve belt. Rather, these peridotite bodies show a prograde metamorphism (M3, figures 18&20)
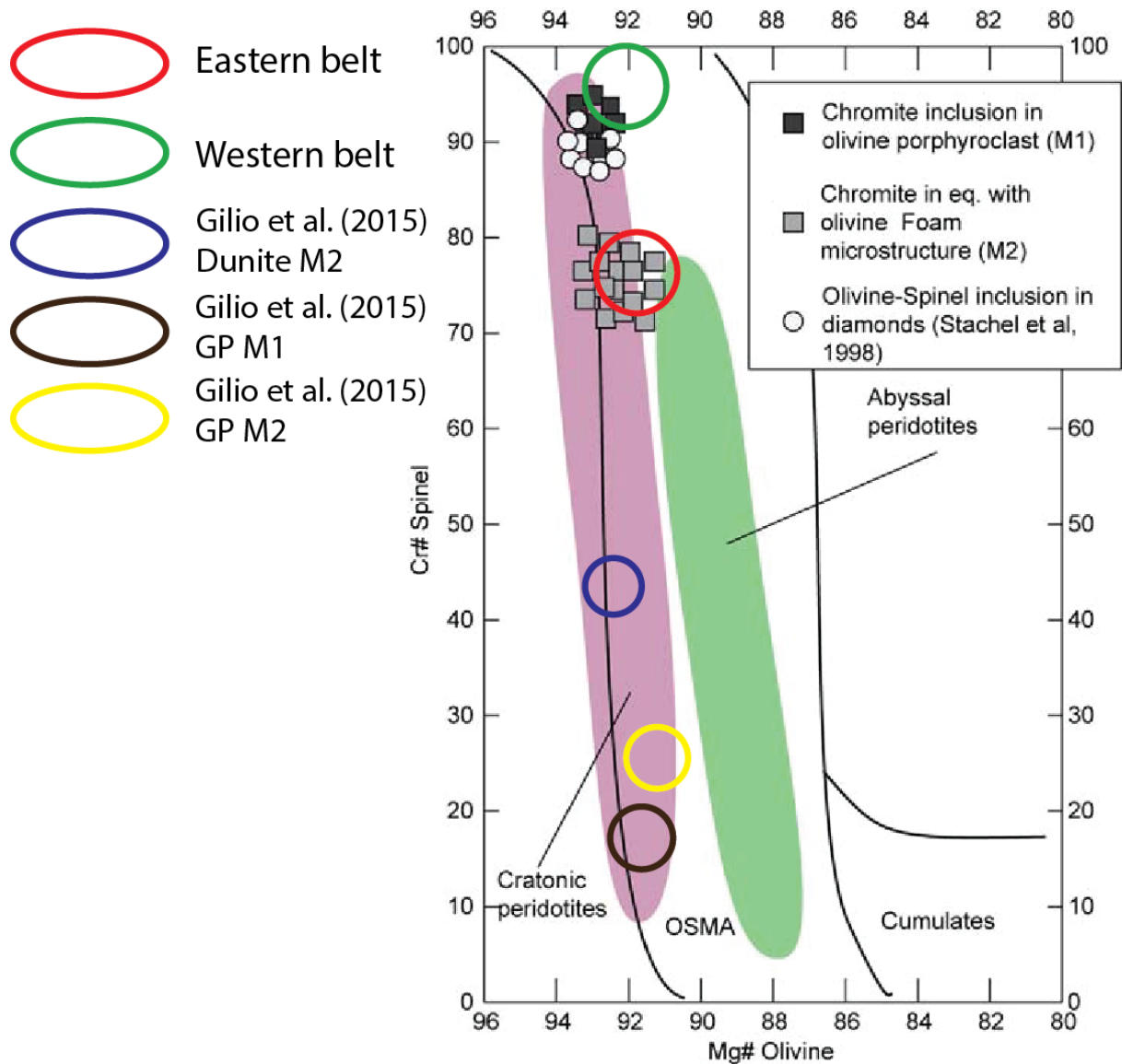
Figure 35. Classification diagram after Arai et al. (1994) showing the different types of peridotites based on Mg# in olivine and Cr# in spinel. The Eastern belt and Western belt both overlap with cratonic type peridotites. For comparison the research of Gilio et al. (2015) on Garnet Peridotites is added.

Arai et al. (2004) found a correlation between metasomatism and the relationship between Mg# in olivine and the Cr# in spinel. Arai found that with increasing metasomatism the Mg# decreases slightly while the Cr# increases. For this research two types of peridotites were used; C-type and F-type, which stand for coarse-grained and fine-grained, respectively. All peridotites are thought to have a mantle-wedge origin. Coarse-grained peridotites are mostly harzburgites with olivine crystals of 5 mm across, where fine-grained peridotites are also harzburgites but with higher amounts of chromian-spinel. Olivine in F-type peridotites is 60-70 µm across (figure 36)(Arai et al., 2004). Comparing this to samples used in this thesis to this classification the Eastern belt is comparable to the F-type where the Western belt is comparable to the C-type peridotite. However, Eastern belt peridotites aren't of mantle-wedge origin, where the Western belt peridotites are. It is therefore suggested that the Western belt has undergone more metasomatism than the Eastern belt.

C-type Peridotite
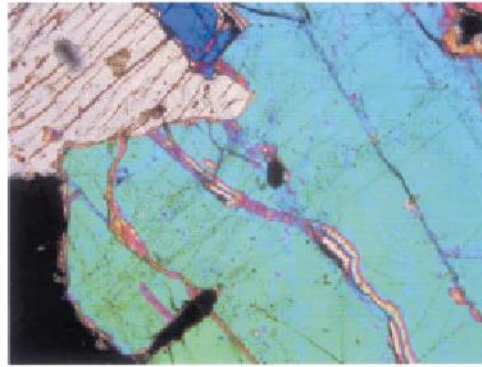
1mm

F-type Peridotite
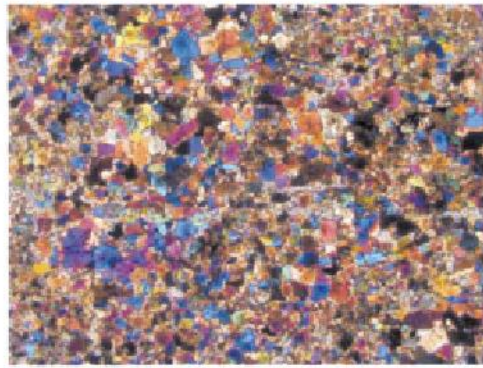
1mm

Figure 36. Illustration of the two different types of peridotites used in Arai et al. (2004).

Barnes and Roeder (2001) discriminated spinel compositions of igneous peridotites of all kinds of different tectonic settings, among them they reviewed ophiolites, alpine ultramafics and abyssal peridotites. They found a strong Cr-Al trend in high-pressure spinel lherzolite bodies. This is not observed in this thesis. Points plotted by Barnes&Roeder are of protolith composition whereas the Western belt spinels are clearly altered by secondary processes. The eastern belt spinels, on the other hand, are less altered and can thus be compared to other results. The area in which the spinels from the eastern belt overlaps partly with the chromitites field (fig 37). Note that the high aluminum content of spinels is restricted to alpine peridotite complexes. Comparing these results to the results of this thesis show that the eastern belt peridotites are a "normal" peridotite type, most probably sheared into the SNC.
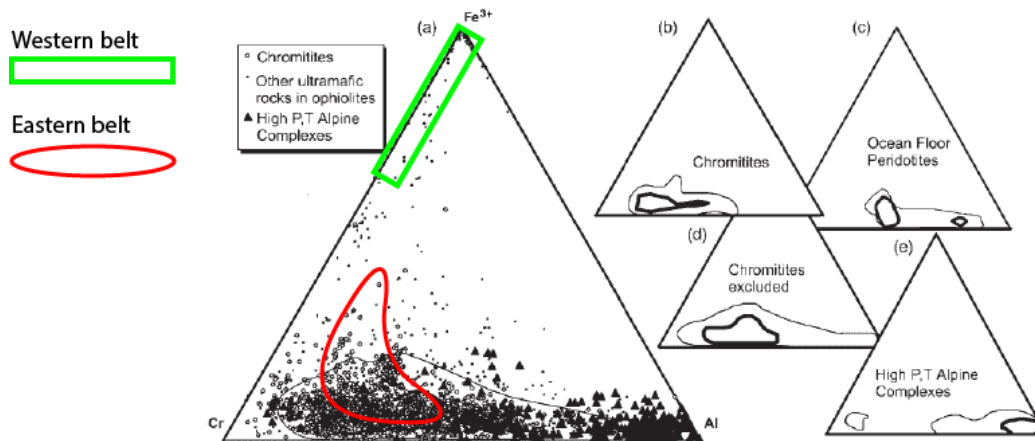
Figure 37. Compositional diagram of spinels in peridotites. The red field represents the eastern belt (M1) and partly overlaps with the chromite field in figure b. The green field represents the western belt (M3) and does not overlap with any field previously determined by Barnes and Roeder (2001)

Griffin et al. (2003) found a relation between the wt% CaO ,Al_2O_3 in peridotites and the age of the mantle from which they formed (figure 38). As the Al and Ca content increases the age of the mantle from which the corresponding peridotites form is younger. This effect is attributed to the absence of Cr-Al phase during the melting phase of Archean xenoliths. However, primary spinel is found in the peridotites sampled in this MSc thesis yet they overlap with the Archean field. This discrepancy can be explained either by small fertilization/modification phases in later era's; or by the fact that the XRF data of the peridotites does not show the true primary composition as these bodies have undergone multiple deformation/metamorphic phases.
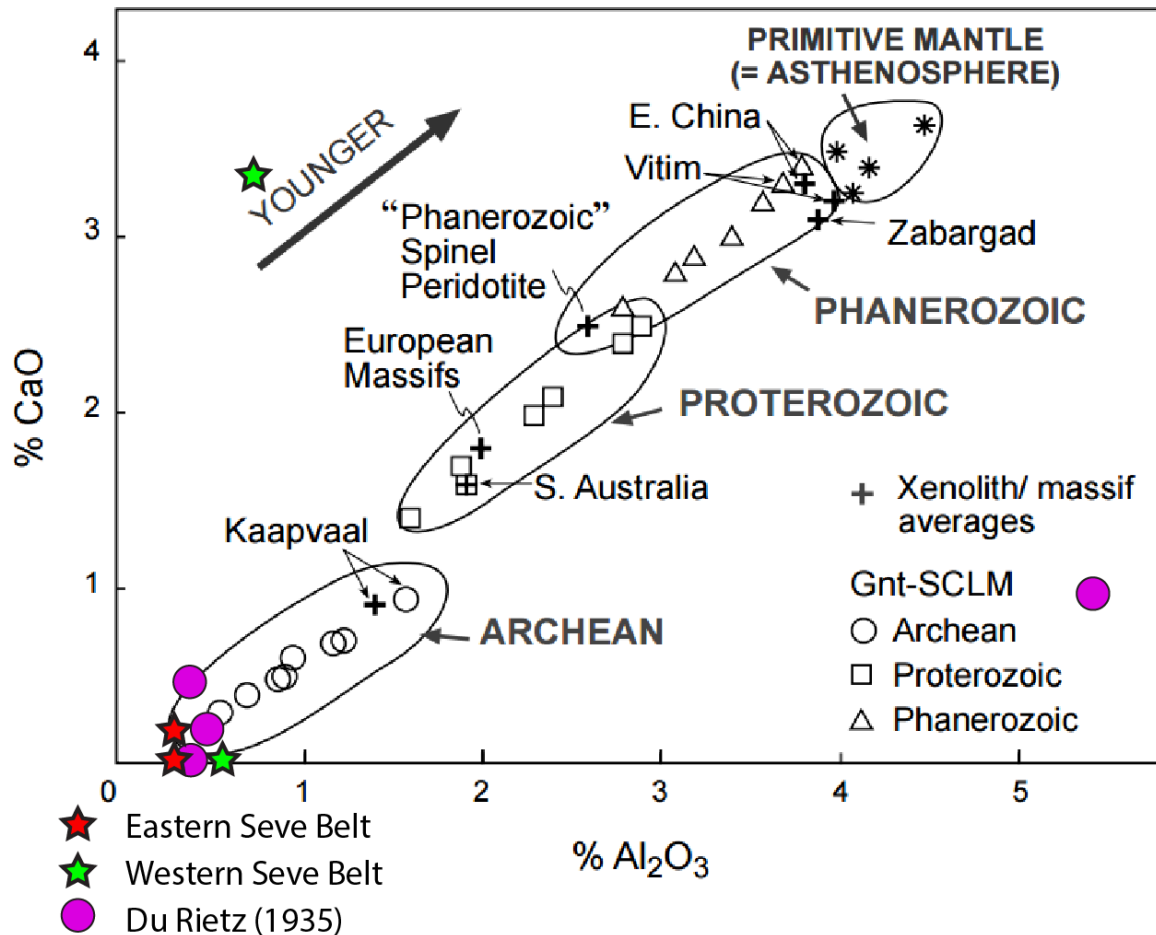
Figure 38. CaO vs. Al₂O₃ for SCLM. XRF measurements are used for the Ca and Al values. As comparison Du Rietz (1935) is added (same peridotites). This data gives an indirect age of the peridotites. (modified after Griffin et al. 2003)

The Eastern and Western Seve belt can be considered, as already noted by Clos et al. (2014), as fragments of a heterogeneous SCLM of Archean , reftactory peridotites and locally refertilized by at least two different Proterozoic events (Clos et al. 2014). These refertilization events have led to a high Mg# (91-93) in both belts.

6.3 P-T-t-paths:

6.3.1 Upper Seve Nappe Peridotites

M1 (protolith)

The M1 assemblage of the Upper Seve Nappe peridotites consists of olivine and spinel with minor amounts of ortho- and clinopyroxenes (<5%) thus classifying the peridotites as spinel bearing dunites. Due to secondary processes very little to no M1 olivines are preserved. Besides, all spinels in the Upper Seve Nappe are altered which makes it very hard, read impossible, to determine the equilibration temperature and pressure of the M1. Assumed is that the peridotite slowly cooled to temperatures < 1200°C (Baker et al., 1995) and eventually equilibrated at subsolidus temperatures as low as 900-850°C. Note that figure 39 doesn't show spinel as a stable phase, reason for this is the absence of Al_2O_3 in the BRC during modelling. However, finding magnetite in the sample does suggest that the has been Al in previous mineral assemblages.

M2 (retrograde metamorphism)

The M2 metamorphic assemblage represents serpentinization. During this process olivine transformed in antigorite at temperatures of 375-500°C (figure 39). For serpentinization to occur water infiltration/percolation is required, these fluids probably came from the underlying subduction zone. Cooling of the peridotite is interpreted to be achieved by a reduction in depth. Temperatures aforementioned can be achieved at depths of 12-15.5 km depth assuming a geothermal gradient of 30°C/km. Pressure conditions during retrograde metamorphism is estimated to be around 0,3-0,5 GPa.

M3 (peak metamorphism)

Peak metamorphic conditions were reached during the M3 metamorphic assemblage with temperatures up to 715°C, this conclusion is based on the absence of orthopyroxene in the M3 metamorphic assemblage. Geothermobarometry was attempted, however, due to the absence of primary olivine and spinel and the absence of clinopyroxene no satisfactory results are found. Tremolite is formed during this peak metamorphism which requires a minimum and maximum temperature of 470 and 720°C, respectively. Comparing the amphibole chemistry with that of Clos et al. (2014) shows no differences, even though Clos et al. took samples in the Central belt. In theory, pressure could be as high as 1 GPa. However, Bucher-Nurminen (1991) identified a Barrovian metamorphic field gradient. Following this metamorphic field gradient indicates a pressure of ~0.4-0.6 GPa.

M4 (retrograde metamorphism)

The M4 metamorphic assemblage is characterized by a decrease in metamorphic grade down to lower greenschist facies. The change is observed in the growth of serpentine, talc, magnesite and chlorite. As the peridotites move towards the surface during this retrograde metamorphism pressure and temperature are close to that of the surface.
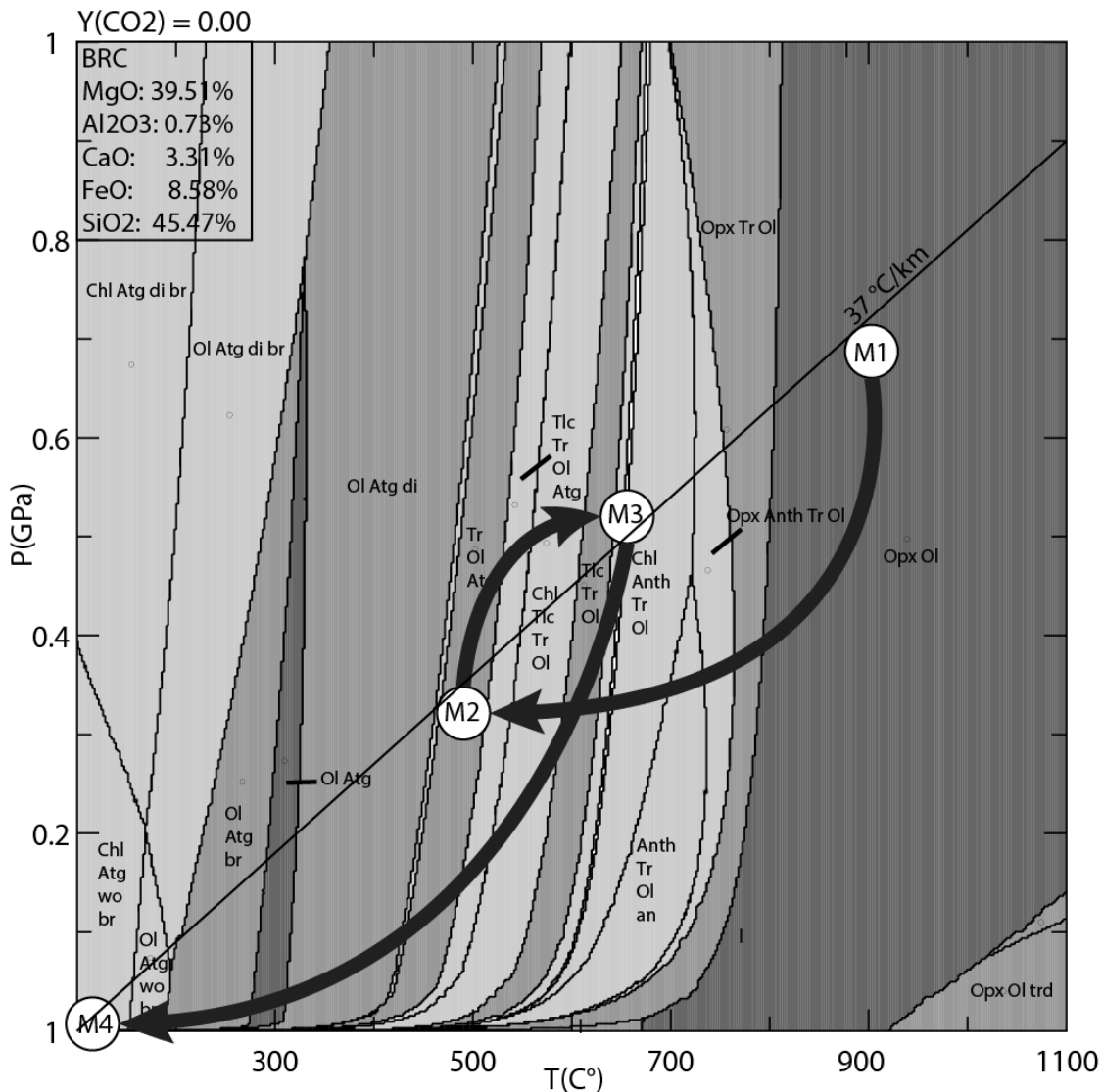
6.3.2 Lower Seve belt peridotites

M1 (protolith)

The M1 mineral assemblage of the Eastern belt peridotites consist of olivine, orthopyroxene and spinel, thus classifying the peridotites as a spinel bearing harzburgite and/or dunites. Temperature for this stability field (figure 40) is >700°C with pressure above 1 GPa. Figure 40 shows no spinel, however, ferri-chromite has been found (figure 19) with chlorite replacing the rim of the spinel.

M2 (retrograde metamorphism)

The M2 assemblage represents the first retrograde metamorphism causing serpentinization. As noted before (section 6.3.1.) water is required for serpentinization. During this process Fe^{2+} is removed from olivine thus increasing the Mg# of olivine, this Fe subsequently forms magnetite. The previous described reaction of olivine to serpentine and magnetite is irreversible. Small amounts of chlorite and serpentine have been formed during this retrograde metamorphism which suggests that there has been little water available. During this retrograde metamorphism orthopyroxene became hydrated as well forming anthophyllite in the process. The temperature for this retrograde metamorphism is estimated at 375-500°C (based on psuedosection, figure 40) whereas pressure is poorly constrained due to a lack of pressure indicators.

M3 (peak metamorphism)

The peak metamorphic assemblage consists of olivine, chlorite and anthophyllite. The estimated temperature for this peak metamorphism is at ~650-700°C as the M3 olivine shows signs of dynamic recrystallization (figure 19). Less amounts of tremolite have been found in the Eastern belt peridotites which suggests that there was either less clinopyroxene in the protolith or the fluids infiltrating the Eastern belt peridotites contained less Ca.

M4 (retrograde metamorphism)

The final metamorphic assemblage found in the eastern belt is similar to the western belt; there is a final serpentinization phase, although this is much less pronounced compared to the western belt. The temperature conditions for this final retrograde metamorphism is similar to the Western belt peridotites.
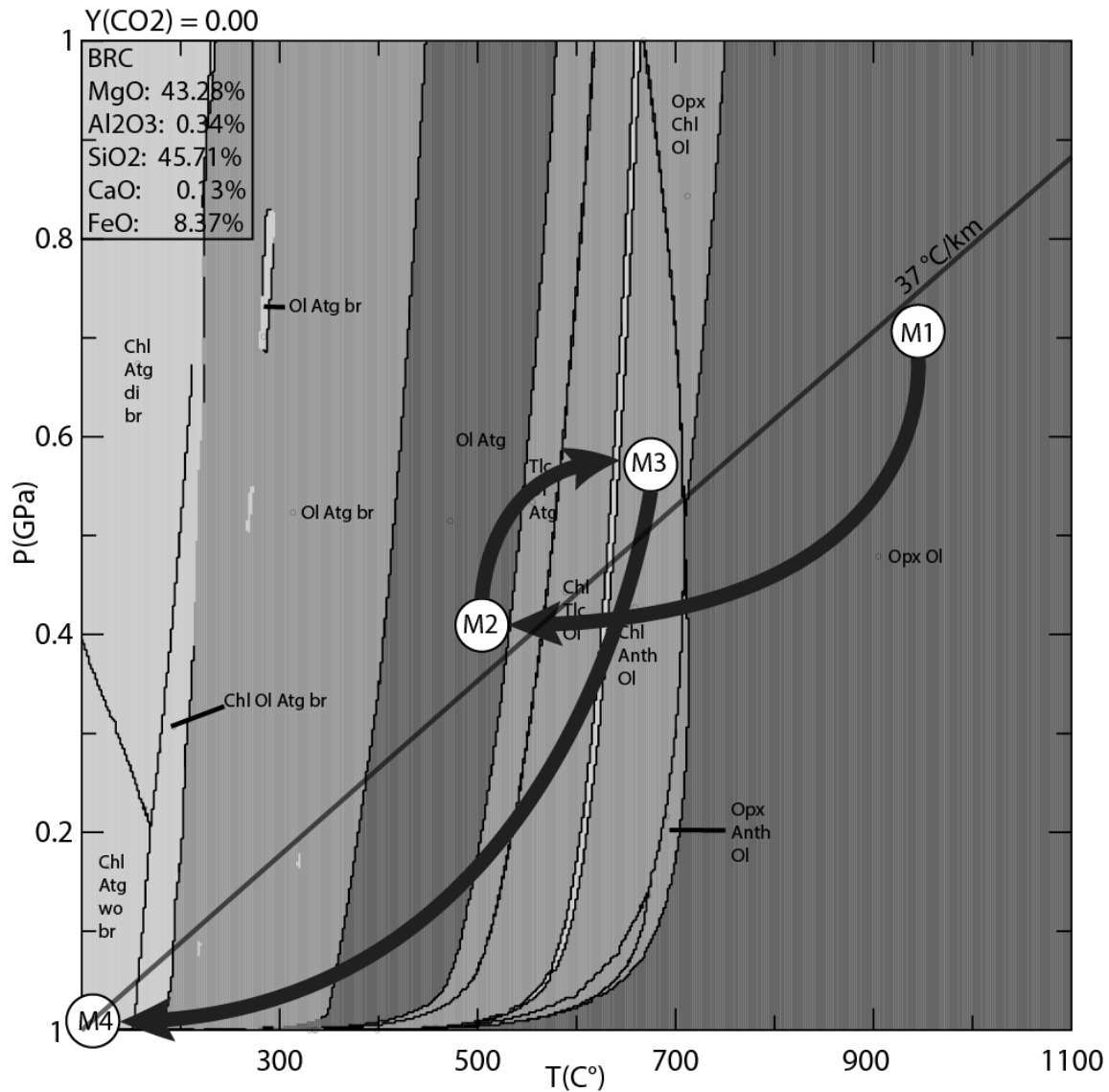
Figure 40. Estimated PT-path for the Eastern belt peridotites of the Seve Nappe. The BRC, shown in the top left corner, is taken from sample 4e1.

6.3.3 Country rock

M1

The M1 mineral assemblage is characterized by the standard pelitic conditions during lithification. It is assumed to consist of muscovite, quartz and albite. The temperature and pressure conditions for this are badly constrained, so just an indication can be given for this sample. The temperature under which this assemblage formed is somewhere in the range of 100-150 C°, whereas the pressure is estimated to be <1kbar.

M2

The temperature for the M2 metamorphic event is estimated between 675-800 C°. The pressure for M2 ranges between 500-600 MPa as the isopleths show (figure 34). Part of this metamorphic phase is found as inclusions in garnet growing at M3, namely the aluminumsilicates which are too small to discriminate with the naked eye and are chemically identical as kyanite and sillimanite are psuedomorphs. However, the habit of sillimanite is

fibrous/needlelike where kyanite is platy. Inclusions in garnet only show small fibres which would mean that sillimanite grew earlier than garnet.

M3

The M3 represents the peak metamorphic conditions which is characterized by the growth of garnet with biotite and kyanite. The pressure for this peak metamorphism is estimated at 5.9 GPa The temperature for this metamorphic assemblage is better constrained than the other metamorphic assssemblages; as zoisite and garnet grow at the same time the temperature must be between 500-600 C° The core of the garnet contain dominantly Mn^{2+} and Ca^{2+} where the rim contains more Fe^{2+} and Mg^{2+}. This indicates that the garnet started growing at relatively low PT-conditions and from there went through a prograde metarmorphism. This metamorphic phase is seen in figure 33 as the white band around the "dirtier" core. Kyanite is found growing together with straight boundaries of garnet , and kyanite is found growing over earlier foliations.

M4

The final metamorphic assemblage represents a retrograde metamorphism back to a metamorphic grade similar to M1. The foliation is also made during this phase as the bands of mica/quartz bend around the garnet. As for the M1 the pressure/temperature conditions are badly constrained ranging between 100-150 C° and 280-460 MPa, respectively.
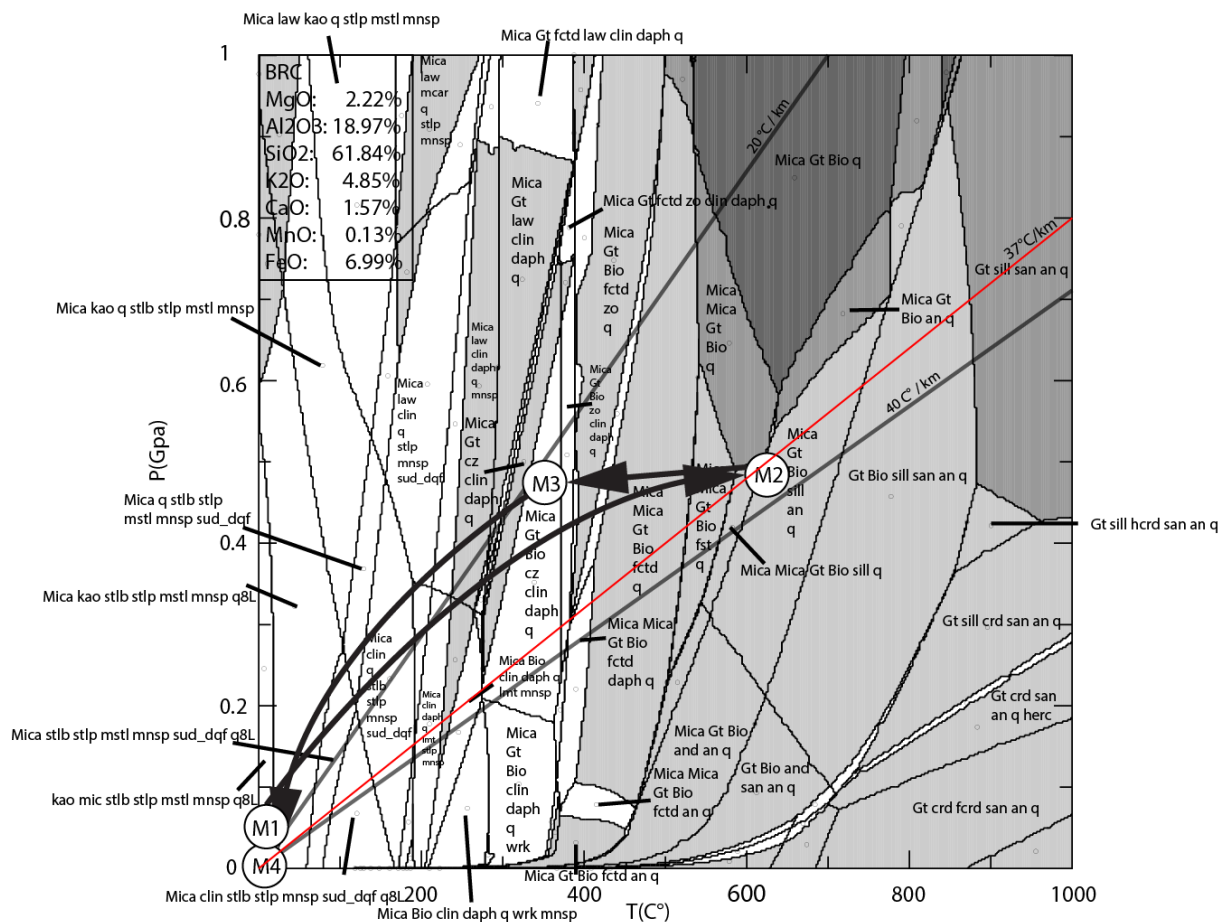
Figure 41. Pt path for the country rock. the psuedosection is made from samples taken for this thesis, the chemical data can be found in the appendix. The solidus is taken from hermann et al (2006). the brc can be found in section 5.3.1.

6.4 Geodynamic model:

6.4.1 Pre-Caledonian & Virisen Arc formation

In the Pre-Caledonian (615-570 Ma) (figure 42) breakup of Laurentia and Baltica occurred (Li et al. 2007). During the breakup, a hyperextended margin formed between a microcontinent and the central belt, which is believed to be another microcontinent separated from the mainland of Baltica.During the formation of the hyperextended margin temperatures increased in the overlying lithospheric mantle which resulted in dynamic recrystallization in the Eastern belt peridotites. Temperatures and differential stresses during this recrystallization event were ~700-785 ⁰C and 30-100 MPa (figure 16). Assumed temperature for this retrograde metamorphism based on metamorphic assemblages is 450 C⁰ (figure 39). The geothermal gradient in a hyperextended margin increases up to 55 C⁰/km (Thompson 1989, Golberg & Leyreloup 1990). To reach temperatures of 450 C⁰ a depth of 8 km is required, this high geothermal gradient is an extreme case. Commonly a geothermal gradient of ~30-35 C⁰/km is assumed, using this gradient means a depth of 12.5-15 km to reach the 450 C⁰. At these depths a pressure is in the order of 3.3-4 kbar which coincides nicely with the estimated PT conditions for the M2 mineral assemblage for the Western belt (figure 39).
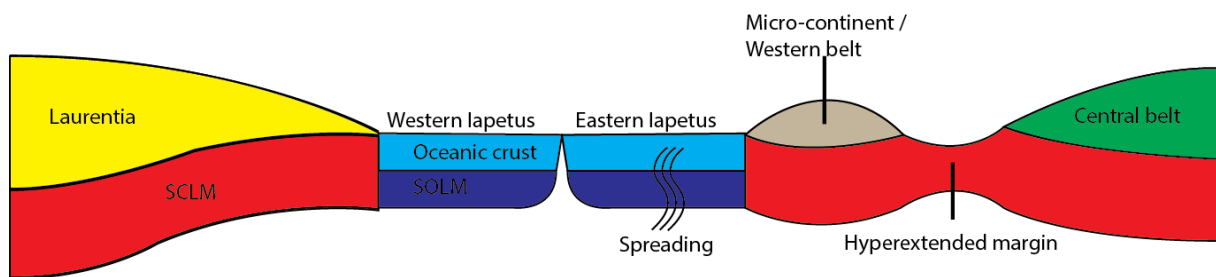
Figure 42. Schematic illustration of the original configuration of Iapetus prior to the onset of convergence of the Scandinavian Caledonides.

During intra-oceanic subduction, the subducting oceanic crust released fluids as a result of heating. These fluids then infiltrated the overlying mantle wedge resulting in lowering the temperature required to generate melt. This resulted in the formation of the Virisen Arc (figure 43). At the hyperextended margin temperatures of the overlying SCLM increased causing dynamic recrystallization in the Eastern Seve belt samples.
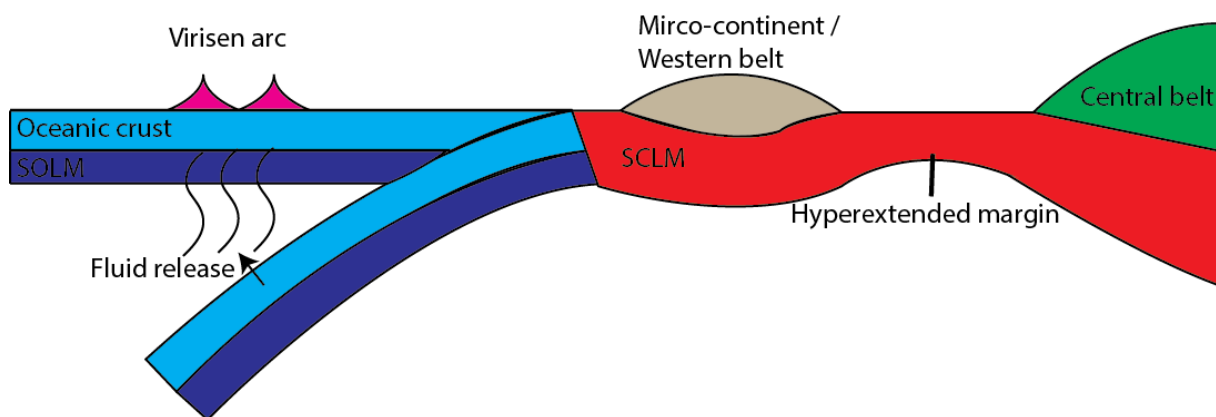
Figure 43 . Formation of the virisen arc pre-Caledonian. As a result of intra-oceanic subduction and fluid-assisted melt the virisen arc formed.

6.4.2 Finnmarkian

As intra-oceanic subduction continued the micro-continent believed currently to be the Western Seve belt collided with the Virisen Arc where the former underthrusted the latter (Brueckner & van Roermund 2004; Roberts et al. 2004; van Staal et al. 1998, 2012). This event is called the Finnmarkian and occurred at ~500 Ma. The Finnmarkian is recorded in the Western belt country rock as an increase in pressure and temperature, with mineral assemblages consisting of, among others, sillimanite and garnet. As the microcontinent experienced a pull of the subducted oceanic crust an opportunity for the introduction of peridotites of the Lower Köli nappe rised. Therefore, during the Finnmarkian the first peridotites were introduced which are currently found at the Lower Köli/Western Seve belt contact.
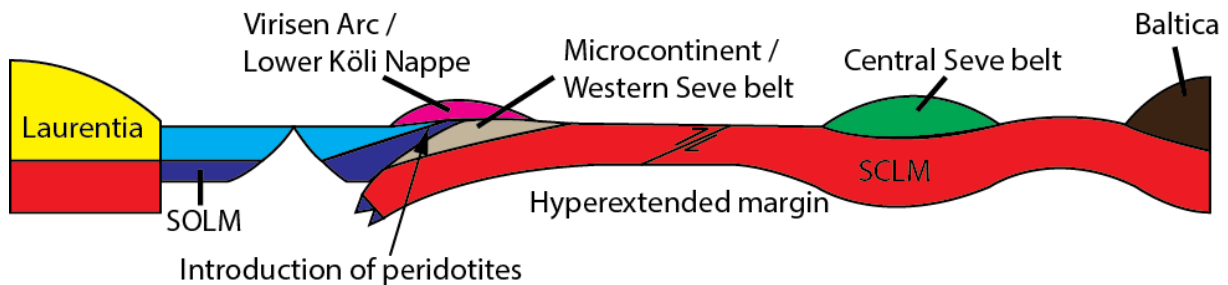
Figure 44. Iillustration of the Finnmarkian orogeny. As a result of the convergence of Laurentia and Baltica the Virisen arc and the microcontinent collided causing the micro-continent to be underthrusted beneath the virisen arc. At this time the peridotites of the Lower Köli nappe were introduced.

6.4.3 Jämtlandian

The next orogenic event is the Jämtlandian (~454 Ma, Brueckner & van Roermund 2004). During the Jämtlandian the Central Seve belt (which drifted from Baltica in earlier stages) subducted down to depths of at least 40 km (occurrence of garnet peridotites does not occur at shallower depths). During the Finnmarkian the Western Seve belt peridotites currently found at the Western- and Central Seve belt contact were introduced to the system. As well as the introduction of peridotites in the Western and Central Seve belt, the Central Seve belt subducted up to eclogite facies. Age determination of this ultra-high pressure deformation shows an age of 457 to 432 Ma, at which time exhumation occurred (Grimmer et al. 2015). Sm-Nd data for mylonitic garnet-mica schist shows a garnet controlled isochron of 462 Ma which is interpreted as a metamorphic growth of garnet. This implies that PT-conditions, when correlating it to the country rock treated in this thesis, would have to be at least 500 C° and 0.6 GPA. During the subduction of the Central belt fluids released from the Central Seve belt resulted in slight serpentinization in the overlying SCLM previously subdcuted beneath the microcontintent consisting of the Western Seve belt and the Virisen Arc during the Finnmarkian (figure 44).
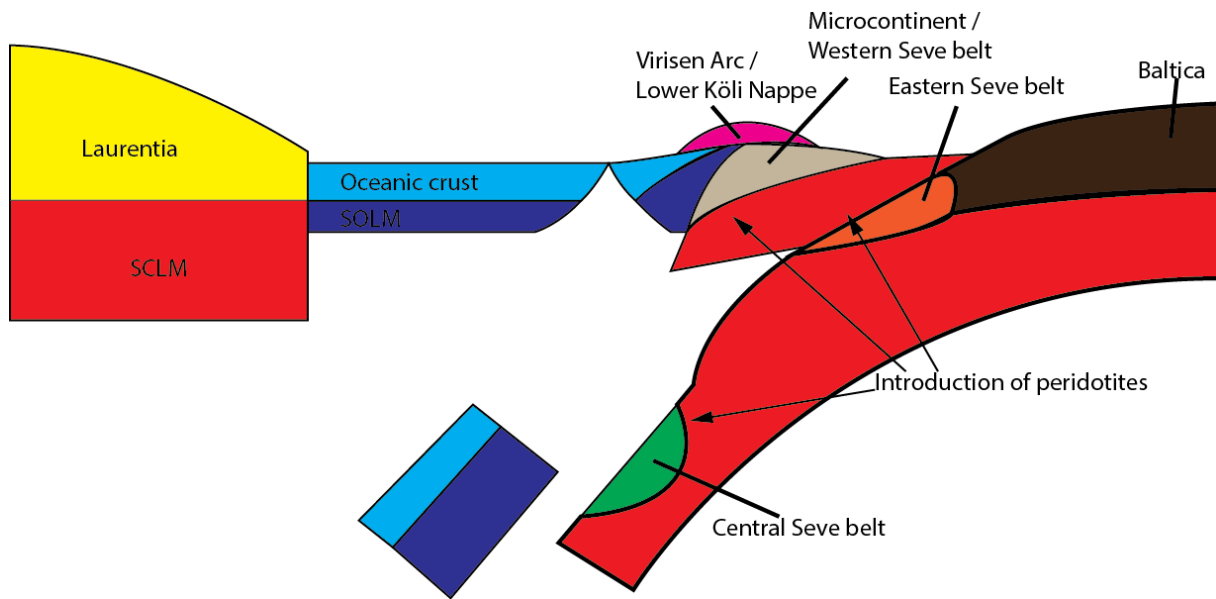
Figure 45. The Jämtlandian orogeny, at this point the peridotites of the western belt got incorporated as a result of shearing. the central belt got subducted up to eclogite-facies depths.

Eventually slab breakoff occurred resulting in eduction of the Central belt resulting in the introduction of the peridotites between the Eastern and Central belt.
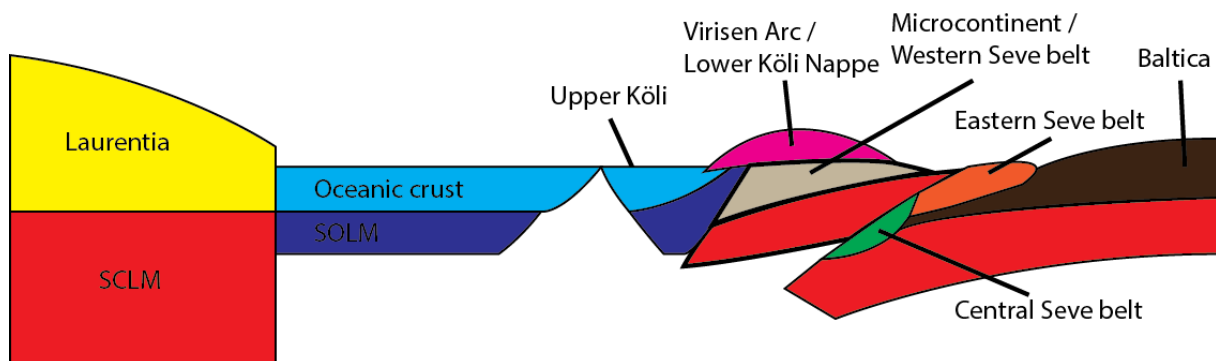
Figure 46. The eduction of the Jämtlandian, at this point the central belt got sheared back into the western and eastern belt. During this eduction peridotites between the Western and Cental Seve belt and the Central and Eastern Seve belt got introduced.

6.4.4 Scandian

The final stage which can be observed is the Scandian Orogeny (~415-400 Ma). This is the collision between Laurentia and Baltica, where the former overthrusts the latter (fig 47; Brueckner & van Roermund 2004). When looking at the P-T-t-paths of the two peridotites and the country rock the temperature and pressure of the eastern belt is higher than those of the country rock and western belt which is not that weird considering the eastern belt lies stratigraphically beneath the other two (Zwart 1974). During the Scandian Orogeny the Köli Nappe Complex got thrusted over the Seve Nappe Complex and formed the final configuration as we find today (Zwart 1974). The burial of the Western Gneiss Region and the Baltic Shield underneath the Seve Nappe Complex caused the same dehydration reactions as discussed before in section 6.4.1. This fluid percolated the above lying SNC causing hydration reactions with olivine resulting in the formation of serpentine seen in the latest metamorphic assemblage. Bucher & Grapes (2005) modelled that the modal volume of olivine at temperatures of 300-400 C° are only 20-25% (fig 49). Pressures and temperatures are in good agreement with the Barrovian metamorphic field gradient associated with continent-continent collision (Bucher-Nurminen 1991).
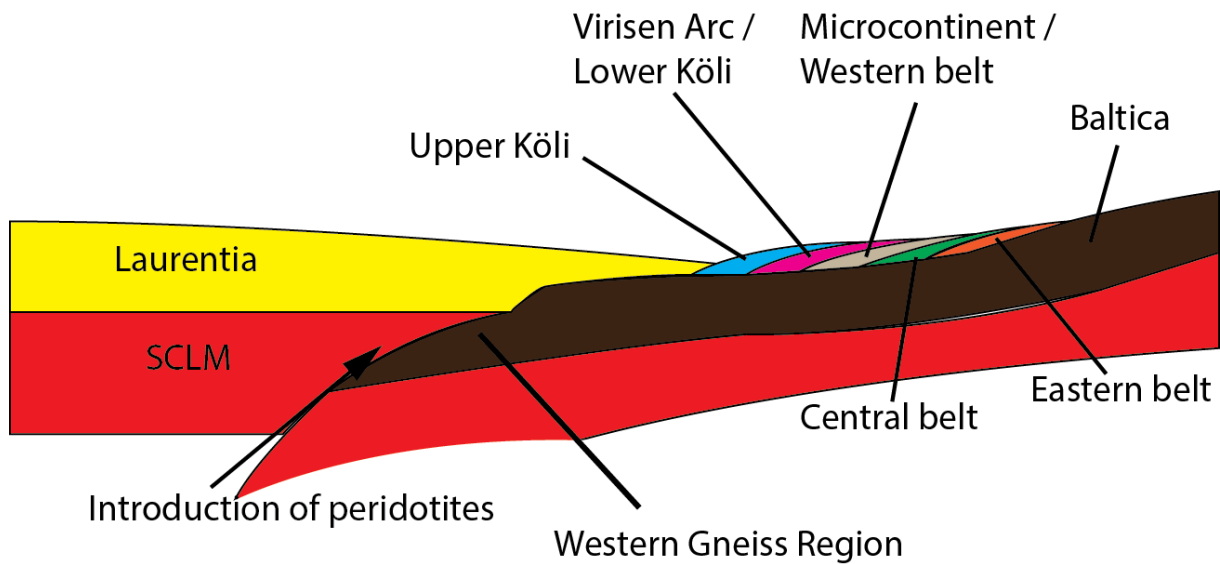
Figure 47. The Scandian orogeny where the western gneiss region subducted to eclogite facies depths. Laurentia thrusted over Baltica and shuffled previously accreted terranes.

As erosion took place the Western gneiss region eventually got exhumed resulting in the current orientation of the Scandinavian Caledonides. During the UHP conditions the continental crust became twice as thick than normal. During exhumation this thickened crust elevated which resulted in the nappes on top of it to slide further to the east (gravitational spreading).
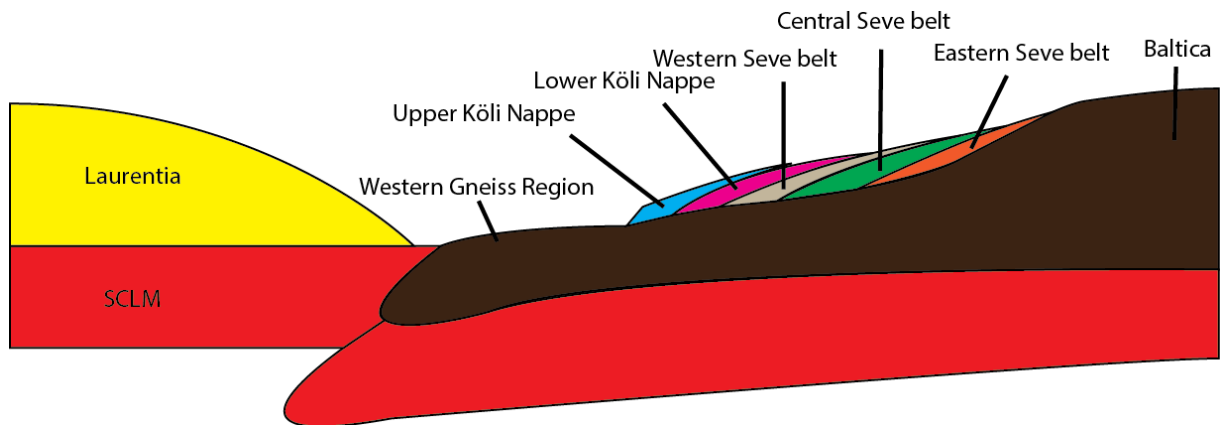
Figure 48. The exhumation of the western gneiss region by orogen normal extension. Note that this part remains speculative.
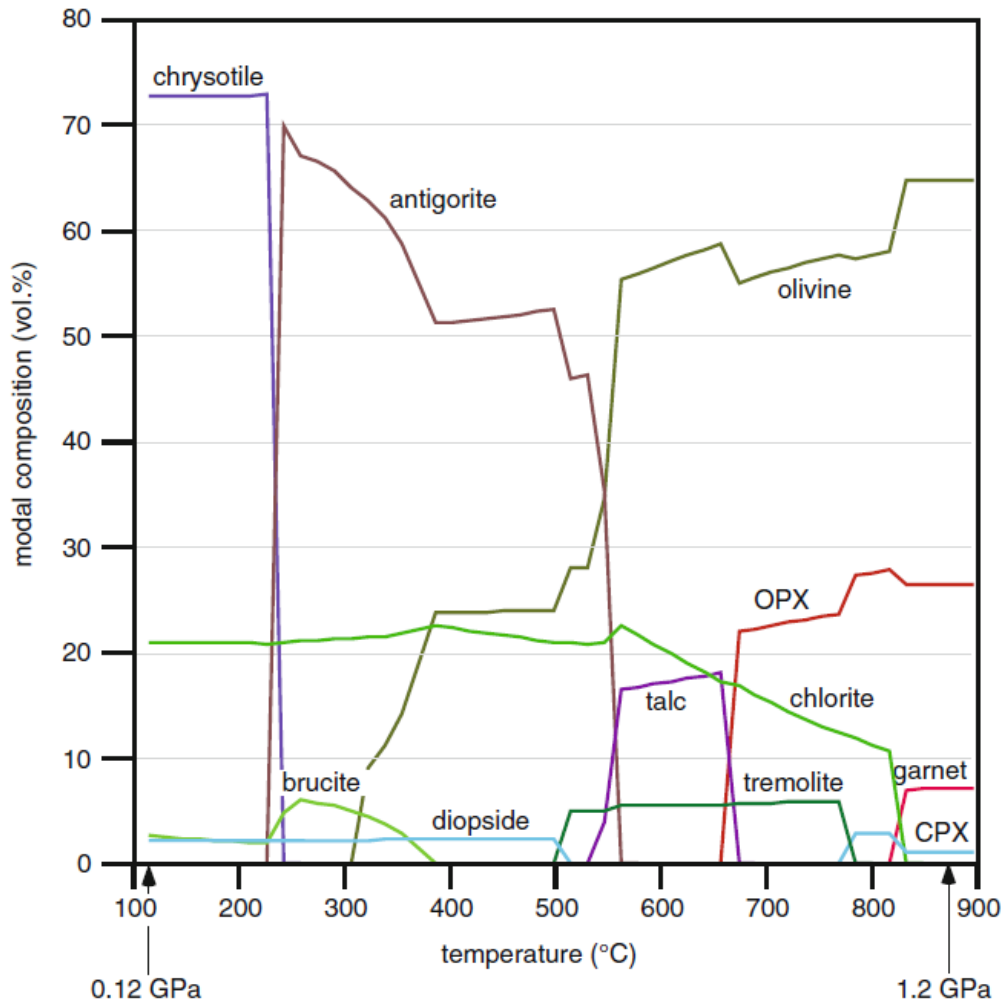
Figure 49. Model metamorphism along a normal geothermal gradient (20 c°/km). after Bucher & Grapes (2005).

6.5 Comparison to the existing models:

When comparing these results to the models of Hacker & Gans (2005) and Roberts (2003) a discrepancy can be found. In the case of Hacker & Gans the Jämtlandian leaves no room for peridotites to be incorporated in the Seve Nappe Complex (fig 14). However, as this thesis and many other papers before (Benders 2015, Brueckner & van Roermund 2004, Clos et al. 2014, Gilio et al 2015), have shown that peridotites are present, the model of Hacker & Gans leaves a big gap as to where the peridotites come from. The model for Roberts (2003) also does not include the introduction or presence of peridotite bodies in the SNC and KNC (figs 8-10). When looking at his model, in contrast to Hacker & Gans' model, it leaves room for interpretation as to where the peridotite bodies got incorporated. However, age determinations leaves a discrepancy between the possible introduction of peridotites and the measured ages (Roberts 2003, Grimmer et al. 2015) therefore also leaving room for improvement for the model of Roberts. Looking at the model of Brueckner & van Roermund (2004) the ages of Grimmer et al. (2005) and the fact that they included emplacement of peridotites shows that they are the best model combined with this thesis' results.

7.0 Conclusion

I. This study shows that the Upper Seve Nappe country rock is metamorphosed to amphibolite facies

II. EMP-analyses show that the Western Seve belt resided in the mantle wedge overlying the subduction zone during the Finnmarkian and Jämtlandian orogeny. The lower belt has sub-cratonic lithosphere provenance.

III. The Western Seve belt peridotites have undergone metasomatism as a response to fluid infiltration/percolation caused by dehydration reactions in the underlying subduction zone (500 & 454 Ma.)

IV. The Eastern Seve belt peridotites have undergone a period of heating in response to a hyperextended margin resulting in dynamic recrystallized olivine with temperatures and differential stresses of 700-785 ^oC and 30-100 Mpa, respectively.

V. Prior to / during the Finnmarkian the country rock of the upper belt was metamorphosed to amphibolite facies forming sillimanite.

VI. During the Jämtlandian the peridotites of the Western and Eastern belts got incorporated in the country rock.

VII. The peak metamorphic conditions for both the lower and upper belt occurred during the Jämtlandian (454 Ma.) in a Barrovian metamorphic field gradient (20^oC/km) .

8.0 future work

I. Geothermobarometry should be done on the peridotites in order to better constrain the PT-conditions of the different metamorphic assemblages.

II. More XRF-measurements and Perple_X modelling should be done on the upper belt country rock to better constrain PT conditions.

9.0 Acknowledgements

10.0 References

Andréasson P.G., 1994, The Baltoscandian margin in Neoproterozoic-early Paleozoic tie: Some constraints and terrane derivation and accretion in the Arctic Scandinavian Caledonides. Tectonophysics. Volume 231, p. 1-32

Arai S., 1994, Characterization of spinel peridotites by olivine-spinel compositional relationships: Review and interpretation. Chemical Geology. Vol. 113. p. 191-204.

Arai S., Takada S., Michibayashi K., Kida M., 2003, Petrology of Peridotite Xenoliths from Iraya Volcano, Phillipines, and its Implication for Dynamic Mantle-Wedge Processes. Journal of Petrology. Vol. 45. No. 2. p. 369-389.

Arai S., Ishimaru S., 2007, Insights into Petrological Characteristics of the Lithosphere of Mantle Wedge beneath Arcs through Peridotite Xenoliths: a Review. Journal of petrology. Vol. 49. No. 4. p. 665-695.

Baker, M. B., Hirschmann, M. M., Ghiorso, M. S., & Stolper, E. M. (1995). Compositions of nearsolidus peridotite melts from experiments and thermodynamic calculations. Nature, 375(6529), Bodinier J.-L., Godard M., 2013, Orogenic, Ophiolitic and Abyssal Peridotites, Treatise on Geochemistry: Second Edition, Volume 3, p. 103-167.

Barnes J.S., Roeder P.L., 2001, The range of spinel compositions in terrestrial mafic and ultramafic rocks. Journal of petrology. Vol. 42. No. 12. p. 2279-2302.

Bial J., Trepmann C.A., 2013, The microstructural record of porphyroclasts and matrix serpentinized peridotite mylonites – from brittle and crystal-plastic deformation to dissolution-precipitation creep. Solid Earth. Vol. 4. p.315-330.

Birter S., 2002, Fluid-rock interacion on alpine-type ultramafic rocks from the Norwegian Caledonides. PhD thesis. Universität Freiburg.

Bodinier J.L., Godard M., 2003, Orogenic, Ophiolitic and Abyssal Peridotites. Treatise on geochemistry. Vol.2. p. 103-170.

Brueckner H.K., 1998. Sinking intrusion model for the emplacement of garnet-bearing peridotites into the continent collision orogens. Geology, 26(7), 631-634

Brueckner H.K., Medaris L.G., 2000, A general model for the intrusion and evolution of 'mantle' garnet peridotites in high-pressure and ultra-high-pressure metamorphic terranes. Journal of Metamorphic Geology, Volume 18, p. 123-133

Brueckner H. K., van Roermund H.M.L., 2004, Dunk tectonics: A multiple subduction/eduction model for the evolution of the Scandinavian Caledonides. Tectonics. Vol. 23. (2).

Brueckner H.K., van Roermund H.L.M., Pearson N.J., 2004, An Archean(?) to Paleozoic evolution for a garnet peridotite lens with sub-Baltic shield affinity within the Seve Nappe Complex of Jämtland, Sweden, Central Scandinavian Caledonides. Journal of petrology. Vol.45. no.2 . p. 415-437.

Brueckner H.K., van Roermund H.L.M., 2007, Concurrent HP metamorphism ono both margins of Iapetus: Ordovician ages for eclogite and garnet pyroxenites from the Seve Nappe Complex, Swedish Caledonides. Journal of geological society. Vol. 164. p. 117-128.

Bucher-Nurminen, K. (1991). Mantle fragments in the Scandinavian Caledonides. Tectonophysics, 190(2), 173-192.

Bucher K., Grapes R., 2011, Petrogenesis of metamorphic rocks. Ch. 5, p. 191-224

Caddick M.J., Konopásek J., Thompson A.B., 2010, Preservation of garnet growth zoning and the duration of prograde metamorphism. Journaly of petrology. Vol.51. no.11. p. 2327-2347.

Calon, T. J., (1979). A study of the Alpine-type peridotites in the Seve-Köli nappe complex central Swedish caledonides with special reference to the Kittelfjäll peridotite. (Doctoral dissertation)

Coleman R.G., 1971, Plate tectonic emplacement of upper mantle peridotites along continental edges. Journal of geophysical research. Vol. 76, no. 5.

Clos, F., Gilio, M., & van Roermund, H. L. (2014). Fragments of deeper parts of the hanging wall mantle preserved as orogenic peridotites in the central belt of the Seve Nappe Complex, Sweden. Lithos, 192, 8-20.

Conolly J., 2005, Computation of phase equilibria by linear programming: A tool for geodynamic modeling and its application to subduction zone decarbonation. Earth and Planetary Science Letters 236: 524-541.

Conolly J., 2009, The geodynamic equiation of state: what and how. Geochemistry, Geophysics, Geosystems 10: Q10014 DOI:10.1029/2009GC002540.

Cuthbert, S. J., & Carswell, D. A. (1990). Formation and exhumation of medium-temperature eclogites in the Scandinavian Caledonides. Eclogite facies rocks*, 180-203.*

Dijkstra A.H., Drury M.R., Vissers R.L.M., et al., 2004, Shear zones in the upper mantle: evidence from alpine- and ophiolite-type peridotite massifs. Geological society, vol. 224, p. 11-24.

Den Tex E., 1969, Origin of ultramafic rocks, their tectonic setting and history: a contribution to the discussion of the paper "the origin of ultramafic and ultrabasic rocks" by PJ Wyllie. Tectonophysics, vol 7(5), p. 475-488

Dick H.J.B., Bullen T., 1984, Chromian spinel as a petrogenetic indicator in abyssal and alpine-type peridotites and spatially associated lavas. Contributed mineral petrology, vol. 86, p. 54-76.

Dunning G.R., 1987, U-Pb zircon ages of Caledonian ophiolites and arc sequences: implications for tectonic setting (abstract). Terra Abstr., EUG IV, Strasbourg, 179

Du Rietz, T. (1935). Peridotites, serpentines, and soapstones of Northern Sweden, with special reference to some occurrences in Northern Jämtland. Geol. Fören. Stock. För. 57*, 133-260.*

Evans B.W., Frost B.R., 1975, Chrome-spinel in progressive metamorphism- a preliminary analysis. Geochimica et. Cosmochica Acta, vol. 39, p. 959-972.

Ewing T.A., Rubatto D., Beltrando M., Hermann J., 2015, Constraints on the thermal evolution of the Adriatic margin during Jurassic continental break-up: U-Pb dating of rutile from the Ivrea-Verbano Zone, Italy. Contributed mineral petrology. Vol. 169, no. 44.

Gayer R.A., Rice A.H.N., Roberts D., Townsend C., Welbon A., 1987, Restoration of the Caledonian Baltoscandian margin from balanced cross-sections: the problem of excess continental crust. Trans. R. Soc. Edinb. Volume 78, p. 197-217

Gee D.G., 1975, A tectonic model for the central part of the Scandinavian Caledonides. American journal of science, vol. 275-a, p. 468-515.

Gee D.G., 1978, Nappe displacement in the Scandinavian Caledonides. Tectonophysics, vol. 47, p. 393-419.

Gee, D. G., Fossen, H., Henriksen, N., & Higgins, A. K. (2008). From the early Paleozoic platforms of Baltica and Laurentia to the Caledonide Orogen of Scandinavia and Greenland. Episodes, 31(1), 44.

Gee D.G., Janák M., Majka J., Robinson P., van Roermund H., 2013, Subduction along and within the Baltoscandian margin during closing of the Iapetus Ocean and Baltica-Laurentia collision. Lithosphere, Volume 5, no. 2, p. 169-178

Gilio, M., Clos, F. & van Roermund, H.L.M. (2015). The Friningen Garnet Peridotite (Central Sweden). A good example of the characteristic PTt path of a cold mantle wedge garnet peridotite. Manuscript submitted for publication.

Golberg J.M., Leyreloup A.F., 1990, High temperature-low pressure Cretaceous metamorphism related to crustal thinning (Eastern North Pyrenean Zone, France). Contributed mineral petrology, vol. 104, p. 194-207.

Greiling R. O., Garfunkel Z., Zachrisson E., 1999, Evolution of the orogenic wedge in the central Scandinavian Caledonides and its interaction with the foreland lithosphere. A reply. GFF, 121:2, 154-154

Greiling R.O., Grimmer C.J., De Wall H., Björk L., 2007, Mesoproterozoic dyke swarms in foreland and nappes of the central Scandinavian Caledonides: structure, magnetic fabric, and geochemistry. Geol. Mag. 144 (3). p. 525-546.

Grimmer J.C., Glodny J., Drüppel K., Greiling R.O., Kontny A., 2015, Early- to mid-Silurian extrusion wedge tectonics in the cental Scandinavian Caledonides. Geology (43). p. 347-350.

Hacker, B. R., & Gans, P. B. (2005). Continental collisions and the creation of ultrahigh-pressure terranes: Petrology and thermochronology of nappes in the central Scandinavian Caledonides. Geological Society of America Bulletin, *117(1-2), 117-134.*

Hawthorne F.C., Oberti R., Harlow G.E., Maresch W.V., Martin R.F., Schumacher J.C., Welch M.D., 2012, Nomenclature of the amphibole supergroup. Mineralogical Society of America. 97(11-12), p. 2031-2048.

Hermann J., Spandler C., Hack A., Korsakov A.V., 2006, Aqueous fluids and hydrous melts in high-pressure and ultra-high pressure rocks: Implications for element transfer in subduction zones. Lithos, vol. 92, p. 399-417.

Holdaway M. J., 1971, Stability of andalusite and the aluminum silicate phase diagram. American Journal of Science, 271, p. 97-131.

Janák, M., van Roermund, H., Majka, J., & Gee, D. (2013). UHP metamorphism recorded by kyanite-bearing eclogite in the Seve Nappe Complex of northern Jämtland, Swedish Caledonides. Gondwana Research, 23(3), 865-879.

Kapsiotis A., Tsikouras B., Gammatikopoulos T.A., Karipi Σ., Hatzipanaqiotoi K., 2007, On the metamorphic modification of Cr-spinel compositions from the ultrabasic rocks of the Pindos ophiolite complex (NW Greece). Bulletin of the Geological Society of Greece, 40(2), p. 781-793

Koons P.O., 1982, An experimental investigation of the behavior of amphibole in the system Na_2O-MgO-Al_2O_3-SiO_2-H_2O at high pressures. Contributions to Mineralogy and Petrology, 79, p. 258-267.

Leake B.E., Wooley A.R., Arps C.E.S., et al., 1997, Nomenclature of amphiboles: report of the subcommittee on amphiboles of the international mineralogical association, commission of new minerals and mineral names. Am. Mineral. Vol. 82, p. 1019-1037

Lee J.K.W., Williams I.S., Ellis D.J., 1997, Pb, U and Th diffusion in natural zircon. Letters to nature.

Li Z.X., Bogdanova S.V., Collins A.S., et al., 2007, Assembly, configuration and break-up history of RondiniaL A synthesis. Precambrian research, vol. 160, p. 179-210.

Li Z.X., Bogdanova S.V., Collins A.S., Davidson A., de Waele B., Ernst R.E., Fitzsimons I.C.W., Fuck R.A., Gladkochub D.P., Jacobs J., Karlstrom K.E., Lu S., Natapov L.M., Paese V., Pisarevsky S.A., Thrane K., Vernikovsky V., 2008. Assembly, configuration, and break-up history of Rodinia: A synthesis. Precambrian Research, 160 (1-2), 179-210

Majka J., Be'eri-Shlevin Y., Gee D.G., Ladenberger A., Claesson S., Konečny P., 2010, Multiple monazite growth in the Åreskutan migmatites: evidence for a polymetamorphic Caledonian evolution of the Seve Nappe Complex in west-central Jämtland, Sweden. Manuscript.

Majka, J., Rosén, Å., Janák, M., Froitzheim, N., Klonowska, I., Manecki, M., ... & Yoshida, K. (2014). Microdiamond discovered in the Seve Nappe (Scandinavian Caledonides) and its exhumation by the "vacuum-cleaner" mechanism. Geology, 42(12), 1107-1110.

Mellini, M., Rumori, C., & Viti, C. (2005). Hydrothermally reset magmatic spinels in retrograde serpentinites: formation of "ferritchromit" rims and chlorite aureoles. Contributions to Mineralogy and Petrology, 149(3), 266-275.

Palme H., O'Neill H. St. C., 2003, Cosmochemical Estimates of Mantle Composition. Treatise on geochemistry. Vol.2, p. 1-38.

Qvale, H., & Stigh, J. (1985). Ultramafic rocks in the Scandinavian Caledonides.The Caledonide Orogen: Scandinavia and Related Areas: Chichester, UK, Wiley, 693-715.

Ramsay D. M., Sturt B.A., 1977, A sub-Caledonian unconformity within the Finnmarkian nappe sequence and its regional significance. Norges geol. Unders., 334, p. 107-116

Roberts D., Walker N., Slagstad T., Solli A., Krill A., 2002. U-Pb zircon ages from the Bymarka ophiolite near Trondheim, central Norwegian Caledonides, and regional implications. Nor. Geol. Tidsskr. 82, 19-30

Roberts D., 2003, The Scandinavian Caledonides: event chronology, palaeogeographic settings and likely modern analogues. Tectonophysics, Volume 365, p. 283-299.

Van Roermund H.L.M., 1989, High-pressure ultramafic rocks from the allochtonous nappes of the Swedish Caledonides. The Caledonide geology of Scandinavia. p. 205-219.

van Roermund, H. L.M., & Bakker, E. (1983). Structure and metamorphism of the Tången—Inviken area, Seve Nappes, Central Scandinavian Caledonides.Geologiska Föreningen i Stockholm Förhandlingar, 105(4), 301-319.

Van Roermund H.L.M., 2009, Mantle-wedge garnet peridotites from the northernmost ultra-high pressure domain of the Western Gneiss Region, SW Norway. European Journal of Mineralogy. Vol 21(6), p. 301-319.

Rowley D.B., 2002, Rate of plate creation and destruction: 180 Ma to present. Geological society of America Bulletin. Vol.114. no.8. p. 927-933.

Sturt B.A., Pringle I., Ramsay D.M., 1978, The Finnmarkian phase of the Caledonian orogeny. Journal of Geological Society London, Volume 135, p. 597-610

Sturt B.A., Roberts D., 1991, Tectonostratigraphic relationships and obduction histories of Scandinavian ophiolitic terranes. In: Peters T. (Ed.), Ophiolite Genesis and Evolution of the Ocean Lithosphere. Min. Petrol. Mineral., Sultanate of Oman, p. 745-769.

Thompson A.B., 1982, Dehydration melting of politic rocks and the generation of H_2O-understurated granitic liquids. American journal of science, vol. 282. p. 1567-1596.

Thompson P.H., 1989, Moderate overthickening of thinned sialic crust and the origin of granitic magmatism and regional metamorphism in low-P-high-T terranes. Geology, vol. 17, no. 6, p. 520-523.

Torsvik, T. H., Smethurst, M. A., Meert, J. G., Van der Voo, R., McKerrow, W. S., Brasier, M. D., ... & Walderhaug, H. J. (1996). Continental break-up and collision in the Neoproterozoic and Palaeozoic—a tale of Baltica and Laurentia.Earth-Science Reviews, 40(3), 229-258.

Torsvik, T. H. (1998). Palaeozoic palaeogeography: a North Atlantic viewpoint.GFF, 120(2), 109-118.

Torsvik, T. H., & Rehnström, E. F. (2001). Cambrian palaeomagnetic data from Baltica: implications for true polar wander and Cambrian palaeogeography. Journal of the Geological Society, 158(2), 321-329.

Torsvik, T. H., & Cocks, L. R. M. (2005). Norway in space and time: a centennial cavalcade. Norwegian Journal of Geology, 85(1-2), 73-86.

Trouw R.A.E., 1973. Structural geology of the Marsfjällen area, Caledonides of Västerbotten, Sweden. Sveriges Geologiske Undersokning, C689, p. 1-155

Tuccillo M.E., Essene E.J., van der Pluijm B.A., 1990, Growth and retrograde zoning in garnets from high-grade metapelites: Implications for pressure-temperature paths. Geology, vol. 18, no. 9, p. 839-842.

Walter, M. J. (1998). Melting of garnet peridotite and the origin of komatiite and depleted lithosphere. Journal of Petrology, 39(1), 29-60.

Williams, P. F., & Zwart, H. J. (1977). A model for the development of the Seve-Köli Caledonian nappe complex. In Energetics of geological processes (p. 169-187).

Wyllie J.P., 1969, The origin of ultramafic and ultrabasic rocks. Tectonophysics, 7(5), p. 437-455.

Yoshinobu A.S., Barnes C.G., Nordgulen Ø., et al., 2002, Ordovician magmatism, deformation, and exhumation in the Caledonides of central Norway: An orphan of the Taconic orogeny?. Geology, vol. 30, no. 10, p. 883-886.

Zane, A., & Weiss, Z. (1998). A procedure for classifying rock-forming chlorites based on microprobe data. Rendiconti Lincei, 9(1), 51-56.

Zhang C., van Roermund H., Zhang L., 2010, Using garnet peridotites as tools to reconstruct paleo-geodynamic settings of fossil continental collision zones. EGU General Assembly Conference Abstracts. Vol. 12, p. 5928)

Zwart H.J., 1974, Structure and metamorphism in the Seve-Köli Nappe Complex (Scandinavian Caledonides) and its implications concerning the formation of metamorphic nappes. Annales de la société géologique de Belgique. 308-311.

11.0 Appendices

11.1 EMP Chemical data

In the tables below the first column shows the mineral thought to represent the measurement. All percentages are in wt%.

11.1.1 2c1b

Comment	Na2O	SiO2	TiO2	Cr2O3	K2O	CaO	MgO	Al2O3	FeO	MnO	NiO
2c1b-kyanite-01	0,01	49,60	0,01	0,01	0,01	0,00	0,00	50,05	0,30	0,01	0,00
2c1b-tita-02	0,05	42,48	0,45	0,01	0,00	4,77	6,43	13,82	31,68	0,29	0,03
2c1b-kyan-03	8,87	67,68	0,00	0,00	0,05	7,15	0,00	16,00	0,24	0,01	0,00
2c1b-titan-04	0,05	0,04	49,62	0,00	0,00	0,02	0,05	0,03	45,47	4,72	0,00
2c1b-sill-05	0,02	0,09	97,73	0,02	0,00	0,23	0,03	0,06	1,52	0,29	0,00
2c1b-garn-06 Line 001	0,06	42,43	0,09	0,00	0,00	6,89	1,39	13,92	24,35	10,87	0,00
2c1b-garn-06 Line 002	0,04	42,40	0,02	0,02	0,00	7,08	1,38	13,90	24,50	10,66	0,00
2c1b-garn-06 Line 003	0,08	42,59	0,03	0,00	0,00	7,08	1,40	13,85	24,75	10,20	0,02
2c1b-garn-06 Line 004	0,04	42,29	0,03	0,00	0,00	6,94	1,32	14,07	25,30	9,99	0,01
2c1b-garn-06 Line 005	0,37	42,06	0,03	0,00	0,69	7,03	1,34	13,87	25,07	9,54	0,00
2c1b-garn-06 Line 006	0,09	42,43	0,10	0,00	0,00	6,81	1,36	14,02	25,85	9,34	0,00
2c1b-garn-06 Line 007	0,09	42,44	0,01	0,01	0,05	7,19	1,37	13,93	26,35	8,57	0,00
2c1b-garn-06 Line 008	0,10	42,21	0,12	0,00	0,01	7,11	1,45	13,86	26,96	8,15	0,03
2c1b-garn-06 Line 009	0,16	42,39	0,02	0,00	0,00	7,48	1,61	13,97	27,02	7,36	0,00
2c1b-garn-06 Line 010	0,10	42,23	0,01	0,00	0,00	6,13	2,05	13,97	28,25	7,25	0,02
2c1b-garn-06 Line 011	0,05	42,21	0,02	0,01	0,00	6,35	2,27	13,99	28,68	6,42	0,00
2c1b-garn-06 Line 012	0,06	42,40	0,04	0,01	0,00	6,40	2,29	13,90	28,86	6,03	0,00
2c1b-garn-06 Line 013	0,07	42,47	0,01	0,00	0,00	6,66	2,58	13,84	28,88	5,50	0,00
2c1b-garn-06 Line 014	0,02	42,39	0,03	0,00	0,00	5,97	2,90	13,97	29,58	5,13	0,00
2c1b-garn-06 Line 015	0,07	42,27	0,00	0,01	0,00	5,06	3,28	13,99	30,34	4,98	0,00
2c1b-garn-06 Line 016	0,05	42,25	0,01	0,00	0,00	4,37	3,86	13,97	30,70	4,79	0,00

	Na2O	SiO2	TiO2	Cr2O3	K2O	CaO	MgO	Al2O3	FeO	MnO	NiO
2c1b-garn-06 Line 017	0,03	42,03	0,02	0,00	0,02	3,57	4,56	13,95	31,18	4,63	0,01
2c1b-garn-06 Line 018	0,10	42,08	0,00	0,00	0,01	2,39	5,24	14,05	31,92	4,21	0,01
2c1b-garn-06 Line 019	0,07	42,16	0,00	0,00	0,00	2,63	6,06	14,12	32,12	2,82	0,01
2c1b-garn-06 Line 020	0,07	42,25	0,00	0,00	0,01	2,72	6,81	14,19	32,18	1,76	0,00
2c1b-alum-06	1,84	59,41	1,10	0,00	7,86	0,01	0,67	27,70	1,30	0,06	0,04
2c1b-sill-07	1,58	58,52	1,55	0,02	8,09	0,05	0,74	27,72	1,61	0,06	0,05
2c1b-kyan-08	1,31	58,73	0,93	0,00	8,52	0,01	1,27	26,61	2,57	0,05	0,00
2c1b-kyan-09	11,40	71,36	0,00	0,00	0,11	2,86	0,02	13,60	0,53	0,11	0,00

11.1.2 3w2xtr

Comment	Na2O	SiO2	TiO2	Cr2O3	K2O	CaO	MgO	Al2O3	FeO	MnO	NiO
3w2xtr-trem-01	0,25	52,84	0,00	0,02	0,04	12,72	32,33	0,31	1,37	0,04	0,06
3w2xtr-ol-02	0,00	32,96	0,00	0,00	0,00	0,01	59,89	0,01	6,82	0,11	0,21
3w2xtr-ol-03	0,02	32,97	0,00	0,00	0,00	0,00	60,06	0,00	6,60	0,13	0,21
3w2xtr-trem-04	0,10	53,18	0,00	0,00	0,02	12,61	32,65	0,05	1,23	0,11	0,05
3w2xtr-spinel-05	0,06	0,06	0,28	15,07	0,00	0,00	2,18	0,05	81,39	0,66	0,27
3w2xtr-Ol-06	0,00	32,70	0,01	0,01	0,00	0,00	60,00	0,00	6,97	0,13	0,18
3w2xtr-Serpl-07	0,03	39,10	0,00	0,00	0,00	0,04	58,42	0,06	1,65	0,53	0,17
3w2xtr-Trem-08	0,12	52,79	0,00	0,01	0,02	12,60	32,93	0,08	1,38	0,06	0,02
3w2xtr-Ol-09	0,02	32,71	0,00	0,00	0,00	0,00	60,32	0,00	6,66	0,13	0,16
3w2xtr-chl-10	0,06	34,03	0,01	1,18	0,02	0,01	52,82	8,20	3,55	0,02	0,10
3w2xtr-Serp-11	0,01	41,17	0,00	0,05	0,00	0,00	55,24	0,45	3,04	0,02	0,02
3w2xtr-Ol-12	0,02	32,44	0,00	0,00	0,01	0,00	60,26	0,00	6,95	0,15	0,17
3w2xtr-trem-13	0,15	52,78	0,01	0,02	0,02	12,54	32,82	0,13	1,45	0,06	0,03
3w2xtr-Mag-14	0,08	0,88	0,00	0,00	0,00	0,01	1,29	0,07	96,35	0,78	0,54
3w2xtr-Trem-15	0,01	32,76	0,00	0,00	0,00	0,00	60,01	0,01	6,94	0,11	0,15
3w2xtr-Ol-16	0,01	32,70	0,00	0,00	0,00	0,00	60,08	0,00	6,91	0,14	0,17
3w2xtr-Serp-17	0,02	41,96	0,01	0,01	0,00	0,00	55,19	0,29	2,42	0,01	0,09

Comment	Na2O	SiO2	TiO2	Cr2O3	K2O	CaO	MgO	Al2O3	FeO	MnO	NiO
3w2xtr-Trem-18	1,34	49,19	0,04	0,26	0,30	13,04	30,26	3,08	2,42	0,04	0,02
3w2xtr-Ol-19	0,04	32,10	0,01	0,00	0,01	0,02	60,53	0,07	6,94	0,14	0,15
3w2xtr-Serp-20	0,02	41,93	0,00	0,02	0,01	0,00	55,06	0,20	2,64	0,03	0,10

11.1.3 ER2C

Comment	Na2O	SiO2	TiO2	Cr2O3	K2O	CaO	MgO	Al2O3	FeO	MnO	NiO
ER2C-Spin-01	0,00	0,03	0,11	10,11	0,00	0,00	5,03	0,36	83,09	0,43	0,83
ER2C-Spin-02	0,02	0,01	0,12	9,80	0,00	0,00	4,82	0,35	83,61	0,42	0,84
ER2C-Spin-03	0,05	0,03	0,13	10,75	0,00	0,01	4,95	0,41	82,37	0,57	0,73
ER2C-Spin-04 Line 001	0,01	0,01	0,11	10,52	0,00	0,00	5,17	0,38	82,61	0,45	0,74
ER2C-Spin-04 Line 002	0,01	0,01	0,09	10,44	0,00	0,00	5,00	0,36	82,84	0,49	0,75
ER2C-Spin-04 Line 003	0,00	0,02	0,10	10,30	0,00	0,00	5,10	0,40	82,80	0,47	0,80
ER2C-Spin-04 Line 004	0,00	0,01	0,13	10,31	0,00	0,00	5,06	0,36	82,80	0,48	0,84
ER2C-Spin-04 Line 005	0,00	0,00	0,12	10,18	0,00	0,00	5,04	0,39	82,98	0,47	0,83
ER2C-Spin-04 Line 006	0,00	0,04	0,09	10,16	0,00	0,00	5,03	0,33	83,12	0,47	0,75
ER2C-Spin-04 Line 007	0,00	0,04	0,08	10,12	0,00	0,00	4,86	0,36	83,36	0,45	0,73
ER2C-Spin-04 Line 008	0,00	0,04	0,12	10,13	0,00	0,00	4,95	0,38	83,08	0,45	0,84
ER2C-Spin-04 Line 009	0,00	0,03	0,13	10,00	0,00	0,00	5,06	0,38	83,21	0,49	0,70
ER2C-Spin-04 Line 010	0,00	0,04	0,10	9,98	0,00	0,01	5,01	0,36	83,20	0,49	0,82
ER2C-Spin-04 Line 011	0,00	0,01	0,09	10,10	0,00	0,00	5,30	0,39	82,85	0,48	0,78
ER2C-Spin-04 Line 012	0,00	0,35	0,12	11,44	0,00	0,10	1,89	0,58	84,28	0,51	0,72
ER2C-Spin-04 Line 013	0,01	0,02	0,13	10,20	0,00	0,01	5,04	0,36	82,95	0,48	0,79
ER2C-Spin-04 Line 014	0,00	0,04	0,10	9,95	0,00	0,01	5,10	0,39	83,19	0,46	0,77
ER2C-Spin-04 Line 015	0,00	0,03	0,14	9,85	0,00	0,01	4,97	0,38	83,35	0,49	0,79
ER2C-Spin-04 Line 016	0,00	0,02	0,10	9,79	0,00	0,00	5,10	0,36	83,39	0,47	0,76
ER2C-Spin-04 Line 017	0,00	0,00	0,11	9,68	0,00	0,00	4,96	0,37	83,53	0,47	0,88
ER2C-Spin-04 Line 018	0,00	0,40	0,09	9,52	0,00	0,00	5,27	0,65	82,89	0,45	0,73
ER2C-Spin-04 Line 019	0,04	4,21	0,09	8,61	0,00	0,02	10,46	0,52	75,00	0,38	0,67

Comment	Na2O	SiO2	TiO2	Cr2O3	K2O	CaO	MgO	Al2O3	FeO	MnO	NiO
ER2C-Spin-04 Line 020	0,00	0,03	0,13	9,48	0,00	0,01	4,93	0,35	83,84	0,44	0,80
ER2C-Spin-04 Line 021	0,00	0,00	0,10	9,52	0,00	0,01	4,97	0,39	83,75	0,43	0,83
ER2C-Spin-04 Line 022	0,00	0,04	0,13	9,49	0,00	0,02	4,99	0,36	83,70	0,43	0,85
ER2C-Spin-04 Line 023	0,02	0,11	0,08	9,15	0,00	0,01	4,70	1,25	83,49	0,43	0,76
ER2C-Spin-04 Line 024	0,00	0,00	0,15	9,99	0,00	0,00	5,20	0,39	82,99	0,49	0,79
ER2C-Spin-04 Line 025	0,00	0,06	0,11	9,87	0,00	0,00	5,43	0,40	82,85	0,47	0,81
ER2C-Chl-04	0,00	33,49	0,00	0,80	0,00	0,02	52,22	9,90	3,39	0,01	0,17
ER2C-ol-04	0,02	32,79	0,00	0,00	0,00	0,01	61,84	0,00	5,01	0,09	0,25
ER2C-ol-04	0,01	32,76	0,00	0,00	0,00	0,01	62,09	0,00	4,78	0,09	0,25
ER2C-serp-04	0,01	33,31	0,00	0,91	0,00	0,01	53,43	9,17	2,98	0,02	0,16
ER2C-magn-04	0,01	0,01	0,12	10,08	0,00	0,01	4,45	0,39	83,73	0,51	0,70
ER2C-OPX-04	0,00	49,44	0,00	0,00	0,00	0,09	46,15	0,23	3,97	0,11	0,00
ER2C-OPX-04	0,00	49,76	0,01	0,00	0,00	0,10	45,98	0,18	3,79	0,12	0,06
ER2C-chr-04	0,00	0,03	0,12	10,87	0,00	0,00	4,17	0,44	83,12	0,58	0,66
ER2C-chl-04	0,00	33,45	0,02	0,70	0,00	0,03	52,19	9,99	3,46	0,02	0,14
ER2C-OPX-04	0,00	49,44	0,01	0,00	0,00	0,09	46,18	0,32	3,80	0,11	0,03

11.1.4 W16

Comment	Na2O	SiO2	TiO2	Cr2O3	K2O	CaO	MgO	Al2O3	FeO	MnO	NiO
W16-magn-01	0,07	0,05	0,05	3,66	0,00	0,00	6,32	0,04	88,55	0,53	0,72
W16-ol-02	0,00	32,74	0,00	0,00	0,00	0,00	64,64	0,01	2,37	0,14	0,11
W16-serp-03	0,01	41,50	0,00	0,03	0,00	0,00	57,07	0,33	1,02	0,01	0,03
W16-ol-04	0,00	32,91	0,00	0,00	0,00	0,01	64,61	0,00	2,21	0,12	0,13
W16-ol-05	0,01	32,70	0,01	0,00	0,00	0,00	64,70	0,00	2,39	0,11	0,10
W16-ol-06	0,01	32,58	0,00	0,00	0,00	0,01	64,72	0,00	2,39	0,13	0,15
W16-magn-07	0,02	10,17	0,00	0,45	0,00	0,00	32,65	0,01	56,06	0,18	0,45
W16-magn-08 Line 001	0,00	0,03	0,08	5,39	0,00	0,00	6,90	0,02	85,91	0,88	0,80
W16-magn-08 Line 002	0,02	0,03	0,12	6,10	0,00	0,00	7,01	0,01	85,04	0,87	0,80

Comment	Na2O	SiO2	TiO2	Cr2O3	K2O	CaO	MgO	Al2O3	FeO	MnO	NiO
W16-magn-08 Line 003	0,07	0,37	0,07	6,82	0,00	0,01	8,32	0,02	82,52	1,01	0,79
W16-magn-08 Line 004	0,05	0,03	0,09	7,32	0,00	0,04	7,54	0,03	83,17	1,01	0,73
W16-magn-08 Line 005	0,04	0,41	0,09	7,61	0,00	0,03	8,21	0,02	81,75	1,09	0,74
W16-magn-08 Line 006	0,03	0,02	0,10	7,94	0,00	0,00	7,88	0,02	82,19	1,04	0,78
W16-magn-08 Line 007	0,00	0,01	0,10	7,72	0,00	0,00	7,74	0,02	82,52	1,13	0,75
W16-magn-08 Line 008	0,00	0,00	0,07	7,23	0,00	0,00	7,53	0,00	83,48	0,95	0,74
W16-magn-08 Line 009	0,00	0,01	0,10	6,65	0,00	0,00	7,44	0,03	84,08	0,92	0,76
W16-magn-08 Line 010	0,00	0,03	0,10	6,15	0,00	0,00	7,19	0,03	84,98	0,81	0,71
W16-magn-08 Line 011	0,03	0,02	0,07	5,58	0,00	0,00	7,10	0,03	85,65	0,76	0,75
W16-magn-08 Line 012	0,06	0,01	0,05	5,03	0,00	0,01	6,84	0,02	86,55	0,69	0,76
W16-magn-08 Line 013	0,03	0,00	0,08	4,66	0,00	0,00	6,74	0,01	87,10	0,63	0,75
W16-magn-08 Line 014	0,03	0,03	0,06	4,29	0,00	0,00	6,41	0,01	87,83	0,60	0,75
W16-ol-022	0,04	32,28	0,01	0,03	0,01	0,01	63,11	0,00	4,18	0,23	0,09
W16-ol-023	0,02	33,11	0,00	0,00	0,01	0,01	63,96	0,03	2,41	0,32	0,13
W16-serp ovg-024	0,02	41,59	0,00	0,03	0,01	0,00	56,89	0,36	1,04	0,01	0,07
W16-magn-025	0,09	0,15	0,10	15,10	0,00	0,00	10,74	0,26	70,60	2,59	0,37
W16-ol-026	0,11	33,42	0,00	0,01	0,01	0,01	62,96	0,08	3,04	0,23	0,14
W16-magn-027	0,02	0,02	0,04	2,63	0,00	0,00	5,28	0,01	90,91	0,43	0,67
W16-Serp-028	0,01	41,73	0,00	0,02	0,00	0,00	56,44	0,27	1,48	0,02	0,03
W16-ol-029	0,06	29,12	0,00	0,01	0,01	0,02	63,01	0,09	7,31	0,24	0,15
W16-Trem-030	0,06	49,82	0,00	0,01	0,01	24,88	24,65	0,00	0,54	0,02	0,01
W16-magn-031	0,03	0,07	0,05	12,16	0,00	0,00	10,16	0,05	75,63	1,27	0,58

11.1.5 4e1

Comment	Na2O	SiO2	TiO2	Cr2O3	K2O	CaO	MgO	Al2O3	FeO	MnO	NiO
4e1-opx-01	0,03	53,31	0,00	0,00	0,00	0,51	40,06	0,02	5,80	0,19	0,08
4e1-ol-02	0,02	32,91	0,00	0,00	0,00	0,02	60,62	0,01	6,20	0,08	0,14
4e1-spinel-03	0,00	0,12	1,36	24,13	0,00	0,03	3,44	1,79	67,92	1,09	0,12

4e1-ol-04	0,02	33,14	0,00	0,00	0,00	0,01	60,12	0,00	6,40	0,09	0,21
4e1-serp-05	0,04	56,63	0,02	0,01	0,01	0,02	42,12	0,04	1,05	0,01	0,06
4e1-antho-06	0,12	53,32	0,00	0,00	0,01	0,43	40,42	0,02	5,47	0,19	0,01
4e1-serp-07	0,05	56,87	0,02	0,02	0,01	0,00	42,06	0,04	0,87	0,00	0,07
4e1-spinel-08	0,01	0,01	0,04	32,41	0,00	0,00	16,58	13,74	36,59	0,62	0,00
4e1-chl-09	1,25	48,58	0,05	0,87	0,20	12,96	29,06	4,52	2,44	0,05	0,04
4e1-serp-10	0,02	38,44	0,00	0,25	0,01	0,06	53,94	0,65	6,35	0,27	0,03
4e1-sulf-11	0,12	0,05	0,00	0,00	0,00	0,02	0,15	0,00	71,24	0,00	28,42
4e1-chrom-12	0,00	0,10	1,10	25,53	0,00	0,00	6,05	2,01	64,00	0,90	0,31
4e1-chl-13	0,00	33,70	0,06	0,96	0,00	0,00	52,05	9,83	3,21	0,02	0,17
4e1-ol-14	0,00	32,84	0,00	0,01	0,00	0,01	59,93	0,00	6,91	0,09	0,20
4e1-ol-15	0,01	53,51	0,01	0,02	0,00	0,39	40,36	0,03	5,42	0,19	0,06
4e1-serp-16	0,04	57,01	0,03	0,02	0,01	0,03	41,54	0,10	1,09	0,01	0,10
4e1-ol-17	0,03	55,18	0,00	0,02	0,01	0,06	42,65	0,18	1,70	0,04	0,13
4e1-spin-18	0,07	0,14	0,00	0,06	0,00	0,02	0,23	0,00	55,97	0,01	43,51
4e1-OPX-19	0,04	53,37	0,02	0,01	0,00	0,51	40,19	0,02	5,56	0,20	0,08
4e1-ol-20	0,04	33,02	0,01	0,00	0,01	0,01	60,28	0,00	6,35	0,09	0,21
4e1-spin-21	0,07	0,40	0,05	33,79	0,00	0,11	16,54	12,52	35,90	0,61	0,00
4e1-spin-22	0,06	0,21	0,92	27,78	0,00	0,03	7,18	1,50	61,14	0,89	0,28
4e1-ol-23	0,02	32,91	0,00	0,00	0,00	0,03	60,34	0,01	6,38	0,10	0,21
4e1-opx-24	0,01	53,86	0,01	0,01	0,00	0,56	39,80	0,04	5,48	0,18	0,04
4e1-spin-25 Line 001	0,02	0,10	0,09	33,15	0,00	0,01	14,49	10,63	40,66	0,76	0,09
4e1-spin-25 Line 002	0,26	0,40	0,03	32,67	0,08	0,06	14,52	11,23	39,99	0,70	0,07
4e1-spin-25 Line 003	0,12	0,05	0,06	33,20	0,01	0,01	14,37	10,65	40,72	0,74	0,05
4e1-spin-25 Line 004	0,05	0,08	0,06	32,84	0,00	0,01	14,45	10,51	41,25	0,71	0,05
4e1-spin-25 Line 005	0,14	0,05	0,02	32,86	0,01	0,00	14,45	10,49	41,31	0,67	0,00
4e1-spin-25 Line 006	0,10	0,07	0,08	32,89	0,01	0,04	14,28	10,39	41,36	0,73	0,06
4e1-spin-25 Line 007	0,10	0,06	0,08	32,81	0,00	0,00	14,22	10,20	41,76	0,72	0,05
4e1-spin-25 Line 008	0,05	0,04	0,10	32,90	0,00	0,00	14,24	10,18	41,74	0,73	0,01

4e1-spin-25 Line 009	0,03	0,05	0,11	32,79	0,01	0,02	14,01	10,00	42,24	0,73	0,00
4e1-spin-25 Line 010	0,05	0,04	0,15	32,49	0,00	0,04	13,75	9,67	43,04	0,70	0,07
4e1-spin-25 Line 011	0,28	0,05	0,16	32,12	0,02	0,03	13,38	9,60	43,66	0,70	0,00
4e1-spin-25 Line 012	0,14	0,11	0,25	32,39	0,02	0,02	13,20	9,15	43,93	0,69	0,11
4e1-spin-25 Line 013	0,18	0,03	0,25	32,23	0,01	0,00	12,68	8,82	44,92	0,77	0,12
4e1-spin-25 Line 014	0,11	0,01	0,28	31,89	0,01	0,03	12,37	8,44	46,03	0,76	0,08
4e1-spin-25 Line 015	0,13	0,03	0,32	31,44	0,00	0,00	11,58	7,75	47,96	0,70	0,08
4e1-spin-25 Line 016	0,19	0,06	0,37	30,82	0,00	0,03	10,46	6,38	50,93	0,70	0,06
4e1-spin-25 Line 017	0,13	0,04	0,55	30,08	0,00	0,04	8,88	4,07	55,25	0,81	0,16
4e1-spin-25 Line 018	0,13	0,05	0,61	29,53	0,00	0,02	7,64	2,31	58,77	0,87	0,08
4e1-spin-25 Line 019	0,15	0,02	0,69	28,59	0,00	0,05	6,35	1,53	61,60	0,88	0,15
4e1-spin-25 Line 020	0,18	0,04	0,90	25,02	0,00	0,01	5,25	1,41	66,05	0,90	0,23
4e1-spin-25 Line 021	0,12	0,06	1,10	19,85	0,00	0,01	3,26	1,10	73,38	0,88	0,24
4e1-spin-46 Line 001	0,00	0,05	0,06	32,99	0,00	0,00	17,04	13,77	35,43	0,65	0,00
4e1-spin-46 Line 002	0,01	0,21	0,03	32,78	0,00	0,04	17,02	13,78	35,42	0,69	0,03
4e1-spin-46 Line 003	0,00	0,00	0,03	32,86	0,00	0,00	16,89	13,79	35,69	0,66	0,06
4e1-spin-46 Line 004	0,00	0,00	0,04	32,87	0,00	0,00	16,97	13,83	35,69	0,59	0,00
4e1-spin-46 Line 005	0,00	0,06	0,01	32,75	0,01	0,01	16,90	13,73	35,87	0,63	0,05
4e1-spin-46 Line 006	0,18	0,04	0,02	32,74	0,00	0,02	16,80	13,66	35,90	0,63	0,00
4e1-spin-46 Line 007	0,00	0,02	0,03	32,57	0,00	0,00	17,02	13,71	35,94	0,62	0,09
4e1-spin-46 Line 008	0,00	0,03	0,01	32,58	0,00	0,01	16,84	13,58	36,27	0,62	0,06
4e1-spin-46 Line 009	0,00	0,02	0,03	32,47	0,00	0,00	16,76	13,44	36,60	0,64	0,03
4e1-spin-46 Line 010	0,00	0,04	0,04	32,38	0,00	0,02	16,60	13,31	36,99	0,61	0,00
4e1-spin-46 Line 011	0,00	0,05	0,00	32,37	0,00	0,02	16,13	13,40	37,32	0,60	0,11
4e1-spin-46 Line 012	0,00	0,00	0,02	32,29	0,00	0,02	16,26	13,06	37,68	0,63	0,03
4e1-spin-46 Line 013	0,00	0,00	0,05	31,98	0,00	0,01	16,10	12,89	38,32	0,63	0,03
4e1-spin-46 Line 014	0,01	0,00	0,12	31,46	0,00	0,00	15,50	12,07	40,15	0,63	0,05
4e1-spin-46 Line 015	0,08	0,05	0,19	30,78	0,00	0,00	14,57	10,91	42,75	0,65	0,02
4e1-spin-46 Line 016	0,03	0,01	0,41	29,27	0,00	0,02	12,19	7,60	49,70	0,66	0,11

	Na2O	SiO2	TiO2	Cr2O3	K2O	CaO	MgO	Al2O3	FeO	MnO	NiO
4e1-spin-46 Line 017	0,00	0,02	0,70	28,21	0,00	0,00	8,21	2,59	59,30	0,82	0,15
4e1-spin-46 Line 018	0,02	0,07	1,26	25,36	0,00	0,01	4,61	2,04	65,40	1,05	0,17
4e1-spin-46 Line 019	0,08	20,49	0,29	20,78	0,00	0,02	18,60	1,39	37,52	0,80	0,04

11.1.5 4e3

Comment	Na2O	SiO2	TiO2	Cr2O3	K2O	CaO	MgO	Al2O3	FeO	MnO	NiO
4e3-ol-hinge-01	0,05	33,00	0,00	0,00	0,00	0,01	60,81	0,00	5,78	0,08	0,27
4e3-opx-02	0,04	53,24	0,01	0,01	0,00	0,57	40,59	0,01	5,27	0,21	0,06
4e3-serp-03	0,02	37,45	0,00	0,01	0,01	0,06	56,66	0,01	5,42	0,07	0,28
4e3-ol-04	0,03	33,10	0,00	0,00	0,00	0,01	60,72	0,00	5,79	0,09	0,24
4e3-ol-05	0,01	32,91	0,00	0,00	0,00	0,01	60,89	0,00	5,85	0,07	0,25
4e3-serp-06	0,10	39,25	0,02	0,00	0,04	0,05	53,86	0,01	6,40	0,08	0,19
4e3-opx-07	0,01	53,41	0,00	0,01	0,00	0,63	40,01	0,02	5,59	0,24	0,08
4e3-trem-08	0,14	53,06	0,01	0,01	0,03	12,27	32,71	0,24	1,39	0,06	0,08
4e3-opx-09	0,04	53,39	0,00	0,01	0,01	0,55	40,46	0,01	5,23	0,20	0,11
4e3-trem-10	0,10	53,34	0,00	0,00	0,02	11,51	33,13	0,17	1,61	0,06	0,07
4e3-trem-11	0,10	53,30	0,01	0,02	0,02	12,17	32,61	0,21	1,40	0,07	0,09
4e3-serp-12	0,00	40,27	0,01	0,00	0,00	0,10	57,25	0,03	2,31	0,03	0,00
4e3-trem-13	0,18	53,09	0,02	0,00	0,09	11,80	32,91	0,22	1,53	0,06	0,09
4e3-trem-14	0,11	52,99	0,01	0,01	0,03	12,31	32,91	0,18	1,35	0,06	0,04

11.1.6 Chromite

Comment	Na2O	SiO2	TiO2	Cr2O3	K2O	CaO	MgO	Al2O3	FeO	MnO	NiO
4e4-chrom-01 Line 001	0,08	0,06	0,14	33,20	0,00	0,02	22,00	10,19	33,60	0,65	0,06
4e4-chrom-01 Line 002	0,25	0,05	0,13	33,15	0,00	0,02	22,13	10,42	33,10	0,63	0,12
4e4-chrom-01 Line 003	0,03	0,01	0,10	33,49	0,00	0,02	21,82	10,03	33,84	0,60	0,05
4e4-chrom-01 Line 004	0,09	0,02	0,06	34,46	0,00	0,02	21,44	9,54	33,78	0,60	0,00
4e4-chrom-01 Line 005	0,07	0,02	0,14	33,31	0,00	0,01	21,97	10,45	33,30	0,60	0,12

4e4-chrom-01 Line 006	0,12	0,08	0,09	33,39	0,01	0,01	22,63	10,66	32,47	0,54	0,01
4e4-chrom-01 Line 007	1,57	0,36	0,10	33,12	0,14	0,13	22,24	10,83	30,95	0,56	0,00
4e4-chrom-01 Line 008	0,03	0,05	0,11	34,07	0,02	0,00	22,57	11,34	31,18	0,58	0,06
4e4-chrom-01 Line 009	0,12	0,16	0,14	32,79	0,00	0,05	23,29	13,03	29,83	0,59	0,01
4e4-chrom-01 Line 010	0,00	0,07	0,13	33,79	0,01	0,02	23,08	11,97	30,33	0,54	0,06
4e4-chrom-01 Line 011	0,05	0,40	0,13	33,52	0,00	0,09	22,00	12,42	30,62	0,62	0,15
4e4-chrom-01 Line 012	0,00	0,00	0,15	33,94	0,00	0,00	23,21	11,62	30,40	0,59	0,10
4e4-chrom-01 Line 013	0,02	0,02	0,12	33,80	0,00	0,00	23,32	11,48	30,59	0,62	0,03
4e4-chrom-01 Line 014	0,00	0,00	0,11	33,61	0,00	0,03	23,31	11,83	30,52	0,54	0,04
4e4-chrom-01 Line 015	0,02	0,00	0,12	33,95	0,00	0,02	23,23	11,09	30,90	0,61	0,06
4e4-chrom-01 Line 016	0,05	2,37	0,10	32,56	0,01	0,48	22,90	10,57	30,37	0,55	0,04
4e4-chrom-01 Line 017	0,00	0,00	0,12	33,67	0,00	0,00	22,42	10,43	32,70	0,59	0,08
4e4-chrom-01 Line 018	0,09	0,08	0,07	33,26	0,00	0,03	21,41	9,72	34,75	0,59	0,01
4e4-chrom-01 Line 019	0,05	0,03	0,13	32,66	0,00	0,02	20,22	7,89	38,28	0,57	0,14
4e4-chrom-01 Line 020	0,05	0,00	0,13	34,80	0,00	0,00	19,01	5,71	39,49	0,69	0,12
4e4-chrom-01 Line 021	0,01	0,02	0,10	33,95	0,00	0,01	17,89	4,65	42,54	0,63	0,20
4e4-chl-01	0,00	34,03	0,00	1,50	0,00	0,01	53,31	9,54	1,46	0,01	0,13
4e4-chl-02	0,03	33,76	0,00	1,12	0,01	0,01	53,40	9,52	1,96	0,02	0,16
4e4-chl-03	0,02	33,95	0,01	1,11	0,00	0,01	53,63	9,52	1,57	0,01	0,17
4e4-chl-04	0,30	33,77	0,02	1,11	0,07	0,07	53,03	9,57	1,92	0,00	0,15
4e4-chl-05	0,00	34,33	0,00	1,29	0,00	0,01	53,24	9,43	1,52	0,03	0,16
4e4-Chro-06	0,05	0,01	0,10	34,14	0,00	0,00	23,25	10,32	31,45	0,59	0,08
4e4-Chro-07	0,03	0,04	0,14	32,72	0,00	0,08	16,87	3,50	45,71	0,71	0,20
4e4-chl-08	0,14	34,83	0,00	1,15	0,05	0,06	53,78	8,04	1,76	0,02	0,17
4e4-chl-09	0,05	33,95	0,02	1,47	0,02	0,05	54,50	8,15	1,60	0,02	0,17

11.2 SEM chemical data

In the following tables SEM measurements can be found. The data is in wt%.

11.2.1 2w1

NiO	MgO	Al2O3	SiO2	Cr2O3	CaO	MnO	FeO	S
0,00	26,76	0,00	58,27	0,00	12,27	0,00	2,70	0,00
0,00	34,21	0,00	64,32	0,00	0,00	0,00	1,46	0,00
3,24	3,02	5,84	37,01	0,00	20,62	13,28	16,99	0,00
0,86	28,86	0,02	58,06	0,00	10,64	0,18	3,37	0,00
0,00	3,11	0,00	0,00	32,63	0,00	0,00	64,26	0,00
0,00	51,03	0,00	38,69	0,00	0,00	0,00	10,28	0,00
0,00	45,16	4,27	46,10	0,00	0,00	0,00	4,47	0,00
0,00	26,76	0,00	58357,00	0,00	12,88	0,00	1,79	0,00
0,00	26,54	0,00	58,92	0,00	12,99	0,00	1,55	0,00
0,00	2,38	0,00	0,00	32,84	0,00	0,00	64,79	0,00
0,00	4,16	0,00	0,00	29,50	0,00	0,00	66,34	0,00
0,00	45,23	3,53	46,48	1,65	0,00	0,00	3,10	0,00
0,00	29,63	0,13	68,19	0,11	0,00	0,00	1,94	0,00
0,00	39,85	0,00	0,00	0,00	57,80	0,00	2,35	0,00
0,00	26,40	0,00	57,72	0,00	13,97	0,00	1,91	0,00
0,00	45,17	3,37	46,92	0,00	0,00	0,00	4,54	0,00
0,00	26,42	0,00	58,63	0,00	13,06	0,00	1,89	0,00
0,00	50,98	0,00	38,33	0,00	0,03	0,00	10,66	0,00
0,00	50,95	0,00	38,39	0,00	0,00	0,00	10,66	0,00
0,00	2,92	0,00	0,00	32,46	0,00	0,00	64,63	0,00
0,00	3,49	0,00	0,00	35,39	0,00	0,00	61,12	0,00
12,49	22,65	0,00	16,86	0,00	0,00	0,00	14,37	29,38
20,43	1,55	0,00	0,00	0,00	0,00	0,00	22,96	45,33
20,16	2,81	0,00	1,41	0,00	0,00	0,00	21,92	44,14

0,00	41,12	0,00	0,00	0,00	55,52	0,00	3,36	0,00
0,00	43,63	3,05	45,20	1,61	1,83	0,00	4,68	0,00
0,00	2,77	0,00	0,00	30,73	0,00	0,00	66,50	0,00
0,00	47,54	0,00	48,63	0,00	0,00	0,00	3,83	0,00
0,00	40,66	0,00	0,00	0,00	55,54	0,00	3,80	0,00
1,76	45,12	3,04	47,48	0,00	0,00	0,00	0,51	0,00
1,74	22,03	0,00	49,54	0,00	2,58	0,00	24,10	0,00
0,00	26,88	0,00	58,65	0,00	12,75	0,00	1,72	0,00
0,00	2,33	0,00	0,00	36,99	0,00	0,00	60,68	0,00
0,00	26,57	0,00	58,77	0,00	13,05	0,00	1,61	0,00
0,00	41,85	0,00	0,00	0,00	55,58	0,00	2,57	0,00
0,00	38,66	0,00	48,85	0,00	0,00	0,00	12,49	0,00

11.2.2 3w2

NiO	MgO	Al2O3	SiO2	Cr2O3	CaO	MnO	FeO	S
0,00	9,41	8,20	0,00	54,05	0,00	0,00	28,25	0,00
0,00	41,40	17,67	35,57	3,22	0,00	0,00	2,14	0,00
0,00	8,06	5,24	0,00	55,00	0,00	0,00	31,59	0,00
0,00	8,75	4,53	0,00	53,41	0,00	0,00	33,14	0,00
0,00	9,67	10,53	0,00	54,68	0,00	0,00	25,12	0,00
0,00	41,01	16,99	35,49	4,02	0,00	0,00	2,48	0,00
0,00	0,00	0,00	0,00	0,00	0,00	0,00		0,00
0,00	8,29	6,49	0,00	53,97	0,00	0,00	31,25	0,00
0,00	40,71	16,93	35,34	4,02	0,00	0,00	3,01	0,00
0,00	7,90	4,83	0,00	56,62	0,00	0,00	30,65	0,00
0,00	6,43	4,85	0,00	49,08	0,00	0,00	27,54	0,00
0,00	8,18	5,94	0,00	54,59	0,00	0,00	31,28	0,00
0,00	8,38	5,10	0,00	55,41	0,00	0,00	31,10	0,00

0,00	0,00	0,00	0,00	0,00	0,00	0,00		0,00
0,00	2,95	0,00	0,00	23,75	0,00	0,00	73,30	0,00
0,00	26,56	0,00	58,00	0,00	13,15	0,00	2,29	0,00
0,00	41,85	13,02	39,39	2,70	0,00	0,00	4,03	0,00
0,00	26,42	0,00	58,22	0,00	13,49	0,00	1,86	0,00
0,00	25,50	1,99	57,06	0,00	13,36	0,00	2,09	0,00
0,00	23,13	0,00	53,58	0,00	21,40	0,00	1,88	0,00
0,00	2,69	0,00	0,00	21,96	0,00	0,00	75,35	0,00
0,00	2,44	0,00	0,00	19,22	0,00	0,00	78,34	0,00
0,00	41,04	15,06	37,19	2,45	0,00	0,00	4,26	0,00
0,00	26,17	0,00	58,11	0,00	13,57	0,00	2,15	0,00
0,00	3,39	0,00	3,12	0,00	0,00	0,00	93,49	0,00
0,00	26,40	0,00	58,27	0,00	13,26	0,00	2,07	0,00
0,00		0,00	0,00	0,00	0,00	0,00		0,00
0,00	51,50	0,00	39,17	0,00	0,00	0,00	9,32	0,00
0,00	49,21	0,00	48,68	0,00	0,00	0,00	2,11	0,00
0,00	51,42	0,00	39,11	0,00	0,00	0,00	9,46	0,00
0,00	51,37	0,00	39,05	0,00	0,00	0,00	9,58	0,00
0,00	51,32	0,00	39,12	0,00	0,00	0,00	9,55	0,00
0,00	51,38	0,00	39,03	0,00	0,00	0,00	9,59	0,00
0,00	51,27	0,00	38,96	0,00	0,00	0,00	9,77	0,00
0,00	51,71	0,00	39,01	0,00	0,00	0,00	9,28	0,00
0,00	51,47	0,00	39,29	0,00	0,00	0,00	9,23	0,00
0,00	51,85	0,00	38,97	0,00	0,00	0,00	9,18	0,00

NiO	MgO	Al2O3	SiO2	Cr2O3	CaO	MnO	FeO	S
0,00	5,47	0,00	0,00	27,86	0,00	0,00	66,67	0,00
0,00	55,28	0,00	39,46	0,00	0,00	0,00	5,26	0,00
0,00	3,80	0,00	0,00	12,03	0,00	0,00	84,17	0,00
0,00	3,86	0,00	0,00	3,32	0,00	0,00	92,82	0,00
0,00	56,72	0,00	39,33	0,00	0,00	0,00	0,48	0,00
0,00	56,80	0,00	39,45	0,00	0,00	0,00	3,75	0,00
0,00	53,42	0,00	40,92	0,00	0,00	0,00	5,66	0,00
0,00	56,55	0,00	39,56	0,00	0,00	0,00	3,90	0,00
0,00	3,99	0,00	0,00	2,98	0,00	0,00	93,14	0,00
0,00	56,49	0,00	39,12	0,00	0,00	0,00	4,38	0,00
0,00	48,67	0,00	49,17	0,00	0,00	0,00	2,16	0,00
0,00	0,00	0,00	0,00	0,00	0,00	0,00	0,00	0,00
0,00	56,44	0,00	39,12	0,00	0,00	0,00	0,54	0,00
0,00	3,62	0,00	0,00	13,73	0,00	0,00	82,62	0,00
0,00	51,10	0,00	45,79	0,00	0,00	0,00	3,11	0,00
0,00	55,92	0,00	39,40	0,00	0,00	0,00	4,69	0,00
0,00	56,57	0,00	39,37	0,00	0,00	0,00	4,06	0,00
0,00	3,23	0,00	0,00	0,00	0,00	0,00	96,77	0,00
0,00	56,85	0,00	39,30	0,00	0,00	0,00	3,86	0,00
0,00	48,57	0,00	48,91	0,00	0,00	0,00	2,52	0,00
0,00	0,00	0,00	0,00	0,00	0,00	0,00	0,00	0,00
0,00	3,78	0,00	0,00	12,35	0,00	0,00	83,87	0,00
0,00	55,08	0,00	40,30	0,00	0,00	0,00	4,63	0,00
0,00	49,81	0,00	47,98	0,00	0,00	0,00	2,20	0,00
0,00	4,67	0,00	0,00	8,53	0,00	0,00	86,79	0,00
0,00	56,65	0,00	39,63	0,00	0,00	0,00	3,72	0,00
0,00	41,07	0,00	54,28	0,00	0,00	0,00	4,65	0,00

NiO	MgO	Al2O3	SiO2	Cr2O3	CaO	MnO	FeO	S
0,00	3,57	0,00	0,00	0,00	0,00	0,00	96,43	0,00
0,00	0,00	0,00	0,00	0,00	0,00	0,00	0,00	0,00
0,00	56,65	0,00	39,32	0,00	0,00	0,00	4,04	0,00
0,00	3,94	0,00	0,00	8,14	0,00	0,00	87,92	0,00
0,00	48,18	2,07	47,82	0,00	0,00	0,00	1,92	0,00
0,00	56,22	0,00	40,02	0,00	0,00	0,00	3,75	0,00
0,00	56,89	0,00	39,29	0,00	0,00	0,00	3,82	0,00
0,00	56,75	0,00	39,41	0,00	0,00	0,00	3,84	0,00
0,00	3,66	0,00	0,00	8,09	0,00	0,00	88,25	0,00
0,00	35,11	2,40	28,81	3,98	0,00	0,00	29,71	0,00

11.2.4 4e3

NiO	MgO	Al2O3	SiO2	Cr2O3	CaO	MnO	FeO	S
0,00	52,50	0,00	39,12	0,00	0,00	0,00	8,39	0,00
0,00	3,87	0,00	0,00	33,33	0,00	0,00	62,80	0,00
0,00	52,53	0,00	39,11	0,00	0,00	0,00	8,36	0,00
0,00	52,56	0,00	39,14	0,00	0,00	0,00	8,30	0,00
0,00	52,54	0,00	39,03	0,00	0,00	0,00	8,42	0,00
0,00	3,05	0,00	0,00	17,03	0,00	0,00	79,92	0,00
0,00	42,43	13,44	38,58	1,93	0,00	0,00	3,63	0,00
0,00	3,89	0,00	0,00	32,72	0,00	0,00	63,38	0,00
0,00	52,72	0,00	39,15	0,00	0,00	0,00	8,14	0,00
0,00	52,69	0,00	39,08	0,00	0,00	0,00	8,23	0,00
0,00	46,52	0,00	46,75	0,00	0,00	0,00	6,73	0,00
0,00	52,67	0,00	38,93	0,00	0,00	0,00	8,41	0,00
0,00	4,13	1,81	0,00	36,49	0,00	0,00	57,57	0,00
0,00	52,47	0,00	39,11	0,00	0,00	0,00	8,42	0,00
0,00	34,04	0,00	59,77	0,00	0,00	0,00	6,18	0,00

0,00	52,63	0,00	39,07	0,00	0,00	0,00	8,30	0,00
0,00	3,63	0,00	0,00	26,01	0,00	0,00	70,36	0,00
0,00	4,54	0,00	0,00	38,71	0,00	0,00	56,75	0,00
0,00	46,03	0,00	41,65	0,00	0,00	0,00	12,31	0,00
0,00	38,04	0,00	55,91	0,00	0,00	0,00	6,05	0,00
0,00	52,52	0,00	39,13	0,00	0,00	0,00	8,35	0,00
0,00	33,69	0,00	60,09	0,00	0,00	0,00	6,22	0,00
0,36	52,51	0,00	38,58	0,00	0,00	0,00	8,56	0,00
0,23	52,29	0,00	39,20	0,00	0,00	0,00	8,28	0,00
0,35	52,30	0,00	38,70	0,00	0,00	0,00	8,65	0,00
0,00	2,68	0,00	0,00	9,66	0,00	0,00	87,65	0,00
0,00	48,89	0,00	44,39	0,00	0,00	0,00	6,71	0,00
0,00	52,64	0,00	39,17	0,00	0,00	0,00	8,19	0,00
0,00	37,65	0,00	56,35	0,00	0,00	0,00	6,00	0,00
0,00	52,63	0,00	38,93	0,00	0,00	0,00	8,44	0,00
0,00	40,86	16,31	36,79	2,39	0,00	0,00	3,64	0,00
0,00	52,39	0,00	38,97	0,00	0,00	0,00	8,65	0,00
0,00	33,19	0,00	59,76	0,00	0,00	0,00	7,05	0,00
0,12	26,69	0,00	58,59	0,00	13,13	0,00	1,48	0,00
0,57	47,29	0,00	45,42	0,00	0,00	0,00	6,72	0,00
18,02	0.00	0,00	0,00	0,00	0,00	0,00	25,88	45,79
0,37	52,76	0,00	38,65	0,00	0,00	0,00	8,22	0,00
0,00	32,87	0,00	59,76	0,00	0,00	0,00	7,37	0,00
0,00	53,05	0,00	39,28	0,00	0,00	0,00	7,67	0,00
0,10	32,70	0,00	59,75	0,00	0,00	0,00	7,45	0,00
0,00	52,53	0,00	39,02	0,00	0,00	0,00	8,45	0,00
0,00	32,76	0,00	59,61	0,00	0,00	0,00	7,63	0,00
0,00	26,01	0,00	58,45	0,00	16,56	0,00	1,97	0,00
0,12	33,08	0,00	59,45	0,00	0,00	0,00	7,35	0,00

0,56	52,32	0,00	38,90	0,00	0,00	0,00	8,22	0,00

11.2.5 4e4

NiO	MgO	Al2O3	SiO2	Cr2O3	CaO	MnO	FeO	S
0,00	6,94	4,34	0,00	57,08	0,00	0,00	31,63	0,00
0,00	8,18	5,29	0,00	57,28	0,00	0,00	29,26	0,00
0,00	8,70	5,62	0,00	55,55	0,00	0,00	30,13	0,00
0,00	8,11	4,45	0,00	55,13	0,00	0,00	32,31	0,00
0,00	7,65	3,22	0,00	54,79	0,00	0,00	34,34	0,00
0,00	8,06	4,87	0,00	54,30	0,00	0,00	32,76	0,00
0,00	8,51	5,57	0,00	56,51	0,00	0,00	29,41	0,00
0,00	9,19	6,95	0,00	56,38	0,00	0,00	27,48	0,00
0,00	10,82	11,18	0,00	54,64	0,00	0,00	23,35	0,00
0,00	10,27	11,27	0,00	55,41	0,00	0,00	23,05	0,00
0,00	10,48	11,99	0,00	55,16	0,00	0,00	22,37	0,00
0,00	10,69	12,27	0,00	54,93	0,00	0,00	22,11	0,00
0,00	11,00	12,08	0,00	54,79	0,00	0,00	22,13	0,00
0,00	10,92	12,67	0,00	54,89	0,00	0,00	21,52	0,00

NiO	MgO	Al2O3	SiO2	Cr2O3	CaO	MnO	FeO	S
0,00	3,50	0,00	0,00	20,31	0,00	0,00	76,19	0,00
0,00	4,14	0,00	0,00	22,03	0,00	0,00	73,83	0,00
0,00	54,60	0,00	38,96	0,00	0,00	0,00	6,45	0,00
0,00	4,52	0,00	0,00	9,39	0,00	0,00	86,09	0,00
0,00	39,72	20,14	34,87	0,00	0,00	0,00	5,27	0,00
0,00	3,81	0,00	0,00	22,57	0,00	0,00	73,62	0,00
0,00	40,44	20,09	34,46	0,00	0,00	0,00	5,00	0,00
0,00	40,04	19,30	35,04	1,35	0,00	0,00	4,27	0,00
0,00	4,56	0,00	0,00	21,94	0,00	0,00	73,51	0,00
0,00	2,95	0,00	0,00	24,50	0,00	0,00	72,55	0,00
0,00	53,94	0,00	38,82	0,00	0,00	0,00	7,25	0,00
0,00	4,08	0,00	0,00	23,45	0,00	0,00	72,48	0,00
0,00	49,86	0,00	46,90	0,00	0,00	0,00	3,24	0,00
0,00	55,16	0,00	39,59	0,00	0,00	0,00	5,24	0,00
0,00	47,25	0,00	50,99	0,00	0,00	0,00	1,76	0,00
0,00	2,82	0,00	1,09	0,00	0,00	0,00	96,09	0,00
0,00	39,81	20,10	34,31	1,34	0,00	0,00	4,44	0,00
0,00	38,54	0,00	55,79	0,00	0,00	0,00	5,67	0,00
0,00	3,15	0,00	0,00	30,15	0,00	0,00	66,70	0,00
0,00	3,15	0,00	0,00	28,57	0,00	0,00	68,28	0,00
0,00	53,52	0,00	38,85	0,00	0,00	0,00	7,63	0,00
0,00	53,67	0,00	38,96	0,00	0,00	0,00	7,38	0,00
0,00	39,96	18,70	34,55	1,71	0,00	0,00	5,07	0,00
0,00	53,47	0,00	39,21	0,00	0,00	0,00	7,32	0,00
0,00	39,64	19,53	33,95	1,88	0,00	0,00	4,99	0,00
0,00	4,08	2,79	0,00	34,31	0,00	0,00	58,82	0,00
0,00	3,40	0,00	0,00	29,50	0,00	0,00	67,11	0,00

0,00	3,16	0,00	0,00	29,02	0,00	0,00	67,81	0,00
0,00	53,77	0,00	38,77	0,00	0,00	0,00	7,46	0,00
0,00	53,53	0,00	38,85	0,00	0,00	0,00	7,62	0,00
0,00	47,97	0,00	47,06	0,00	0,00	0,00	4,97	0,00
0,00	40,11	21,50	33,55	0,00	0,00	0,00	4,84	0,00
0,00	7,34	0,00	0,00	28,44	0,00	0,00	64,22	0,00
0,00	53,66	0,00	38,90	0,00	0,00	0,00	7,43	0,00
0,00	53,24	0,00	38,56	0,00	0,00	0,00	8,20	0,00
0,00	5,00	1,93	0,00	25,87	0,00	0,00	67,20	0,00
0,00	39,61	22,02	34,24	0,00	0,00	0,00	4,13	0,00
0,00	53,13	0,00	39,30	0,00	0,00	0,00	7,57	0,00
0,00	39,76	21,15	34,73	0,00	0,00	0,00	4,37	0,00
0,00	26,16	2,02	56,74	0,00	12,49	0,00	2,59	0,00

11.3 Overview thin sections

The star in the overview of the thin sections show the places at which EMP-measurements have been taken. The squares show the places where photos have been taken. In the table below a clear overview which sample has been taken from which belt is shown.

Western Belt	Central Belt	Eastern Belt/Central Belt	Köli Nappe
2c1b	Er2c	4e1	W16
2w1		4e1a	
2w1 (2)		4e4	
3w1		4e3	
3w1 (2)		5e1	
		5e1 (2)	

Overview of the thin section used for EMP-analyses. There is one clear foliation which cuts the garnets. The main foliation is expressed by quartz, biotite and muscovite. The large square is photo A&B in figure 21. The smaller square is photo C in figure 21.

Overview of a thin section made from the peridtotite located at 2w1 (figure 15). Two different textures can be seen in this thin section. The smoother texture consists of magnesite and talc. The rougher texture consists of olivine. Every black spot is magnetite. The larger square is photo A in figure 17, the smaller square is photo D in figure 17.
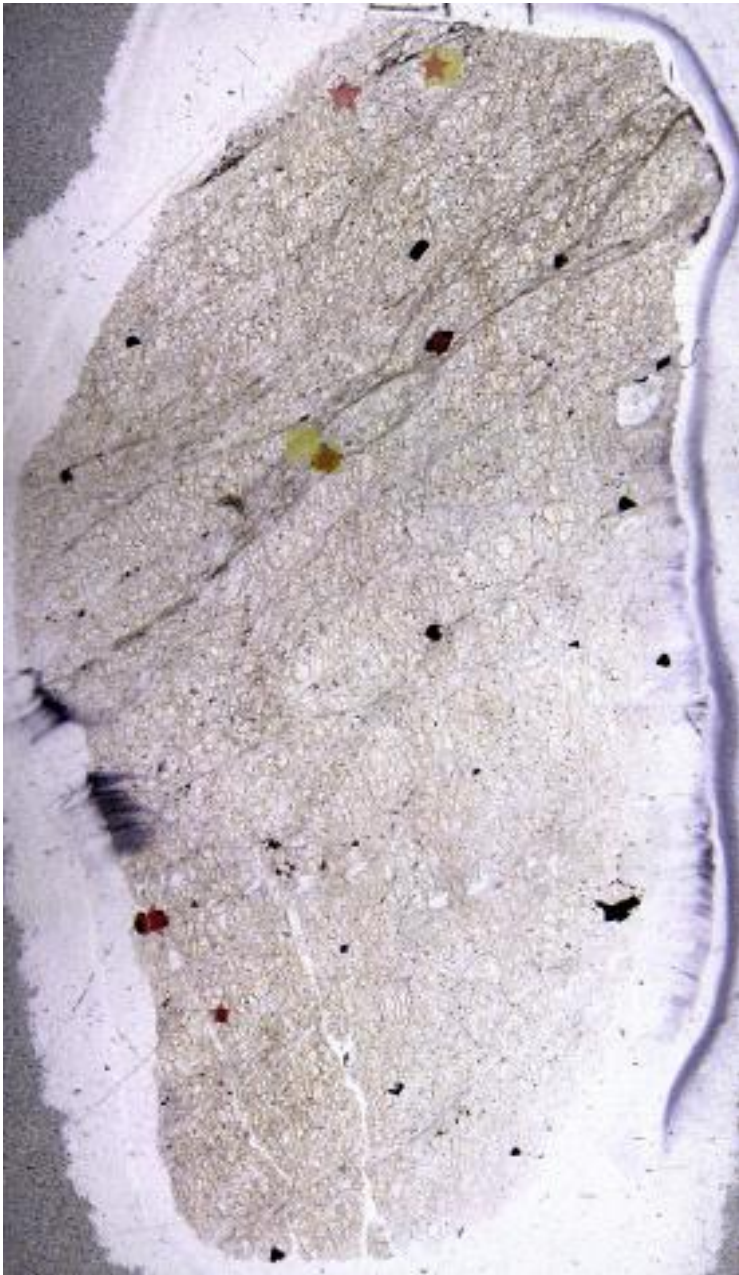
Overview of a thin section made from the peridotite body located at 2w1 (figure 15). The lower right part consists mostly of talc growing over olivine. The center left part of the thin section is olivine with slithers of chlorite, serpentine and talc. The square in the upper right corner is photo F in figure 21, the other square is photo E in figure 21.

Overview of a thin section of the peridotite located at 3w1 (figure 15). This thin section consists 90% of olivine with inclusions of magnetite, serpentine and talc. The centre right square is photo F in figure 17.
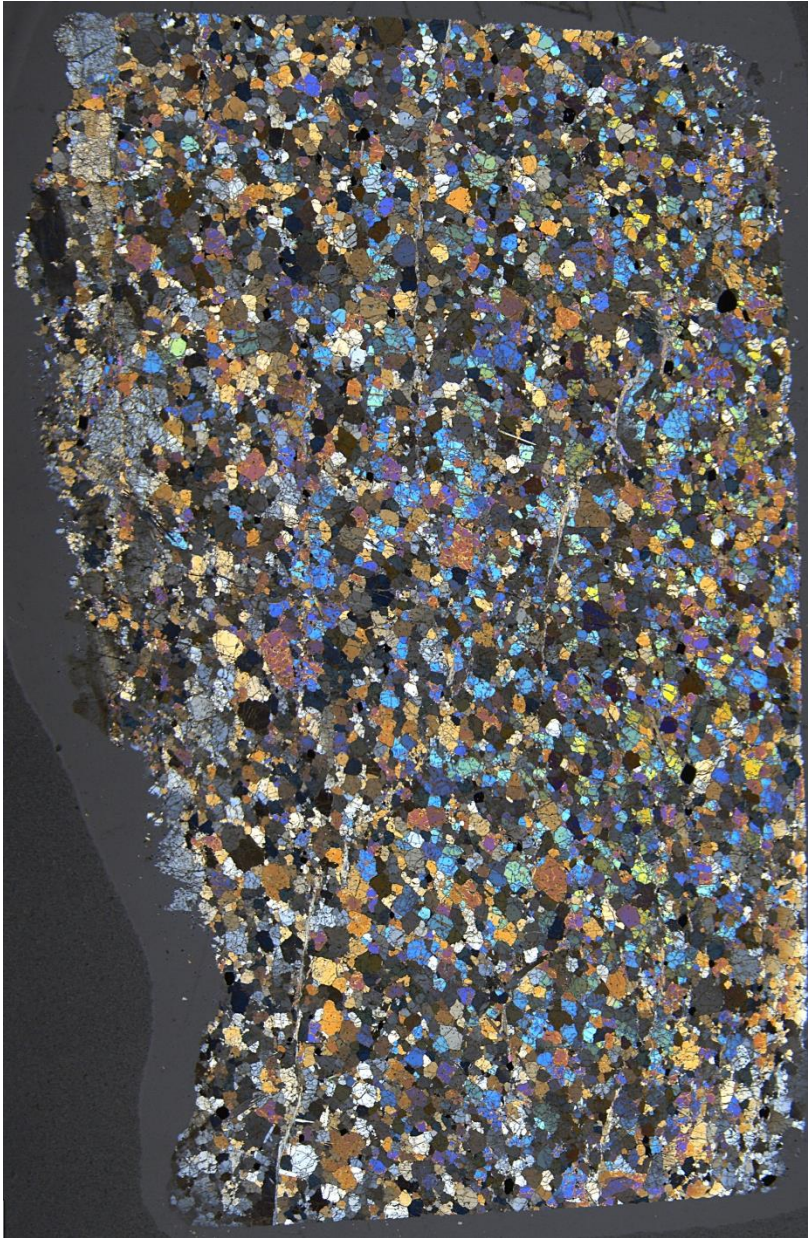
Overview of a thin section of the peridotite located at 3w1 (figure 15). This thin section consists in the upper left corner (white area) of tremolite radiantly growing over olivine. The black dots are all magnetite, where the fractured pattern throughout the section is olivine with serpentine defining some foliation. The top square is photo B in figure 17.

Overview of a thin section of the peridotite sampled at location 4e1 (figure 15). In this thin section a clear foliation expressed by mylonitic textures consisting of olivine, amphibole and serpentine. The black spots are al-rich spinels. The center square is photo A&B in figure 19, the upper square is photo D in figure 19.
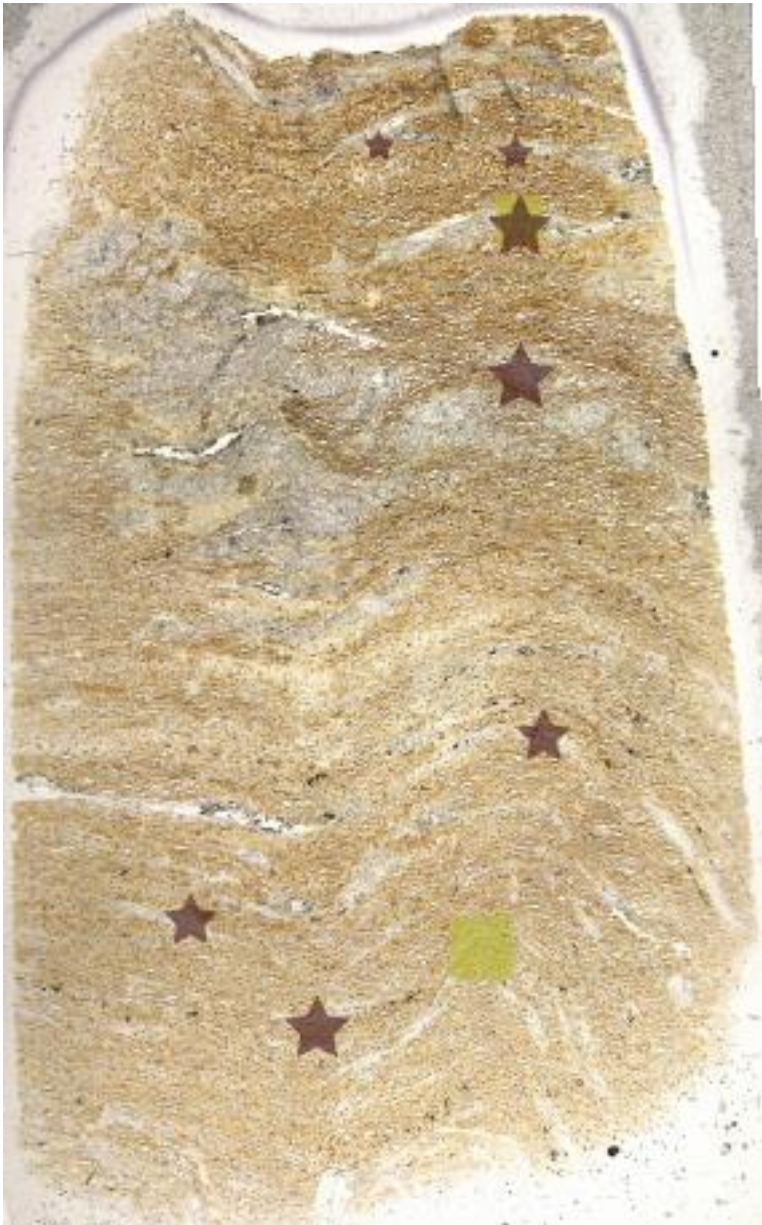
Overview of a thin section of the peridotite sampled at location 4e1 (figure 15). This thin section consists of very small (< mm) olivine grains which are relatively strain-free (see next picture). The black dots are Cr-rich spinel which lie mainly on the Fe-Cr trend. The lower square is photo C in figure 19.

Overview of a thin section made from the peridotite sampled at 4e1 (figure 15) in XPL. For a short description see previous picture.

Overview of a thin section made from the peridotite sampled at 4e4 (figure 15). This sample is taken from a spinel bank inside a larger peridotite body. The spinel grains are separated by chlorite. Measurements have shown that the spinel is mainly Cr-rich with some exceptions being Al-rich.

Overview of a thin section made from the peridotite sampled at location 4e3 (figure 15). In this thin section a clear fold is observed (lower right part). The main minerals in this fold are amphibole and olivine. The lower square is photo E in figure 19, the upper square is photo F in figure 19.

Overview of a thin section made from the peridotite sampled at location 5e1 (figure 15). The olivine grains in this thin section are small (< 1mm) and are relatively strain-free. Two bands of spinel can be observed which consist of Cr-rich spinel. The foliation is expressed by serpentine growing in between and over the olivine grains.

Overview of a thin section made from the peridotite located at 5e1 (figure 15). The foliation in this thin section is expressed by serpentine overgrowing olivine grains. The most abundant mineral is olivine with minor amounts of Cr-rich spinel and tremolite and anthophyllite.

Overview of a thin section made from the peridotite located at ER2C (figure 15). This sample consists mainly of olivine and orthopyroxene with minor amounts of tremolite and Al-rich and Cr-rich spinel.

Overview of a thin section made from the peridotite sampled at location W16 (figure 15). The thin section consists mainly of tremolite, large (1 cm) olivine grains which are overgrown with serpentine, massive serpentine and magnetite (black spots).